THE ROLE OF SECRETION ASSOCIATED RAS RELATED GTPase 1B IN SKELETAL MUSCLE INSULIN SIGNALING

by

Maggie Pickard

Submitted in partial fulfillment of the requirements

For the degree of Master of Science

at

Dalhousie University
Halifax, Nova Scotia
April 2023

Table of contents

List of tables

List of figures

Abstract

Dysfunctional branched-chain amino acid (BCAA) catabolism increases intracellular branched-chain keto acids (BCKA), which inhibit insulin signaling. The discovery of Secretion Associated Ras-related GTPase-1B (Sar1b), a leucine sensor, raised the question if Sar1b alters BCAA flux in the muscle to influence insulin action, mitochondrial function, and protein synthesis. In my thesis, I examined if nutrient overload changes Sar1b content in the muscle, influencing intracellular BCKA levels, and thereby perturbing insulin signaling, substrate metabolism, and mitochondrial function. Increased circulating BCKAs in diet-induced obese mice were associated with decreased Sar1b protein content in the gastrocnemius muscle. In C2C12 cells, Sar1b knockdown increased intracellular BCKA content, reduced pyruvate-linked mitochondrial respiration with a concomitant decline of insulin-stimulated phosphorylation of protein kinase B, glycogen synthase kinase, ribosomal S6, p70S6K, mTOR, and extracellular receptor kinase. Increased understanding of Sar1b and its skeletal muscle interacting partners will uncover novel therapeutic targets to maintain insulin homeostasis during obesity.

List of abbreviations and symbols

aaRS	aminoacyl transfer RNA synthetase
ACC	acetyl-CoA carboxylase
ADP	adenosine diphosphate
AGE	advanced glycation end-products
ANOVA	analysis of variance
ARF	ADP-ribosylation factor
AS160	AKT substrate 160
ATP	adenosine triphosphate
BCAA	branched-chain amino acid
BCAT	branched-chain aminotransferase
BCKA	branched-chain keto acid
BCKDH	BCKA dehydrogenase complex
BCKDK	BCKDH kinase
BLAST	Basic Local Alignment Search Tool
BMI	body mass index
BSA	bovine serum albumin
cDNA	complementary DNA
CM	chylomicron
COPII	coat protein complex II
CPT	carnitine palmitoyl-transferase
CRD	chylomicron retention disease
CVD	cardiovascular disease
DAG	diacylglycerol
DIO	diet-induced obesity
DMEM	Dulbecco's modified eagle medium
DMEM-HG	Dulbecco's modified eagle medium high glucose
DNA	deoxyribonucleic acid
DTT	dithiothreitol
EDL	extensor digitorum longus

eEF2	eukaryotic elongation factor 2
EIF4E	eukaryotic initiation factor 4E
ER	endoplasmic reticulum
ERK	extracellular receptor kinase
ETS	electron transport system
FA	fatty acid
FAO	fatty acid oxidation
FATP	fatty acid transport protein
FBS	fetal bovine serum
GAP	GTPase activating protein
GATOR	GAP activity towards RAGs
GCN2	general control non-derepressible 2
GEF	guanyl nucleotide exchange factor
GLUT	glucose transport protein
Grb2	growth factor receptor-bound protein 2
GS	glycogen synthase
GSK3	glycogen synthase kinase 3
GSV	glucose storage vesicle
GTP	guanosine triphosphate
HFHS	high-fat high-sucrose
INPP4B	inositol polyphosphate-4-phosphatase type II B
IR	insulin receptor
IRS	insulin receptor substrate
ISTD	internal standard
ITD	internal standard
JNK	janus kinase
KIC	4-methyl 2-oxopentanoic acid sodium salt
KIV	sodium-3-methyl-2-oxobutyrate
KIVd7	sodium-2-Keto-3-methyl-d3-butyrate-3,4,4,4d4
KMV	3-methyl-2-oxovaleric acid sodium salt
LPA	lysophosphatidic acid

MAPK	mitogen-activated protein kinase
MiR05	mitochondrial respiration medium
MRM	multiple reaction media
mRNA	messenger RNA
mTORC	mammalian target of rapamycin complex
NTC	no template control
OXPHOS	oxidative phosphorylation
PAGE	polyacrylamide gel electrophoresis
PARP	poly-ADP ribose polymerase
PBS	phosphate-buffered saline
PDH	pyruvate dehydrogenase
PDK	phosphoinositide-dependent kinase
PFA	paraformaldehyde
PH	pleckstrin homology
PHLPP	pleckstrin homology domain leucine-rich repeat protein phosphatases
PI3K	phosphatidylinositol-3-kinase
PIP3	phosphatidylinositol-3,4,5-triphosphate
PKB	protein kinase B
PKC	protein kinase C
PPARα	peroxisome proliferator-activated receptor α
PP2A	protein phosphatase 2A
PP2C	protein phosphatase 2C
PTEN	Phosphatase and tensin homolog deleted on chromosome 10
PTP	protein tyrosine phosphatase
Pyr	pyruvate
qPCR	quantitative polymerase chain reaction
RER1	retention in endoplasmic reticulum sorting receptor 1
RNA	ribonucleic acid
ROS	reactive oxygen species
RPL7	ribosomal protein L7
Sar1b	secretion associated ras-related GTPase 1b

SDS	sodium dodecyl sulphate
SEM	standard error of the mean
SFA	saturated fatty aid
SH2	Src homology 2
SiRNA	small interfering RNA
SOS	son of sevenless
SUnSET	surface sensing of translation
S6K1/P70S6K	Ribosomal protein S6 kinase beta1
TAG	triacylglycerol
TBS	tris-buffered saline
TBS-T	tris-buffered saline-tween
TCA	tricarboxylic acid
TLR	Toll-like receptors
TNFα	tumour necrosis factor α
TSC2	tuberous sclerosis factor 2
T2D	type II diabetes
UPLC	ultra-performance liquid chromatography
VEH	vehicle
VLDL	very low-density lipoprotein
WDR	WD repeat domain
4EBP1	eIF4E-binding protein

Acknowledgements

Foremost, I would like to thank my supervisor Dr. Thomas Pulinilkunnil for his continuous support during my graduate training. Throughout my graduate program, Thomas has shared an incredible enthusiasm for science, research, and creative approaches to scientific investigation. I have greatly appreciated the opportunities Thomas has given me to refine my critical thinking skills, research approach and scientific writing. I would also like to acknowledge the support and guidance of Dr. Petra Kienesberger, who has always been a constant source of encouragement and encouraged me to think critically and conduct thorough research. I am also thankful to my thesis advisory committee members, Dr. Barbara Karten, and Dr. Yassine El-Hiani, for their guidance and encouragement throughout this project. My committee has always helped me think about my project in a new light and kept me on track to completing my goals.

I want to thank all my colleagues in the Pulinilkunnil-Kienesberger laboratories, past and present. This work would not have been possible without their endless support and friendship. I would like to specifically acknowledge Adithi Pisapathi for your friendship and support since the start of our program – I could not have done this without you. Dr. Logan Slade, thank you for your guidance, patience, and words of reassurance and for always answering my endless questions throughout this project. Angela Zemingui, thank you for your contributions to this work and for a great summer of work in the lab. Thank you also to Angella Mercer, Wai Naing, Sundaram Pakkiriswami, Anu Jose and Ana Dekic for technical support, words of encouragement and support, and helpful insights throughout my time in the lab.

I would also like to thank all the members of Dr. Keith Brunt and Dr. Tony Reiman's laboratories for their friendship, encouragement, and helpfulness in working in our shared lab space. Having kind, genuine people to share space with made all the difference in navigating my time in this program. I also want to thank Dr. Rattina Dasse Nadaradjan for his technical assistance and support in the DMNB lab, regardless of the task. I would also like to thank the administrative staff at Dalhousie Medicine New Brunswick and the department of Biochemistry and Molecular Biology for their patience and help in navigating the non-laboratory components of this degree program. I would also like to thank the funding agencies that supported my MSc research: NSERC, Diabetes Canada and the New Brunswick Health Research Foundation.

Finally, to my incredible support system, here in Saint John and elsewhere, who helped me through the hard days of this program, thank you so much for being there for me, always encouraging me, and making me laugh and smile when it's what I needed the most. I could not do it without your support. Thank you, especially Tori; I don't know what I would have done without your friendship in and out of the lab, and I'm so thankful to have met you. Lastly, I am beyond thankful for my parents. Without you encouraging, reassuring, and motivating me to do my best, none of this would be possible. Thank you for being my rocks.

Disclaimer: Maggie Pickard designed and performed all experiments and analyzed results. Dipsikha Biswas performed diet experiments and processed mouse tissue samples presented in Figure 3.1-3.3, Maggie Pickard probed western blot membranes and analyzed the present data. Angela Zemingui performed experiments in H9C2 cells shown in Figure 3.7. Angella Mercer performed UPLC MS analysis shown in Figure 3.11-3.12.

Chapter 1: Introduction

1.1 Obesity, insulin resistance, type 2 diabetes: the triad of metabolic syndrome

Obesity is defined as excess body weight for a given height and remains a global health concern. The pathogenesis of obesity is multifactorial, with environmental, sociocultural, physiological, medical, behavioural, genetic, and epigenetic factors contributing to its cause and progression[1]. The most widely used criterion to classify obesity is body mass index (BMI) (weight in kg/height in m^2), specifically to define overweight (BMI 25 to 29.9 kg/m^2) and obesity (BMI > 30 kg/m^2)[1]. BMI is not necessarily an accurate measure of adiposity, but a population-based anthropometric measurement used in epidemiological tracking. Since 1980, the global rate of obesity has nearly tripled and continues to rise. According to the world health organization, approximately 2 billion adults are overweight, and 625 million are obese[2,3]. Current projections indicate 1 billion people worldwide will be living with obesity by the year 2025[4]. Moreover, pediatric obesity, in both childhood and adolescence, constitutes a major public health crisis. Despite the alarming prevalence and substantial heritability of obesity, the causative mechanisms remain largely unexplained. Therefore, advancing knowledge on obesity complications is paramount to devising strategies for prevention and treatment.

Obesity is a persistent and pernicious driver of global mortality and morbidity. It is a chronic illness rather than a disease risk factor since weight gain and related comorbidities are driven by metabolic remodelling and excess fat accumulation. Obesity renders patients susceptible to developing metabolic syndrome, a cluster of conditions including hypertension, insulin resistance, hyperglycemia, and hyperlipidemia associated with increased risk of type 2 diabetes (T2D), cancer, and cardiovascular disease (CVD)[1,5,6]. Obesity is characterized by positive energy imbalance from excessive nutrient consumption wherein energy intake outweighs energy expenditure[5]. High sugar, high-calorie diets, genetic factors, and limited physical activity are the main contributors to obesity[6]. That said, while dietary and lifestyle interventions are critical for managing weight gain, these interventions show minimal efficacy in reversing morbidity and mortality without significant side effects[6]. Therefore, it is pertinent to understand the biological mechanisms of metabolic remodelling in multiple tissues during obesity to uncover druggable targets to reverse/arrest obesity-related complications.

During obesity, elevation in circulating nutrients like glucose, fatty acids, and amino acids leads to the uncontrolled secretion of insulin and adipocytokines such as leptin and resistin.

Elevated lipids and amino acids during obesity render tissues and cells resistant to insulin action[7]. Insulin resistance is the state of reduced responsiveness to high insulin levels. Persistent insulin resistance causes pancreatic beta cell insufficiency and dysfunction, leading to the development of T2D[7]. In addition to whole-body metabolic effects, obesity and associated insulin resistance remodel metabolism and function in distinct insulin-responsive tissues, including the liver, adipose tissue, and skeletal muscle[8-10].

Since skeletal muscle is the largest insulin-sensitive organ and the site of insulin-sensitive glucose uptake[11], alterations in skeletal muscle insulin signaling during obesity are sufficient to promote metabolic maladaptation, lipid accumulation, and muscle dysfunction and injury. Furthermore, skeletal muscle metabolism is crucial for whole-body glucose homeostasis, which is severely impacted by obesity and T2D[9]. Therefore, understanding the molecular underpinnings of skeletal muscle insulin signaling during obesity is critical for improving glucose homeostasis and attenuating lipotoxic complications in the muscle. This approach will likely uncover novel pathways and druggable targets to improve insulin signaling and sensitivity during obesity, halting the progression to T2D.

1.2 Skeletal muscle insulin signaling and energy metabolism

1.2.1 Insulin signaling pathways stimulating glucose uptake and utilization

Skeletal muscle glucose uptake is facilitated by glucose delivery to myofibers, transport into myofibers, and irreversible phosphorylation of glucose within the myofibers[12]. The initial step of insulin-mediated glucose uptake is mediated by glucose transport proteins (GLUT). GLUT4 is one of 13 sugar transporters (GLUT1-13) and is the predominant isoform involved in skeletal muscle glucose uptake[13]. Decreased insulin secretion during fasting inactivates GLUT4 transporters by restricting GLUT4 within intracellular glucose storage vesicles (GSV)[14]. However, nutrient consumption increases circulating insulin to trigger GLUT4 activation and translocation to the plasma membrane[14] to drive glucose uptake and transport into the cell[11,13,14].

The insulin receptor (IR) resides mainly on the cell surface and structurally constitutes a disulphide-linked α/β heterodimer glycoprotein. Insulin binding to the α subunit of the receptor activates IR and alleviates protein tyrosine phosphatase (PTP)-mediated repression of the β subunit's tyrosine kinase activity[11,15] to trans-phosphorylate tyrosine residues in β subunits. Indeed, PTP1B deletion in mice improves insulin sensitivity by increasing insulin-dependent tyrosine phosphorylation of the insulin receptor[16,17].

Autophosphorylation of IR at distinct tyrosine residues serves as docking sites[11,15,18] for downstream insulin signaling substrates. Specifically, IR autophosphorylates at Tyr-960 in its intracellular juxta membrane region, which creates the recognition site for the insulin receptor substrate (IRS) proteins[11,15,18]. Insulin induces IRS-1 binding to the IR recognition site at p-Tyr-960, and IRS-1 is subsequently phosphorylated at multiple tyrosine residues to become active[11]. Mice with a combined deficiency of IRS-1 and IRS2 in the skeletal muscle displayed systemic insulin resistance and impaired insulin-stimulated glucose uptake[19] in isolated skeletal muscles. However, in L6 myotubes, insulin-stimulated GLUT4 translocation and glucose uptake were regulated primarily by IRS-1[20], highlighting the role of both IRS-1 and IRS-2 in glucose utilization.

Activated IRS-1 acts as a signaling scaffold to bind downstream effector molecules at their Src homology 2 (SH2) domains[11]. One critical node of intracellular effectors is the phosphatidylinositol-3-kinase (PI3K)-AKT/Protein Kinase B (PKB) pathway, which mediates skeletal muscle glucose uptake, glycogen synthesis, and protein synthesis[11,21]. Tyrosine phosphorylated IRS-1 binds to and activates PI3K after recruitment to the plasma membrane[11,21]. PI3K is a heterodimeric class 1A three-kinase with serine kinase activity[11,21]. When activated in response to IRS-1 binding, PI3K catalyzes the formation of phosphatidylinositol-3,4,5-triphosphate (PIP3). PIP3, a lipid messenger protein, is a docking site for binding downstream signaling molecules at their plectron homology (PH) domains, such as AKT/PKB[11,21]. The prevailing hypothesis is that reducing insulin-stimulated AKT activation in the skeletal muscle decreases glucose uptake and GLUT-4 translocation, leading to hyperglycemia and systemic insulin resistance.

There are three isoforms of AKT (AKT1-3), with AKT2 accounting for ~90% of the AKT in the muscle[22]. Combined cardiac and skeletal muscle-specific deletion of AKT1 alone, which accounts for less than 10% of the AKT expressed in skeletal muscle, does not affect muscle growth or glucose homeostasis[23]. However, whole-body deletion of AKT2[24] and muscle-specific combined short-term deletion of AKT1 and AKT2[22] led to impaired insulin-mediated glucose uptake, suggesting that skeletal muscle AKT1 functionally compensates for the absence of AKT2 to preserve insulin signaling. A recent study demonstrated that AKT has a time-dependent effect on insulin sensitivity, as short-term AKT deletion results in insulin resistance, while a more chronic deletion does not impair insulin signaling but induces mitochondrial dysfunction[22].

Recruitment and translocation of AKT from the cytosol to the plasma membrane occur in response to PIP3 production. On the plasma membrane, AKT binds to PIP3 and undergoes a conformational change[11,25]. This conformational change allows for the phosphorylation of AKT at two critical sites: by the mammalian/mechanistic target of rapamycin complex 2 (mTORC2) on serine 473 (s473) in the C-terminal hydrophobic motif harbouring carboxy-regulating domain and by a phosphoinositide-dependent kinase (PDK1) on threonine 308 (T308) in the kinase domain or catalytic T-loop[11,25]. Phosphorylation of both residues is obligatory for maximal activation of the kinase. AKT is inhibited by lipid phosphatases such as Phosphatase and tensin homolog deleted on chromosome 10 (PTEN) and inositol polyphosphate-4-phosphatase type II B (INPP4B). Furthermore, protein phosphatase 2A (PP2A) dephosphorylates AKT T308, leading to kinase inactivation[26]. In addition, the recently uncovered PH domain leucine-rich repeat protein phosphatases (PHLPP1 and PHLPP2) function[27] as physiological AKT S473 phosphatases[28] to terminate AKT signaling.

AKT is a serine-threonine kinase which directly phosphorylates proteins within a consensus recognition motif of R-X-R-X-X-S/T-f (where X is any amino acid and f denotes a preference for large hydrophobic residues) to either activate or inhibit the target protein function. One of the primary targets of AKT is the inhibitory phosphorylation of glycogen synthase kinase 3 (GSK-3), a constitutively active serine/threonine kinase and inhibitor of glycogen synthesis[11,29]. GSK3 has two isoforms, α and β, whose activity is inhibited via phosphorylation by activated AKT at Ser-21 and Ser-9, respectively[11]. Insulin-dependent inhibition of GSK3 decreases its ability to phosphorylate and inhibit glycogen synthase (GS), allowing GS to stimulate glycogenesis[11,29]. AKT also inhibits AKT substrate 160 (AS160) via phosphorylation at Thr-642 and Ser-588[11,30]. This inhibitory phosphorylation eliminates the guanosine triphosphate (GTP)-ase activating (GAP) activity of AS160, allowing for the activation of Rab G proteins, which stimulate the translocation of GLUT4 to the plasma membrane, a critical event in skeletal muscle glucose uptake[11,30].

In addition to the PI3K-AKT arm of insulin signaling, IRS-2, in combination with the adapter protein containingSH2 domains, also activates the mitogen-activated protein kinase (MAPK) pathway, which controls gene expression, mitogenesis (cell growth) and cell differentiation[31,32]. Growth factor receptor bound protein 2 (Grb2) acts as an adapter protein in a complex with the son of sevenless (SOS) protein, binding the insulin-activated SH2-IRS complex and translocating to the membrane[31,32]. The Grb2/SOS complex exerts guanyl nucleotide exchange

factor (GEF) activity toward ras (MAP4K), which subsequently associates with serine-threonine kinase C-Raf (MAP3K) at the membrane. Membrane-localized Raf phosphorylates and activates MEK (MAP2K), which is translocated from the cytoplasm to the nucleus in the presence of insulin[33,34]. MEK phosphorylates tyrosine and threonine residues of extracellular receptor kinase (ERK) 1 and 2 isozymes, resulting in ERK activation[31,32]. While responding to stress or survival stimuli, activated ERK1-2 dimerizes and translocates to the nucleus to transcribe genes involved in cell growth and differentiation[35].

1.2.2 Insulin signaling and substrate preference in the skeletal muscle

Insulin not only facilitates glucose homeostasis, but it also regulates substrate preference for energy generation in the skeletal muscle. The skeletal muscle utilizes primarily glucose or free fatty acids (FAs) as the energy source to produce adenosine triphosphate (ATP)[36]. Under fed conditions, increased plasma glucose levels trigger insulin release, stimulating muscle glucose uptake. Glucose from the circulation is transported into the skeletal myocyte via GLUTs in an insulin-dependent process, which is converted into pyruvate via glycolysis[36,37]. Pyruvate undergoes decarboxylation via pyruvate dehydrogenase (PDH) to form acetyl-CoA, which then undergoes mitochondrial oxidative phosphorylation in the presence of molecular oxygen to yield ATP, H_2O and CO_2[38].

The flux of acetyl-CoA into mitochondria derived from either glucose or FA acts as the nodal point for substrate metabolism as proposed by Sir Philip Randle and colleagues[39]. The Randle cycle states that increased availability of one substrate would decrease the oxidation and thus the utilization of the competing substrate[40]. During states of nutritional abundance, glucose utilization dominates, wherein pyruvate-derived acetyl CoA is favoured for oxidation by relieving the inhibition of PDH by PDH kinase. Insulin inhibits PDH kinase, thereby increasing PDH dephosphorylation and increasing glycolysis[39,41]. However, during starvation or nutritional insufficiency, decreases in circulating insulin diminish glucose use and relieve the inhibition of lipolysis, leading to increased systemic FAs and lipoprotein triacylglycerol (TAG) which are preferentially used for energy[36,42].

Augmented insulin during the fed state inhibits fatty acid oxidation (FAO)[36,37] by increasing PDH activity, decreasing acetyl-CoA/free CoA and downregulating NADH/NAD^+ ratios. Insulin-dependent AKT activation is required for PDH activation[43]. However, during fasting conditions, increased fatty acid-derived acetyl-CoA/free CoA and NADH/NAD^+ ratios activate PDH kinase and inhibit PDH, decreasing glucose oxidation. Furthermore, the rate of FA β-oxidation is also regulated

by the intracellular levels of malonyl-CoA, derived from cytosolic acetyl-CoA via acetyl-CoA carboxylase (ACC), an inhibitor of carnitine palmitoyl transferase 1 (CPT-1)[42]. In the fed state, malonyl CoA allosterically inhibits CPT-1, the rate-limiting enzyme involved in mitochondrial FA import and subsequent oxidation[42]. Fasting depletes intramyocellular malonyl-CoA content, relieving CPT-1 inhibition and leading to high FAO. Therefore, insulin inhibits FAO by increasing glucose oxidation, allowing the skeletal muscle to preferentially use glucose as a substrate[42]. Insulin also has a role in metabolizing amino acids as a tertiary energy source. Like glucose, increased plasma levels of select amino acids can stimulate insulin release from pancreatic β cells[44]. Indeed, skeletal muscle insulin infusion augments net amino acid uptake, increasing amino acid delivery to the muscle[45].

Insulin is a mitogenic hormone which prevents amino acid mobilization, enabling the storage of amino acids into proteins[46]. Insulin activates protein synthesis via its downstream effector, the mammalian or mechanistic target of rapamycin (mTOR)[47]. Insulin signaling stimulates AKT, which phosphorylates and inactivates tuberous sclerosis factor 2 (TSC2). Active TSC2 is a GTPase activating protein (GAP) which accelerates GTP hydrolysis to GDP, enabling the addition of GDP to Rheb inactivating Rheb [47]. By inactivating TSC2, AKT allows for Rheb to remain GTP-bound. GTP-bound Rheb localizes at the lysosome and binds to and activatesmTOR[47,48]. Following a conformational change after Rheb binding, mTOR is phosphorylated and activated by several kinases, including AKT, mTOR exists in two distinct complexes, mTOR complex 1 (mTORC1) and mTOR complex 2 (mTORC2). mTORC1 regulates the function of proteins involved in the initiation and elongation stages of messenger ribonucleic acid (mRNA) translation. Following insulin receptor activation, mTORC1 activates ribosomal protein S6 kinase beta-1 (S6K1/P70S6K), which further phosphorylates the S6 ribosomal protein to regulate the expression of eukaryotic initiation factor 4E (eIF4E) and eukaryotic elongation factor 2 (eEF2)[47,48], readouts of increased protein synthesis and ribosomal biogenesis. mTOR also performs inhibitory phosphorylation of 4E-BP1 at either Thr37, Thr46, Thr70 or Ser65, thereby relieving its inhibition of eIF4E and facilitating protein synthesis[47,48].

1.3 Metabolic inflexibility and skeletal muscle insulin resistance

During obesity and diabetes, lack of insulin or insulin function impairs GLUT translocation, leading to systemic hyperglycemia with a concomitant decline in muscle glucose uptake, glycolysis, and glucose oxidation[9]. Therefore, to compensate for ATP deficit from glucose oxidation, adaptive

molecular events ensue to provide uninterrupted FA supply and oxidation. Enhanced adipose tissue lipolysis and very low-density lipoprotein (VLDL) secretion from the liver increases systemic FA and TAG[49]. Within the muscle, there is an increase in the activity of TAG-synthesizing enzymes, resulting in TAG accumulation. To mobilize FA from circulating and intracellular TAG, the activity of extracellular LPL and intracellular TAG hydrolases (ATGL & HSL) increases, leading to superfluous FA availability to skeletal muscle[49]. Elevated intracellular FA during obesity and diabetes activates peroxisome proliferator-activated receptor α (PPARα), which promotes the expression of genes involved in FAO, inhibiting glucose utilization[49]. Increased demand and supply of FA promotes FA uptake, accumulation, and formation of intracellular FA derivatives or lipotoxic intermediates, such as fatty acyl coenzyme A (CoA), diacylglycerol (DAG) and ceramides, long chain acyl CoAs and/or acylcarnitines[50]. FA inhibition of insulin signaling is the basis of obesity-mediated insulin resistance and T2D[9]. Lipotoxic species directly or indirectly interfere with insulin signaling and glucose transport via various mechanisms, as discussed in the subsequent sections of this chapter. However, lipotoxicity is not the only consequence of metabolic inflexibility during obesity and diabetes. Hyperglycemia and ensuing glucotoxicity are also an outcome of metabolic maladaptation. Indeed, a 2018 study demonstrated that a subtle elevation in plasma glucose concentration in healthy individuals for only three days induced insulin resistance[51]. Pathological outcomes of impaired insulin signaling precipitate complications of glucotoxicity and lipotoxicity that in turn induce mitochondrial dysfunction, reactive oxygen species (ROS) overload, ER stress, and proteotoxicity, which all feed-forward metabolic inflexibility within the skeletal muscle observed in obesity and diabetes.

Optimal insulin signaling is a prerequisite for mitochondrial metabolism and function. Evidence from human and animal models of insulin resistance and T2D suggest that the development of skeletal muscle insulin resistance[52] is accompanied by decreases in mitochondrial respiration and increasing mitochondrial dysfunction[53-55]. However, there are also reports showing no mitochondrial dysfunction in models of insulin resistance and T2D[52,56], questioning the causative role of mitochondrial dysfunction for the onset of insulin resistance. Therefore, while it is critical to understand the relationship between insulin signaling and mitochondrial homeostasis, the aberrations in distal and proximal pathways of insulin signal transduction must be carefully studied and understood to develop therapies to ameliorate obesity-related insulin resistance and type 2 diabetes.

1.3.1 Insulin resistance overview

The current hypothesis on mechanisms that mediate insulin resistance and impaired insulin action is attributed to defects in signaling components of insulin signal transduction or are secondary to complications of metabolic dysfunction. Prior studies have now demonstrated that i) insulin resistance is observed in rodents and humans in the absence of decreased signal transduction; ii) mere changes to the proximal insulin signaling components like IR, IRS-1, or AKT do not completely explain insulin resistance; iii) circumventing growth factors receptor signaling is not sufficient to block the defect observed in insulin resistance, and iv) insulin resistance in skeletal muscle is most prominent at the level of glucose transport[57-60].

Although fatty acids inhibit the insulin-dependent translocation of GLUT4 to the plasma membrane, there is no evidence that this inhibition involves an allosteric modification. This suggests that lipotoxic intermediates likely deregulate muscle insulin signaling by impacting not just the proximal but also the distal signaling axis of insulin signal transduction, constituting proteins downstream of AKT such as protein kinase C (PKC), Janus kinase (JNK), GSK3 and ERK [11]. These serine-threonine kinases induce inhibitory serine phosphorylation of IRS-1. Serine phosphorylation at its PH domain limits the ability of IRS-1 to bind to the plasma membrane and the IR[11]. Serine phosphorylation of the PTB or carboxyl domain limits the interactions of IRS with PI3K, minimizing the activation of PI3K[61]. Rodent models have shown hyper-serine phosphorylation in insulin-resistance models at Ser302, Ser307, Ser612, and Ser632; while human serine phosphorylation sites include Ser636 and Ser312[11,62,63]. These protein kinases are also involved in divergent signaling pathways stimulated by insulin, nutrient overload, inflammation, cell stress and mitochondrial dysfunction, which will be reviewed below.

1.3.2 GSK-JNK-PKC signaling in skeletal muscle insulin resistance

In the muscle, excessive FA uptake increases fatty acyl-CoA to form lysophosphatidic acid (LPA), DAGs, and TAGs[9] via lipogenesis. Indeed, in obesity, DAG accumulation is observed in insulin-sensitive tissues, particularly the liver and skeletal muscle[9]. DAGs can occur in three stereoisomers: sn-1,3 DAG, sn-1,2 DAG and sn-2,3 DAG. 1,2 DAGs accumulate in the sarcolemma and intracellular membranes of the endoplasmic reticulum (ER) and mitochondria to activate PKC. Novel PKC isoforms include PKCδ, PKCε, PKCη and PKCθ. In the skeletal muscle, DAG accumulation activates skeletal muscle PKC-θ, stimulating its translocation to the plasma membrane[9,64]. Active PKC-θ inhibits IRS-1 activation via inhibitory serine phosphorylation at

Ser1101, blocking IRS-1 insulin-stimulated tyrosine phosphorylation[9,64]. PKC-θ expression is increased in the soleus muscle of diabetic rats and high fat-induced defects in insulin signaling and glucose transport[65] are ameliorated in PKCθ-KO mice. Furthermore, in obesity, JNK, a stress-activated MAPK effector protein, is activated by high levels of pro-inflammatory cytokines such as tumour necrosis factor α (TNFα), ER stress, and increased ROS[66,67]. JNK is activated and phosphorylated by ERK, downstream of insulin-Raf activation[66-69] in insulin-target tissues, including the skeletal muscle[66-68]. Both JNK-1 and JNK-2 isoforms can phosphorylate IRS-1 at ser-307, and potentially other serine residues to inhibit its activation and insulin signaling in the muscle[66-68].

Under healthy conditions, GSK3β is phosphorylated and inhibited by AKT downstream of insulin-IRS-PI3K activation[70]. However, in obesity and T2D, lipotoxicity elevates GSK3β activity. Moreover, GSK3β directly inhibits insulin signaling by phosphorylating IRS-1 at Ser332[11,70]. Additionally, chronic hyperglycemia (high glucose) activates GSK3β, facilitating ubiquitin-mediated proteasome degradation of IRS-1 in an IR-independent manner[71] to induce insulin resistance.

1.3.3 Glucotoxicity and lipotoxicity disrupt skeletal muscle insulin signaling

Glucotoxicity occurs when a cell/tissue is chronically exposed to elevated glucose (hyperglycemia). Chronic hyperglycemia is a leading cause of insulin resistance in the skeletal muscle and drives the progression to T2D[72]. Hyperglycemia stems from increased glucose production by the liver and decreased glucose uptake by the skeletal muscle[51,72] following decreased insulin content and/or action[72]. Hyperglycemia activates four distinct pathways; 1) ROS generation and activation of poly-ADP ribose polymerase (PARP), 2) activation of PKC, 3) increased glucose flux through the aldose reductase pathway, and 4) formation of glucose-derived advanced glycation end-products (AGE)[41,73-76]. Hyperglycemia-induced insulin resistance also involves impaired insulin-mediated nonoxidative glucose disposal[51]. Glycogen synthesis is the primary route of nonoxidative glucose disposal, which is regulated by the activity of GS[51]. Increased GSK3β activity during hyperglycemia leads to phosphorylation and inhibition of GS[51,77]. Overall, chronically elevated glucose levels are a key contributor to disturbances in skeletal muscle insulin-mediated glucose homeostasis pathways and insulin resistance [51,77].

Lipotoxicity occurs because of the accumulation of lipotoxic intermediates, causing tissue injury and apoptosis. During FA overload, loss of insulin action and the concomitant inability of

adipose tissue to store FA led to increased circulating FA and spillover into oxidative tissues, leading to high FA metabolism and TAG turnover[78]. Lipotoxicity induces oxidative and ER stress, mitochondrial and lysosomal dysfunction, inflammation, and insulin resistance. DAG, the catabolic intermediate of TAG, accumulates in the myotubes after acute exposure to increased FA levels (300 μM of palmitate and oleate)[78].

Excess of palmitate, a saturated fatty acid (SFA), contributes to insulin resistance by increasing DAG and pro-inflammatory signaling, through binding to Toll-Like Receptors (TLRs)[79]. SFAs activate pro-inflammatory pathways and stress kinases such as JNK. Palmitate is transported into the cell via the action of fatty acid transport proteins (FATP) and shuttled to the mitochondria (Figure 1.1), where excess fat oxidation drives ROS production, another contributing factor to insulin resistance[79]. Furthermore, palmitate enhances the synthesis of ceramides which directly inactivate AKT signaling by activating PP2A and PKCζ[79-81]. PP2A dephosphorylates AKT at Thr308 and Ser473, rendering it inactive and unable to stimulate glucose uptake, while PKCζ phosphorylates AKT at Thr43, preventing its translocation to the plasma membrane and subsequent activation[79-81]. Furthermore, ceramides are also activators of pro-inflammatory molecules like JNK, further contributing to insulin resistance[82].

1.3.4 Inhibition of insulin signaling via mTOR activation

Nutrient overload is associated with glucotoxicity, lipotoxicity, and hyperinsulinemia, leading to the overactivation of mitogenic pathways. The nutrient- sensor mTOR facilitates insulin-induced activation of cellular anabolism and growth. Chronic hyperactivation of mTORC1 drives β-cell malfunction and impairs insulin signaling[48,83]. mTORC1 activation stimulates S6K1 to phosphorylate IRS-1 serine residues, preventing its subsequent activation, a negative feedback mechanism that protects the cell to further insulin stimulation at the end of the pathway[47,83]. However, mTORC1 is chronically activated under excess nutrient consumption, specifically by branched-chain amino acids (BCAAs), which leads to sustained S6K1 stimulation and increased inhibitory phosphorylation of IRS-1[47,83]. Indeed, mice lacking S6K1 showed decreased diet-induced insulin resistance[84]. mTORC1 can also directly promote the degradation of IRS and activate Grb10, a negative regulator of the insulin receptor[83,85]. Thus, overactive mTORC1 impairs insulin signaling and exerts a critical influence on skeletal muscle glucose, lipid, and amino acid homeostasis.

1.4 BCAA metabolism and sensing in the skeletal muscle

1.4.1 Defective BCAA catabolism inhibits muscle insulin signaling

BCAAs (isoleucine, leucine, and valine) are essential amino acids characterized by a branched side chain in their structure. BCAAs account for 20% of the protein intake in the human diet and play a critical role in regulating protein synthesis, energy metabolism, and insulin signaling[86,87]. Unlike other amino acids mainly metabolized in the liver, the skeletal muscle is the primary site of BCAA catabolism[87]. BCAAs are converted to their α keto-acid counterparts, the branched-chain keto acids (BCKAs), by a transamination reaction catalyzed by branched-chain aminotransferase (BCAT). BCAT exists in two isoforms: BCAT1 in the cytosol and BCAT2 in the mitochondria[87], and BCAT2 is the primary isoform catalyzing skeletal muscle BCAA breakdown[87]. BCKAs are subsequently oxidized by the branched-chain keto acid dehydrogenase (BCKDH) complex in the inner mitochondrial matrix. BCKDH activity is tightly controlled by BCKDH kinase (BCKDK)-mediated inhibitory phosphorylation or BCKDH activation by protein phosphatase 2C (PP2Cm)[87]. The resulting branched chain acyl-CoA derivatives from the BCKDH reaction are metabolized to acyl CoAs to contribute carbons to the tricarboxylic acid (TCA) cycle[87]. Studies have shown recently that metabolic alterations in BCAA catabolism may be a more robust indicator of disease progression than altered BCAA levels alone[88-90].

Prior studies investigating the correlation between increased circulating plasma BCAAs and incidence of obesity, insulin resistance, and T2D have presented inconsistent results on whether elevated BCAA overload is protective or detrimental in pathological states[87,91,92]. Notably, in rodent models, diet-induced obesity (DIO) decreases skeletal muscle content of BCAA catabolizing enzymes, increasing intracellular BCKA content and contributing to insulin resistance[93]. Treatment with exogenous BCKAs and overexpression of BCKDK inhibited insulin signaling in C2C12 myotubes[93]. This study also demonstrated that BCKA overload activated mTORC1 and protein synthesis. The mechanism by which disruptive BCAA catabolism and BCKA overload impaired insulin signaling could likely be attributed to mTORC1 activation since rapamycin treatment rescued the impact of BCKA overload on insulin signaling[93]. These findings support the notion that dysregulation in BCAA metabolism and overactivation of the mTOR signaling pathway in the skeletal muscle is sufficient to disrupt insulin signaling. However, emerging studies examine mechanisms by which BCAA are transported and/or sensed within the muscle to activate mTOR and/or other insulin resistance-inducing pathways.

1.4.2 mTOR activation, BCAA sensing, and plausible impact on skeletal muscle insulin signaling

Amino acids are recycled and allocated for protein biosynthesis during nutrient insufficiency. During starvation (insulin deficiency), amino acid catabolism is induced to produce fuels such as glucose and ketone bodies for use by the skeletal muscle[94]. Therefore, accurate sensing of amino-acid type and content in the muscle is vital for efficiently regulating protein and amino-acid synthesis and catabolism by modulating insulin signaling pathways. Since no amino acid compensates for the absence of another, the cell must be able to detect the lack of any amino acid efficiently to prevent potential failures in protein synthesis. Multiple sensors for amino acids have been identified however, how they work is unknown; an intra-lysosomal sensor that transduces the signal through the membrane, a lysosomal transmembrane sensor that both detects and transduces the signal and a cytoplasmic sensor that operates downstream of amino-acid export from the lysosome[95].

One of the intracellular amino acid sensors is general control non-derepressible 2 (GCN2)[96]. During low levels of any amino acid, its cognate aminoacyl-transfer RNA (tRNA) synthetase (aaRS) does not load the tRNA. The unloaded tRNA is detected by GCN2 kinase, which halts translation initiation by inactivating eukaryotic translation initiation factor 2α[96]. In addition to amino acid sensing at the whole cell level, amino acids are also sensed at the organelle level. mTORC1 is activated downstream of elevated intracellular amino acids by recruitment to the outer lysosomal surface by a Rag GTPase. mTOR sensing of amino acid input requires coordination from protein complexes, GAP activity towards Rags-1 and 2 (GATOR1 and GATOR2) that control the recruitment and activation of mTOR to the lysosomal surface[48]. Additionally, mTOR lysosomal translocation requires the bound form of RagA or RagB and the GDP-bound form of RagC or RagD; the ragulator complex acts in concert with GATOR1 as GEF and GAP for RagA/B, respectively, to activate the complex[48,97]. Amino acid sensors coordinate the ability of the GATOR complexes to respond to amino acid availability.

One well-characterized BCAA (leucine) sensor is sestrin2, a negative regulator of mTOR[98]. With sufficient leucine, leucine binds to sestrin2, causing it to dissociate from GATOR2[98]. This allows GATOR2 to bind to and activate mTOR, coordinating its lysosomal recruitment[98]. Indeed, overexpression of sestrin2 increases autophagy, blocks mTOR activation, and enhances insulin signaling and glucose uptake in muscle cells. Furthermore, endogenous sestrins maintain insulin-dependent AKT activation in diet-induced obesity, and this effect is primarily observed in the liver

and skeletal muscle. Sestrin2 also directly binds to the PH domain of AKT and induces AKT translocation to the plasma membrane. These results uncover a signaling mechanism whereby Sestrin2 activates AKT through GATOR2 and mTORC2[99]. Silencing WD repeat domain 24 (WDR24), the GATOR2 component essential for the Sestrin2–GATOR2 interaction, or WDR59, the GATOR2 component essential for the GATOR2–mTORC2 interaction, completely ablated Sestrin2-induced AKT activation[99]. In agreement with these findings, sestrin-deficient animals and flies display severe insulin resistance and glucose intolerance[99], suggesting that intracellular sensors of BCAA have a profound role in impacting insulin signaling and function. Interestingly, a novel leucine sensor and mTOR inhibitor that works similarly to sestrin2 was recently identified, and it is highly expressed in the skeletal muscle; Secretion-associated ras-related GTPase 1b (Sar1b)[100]. With Sar1b's recent discovery as a leucine sensor and negative regulator of mTOR, it remains to be seen whether this protein might have a role in skeletal muscle insulin and mTOR signaling[100].

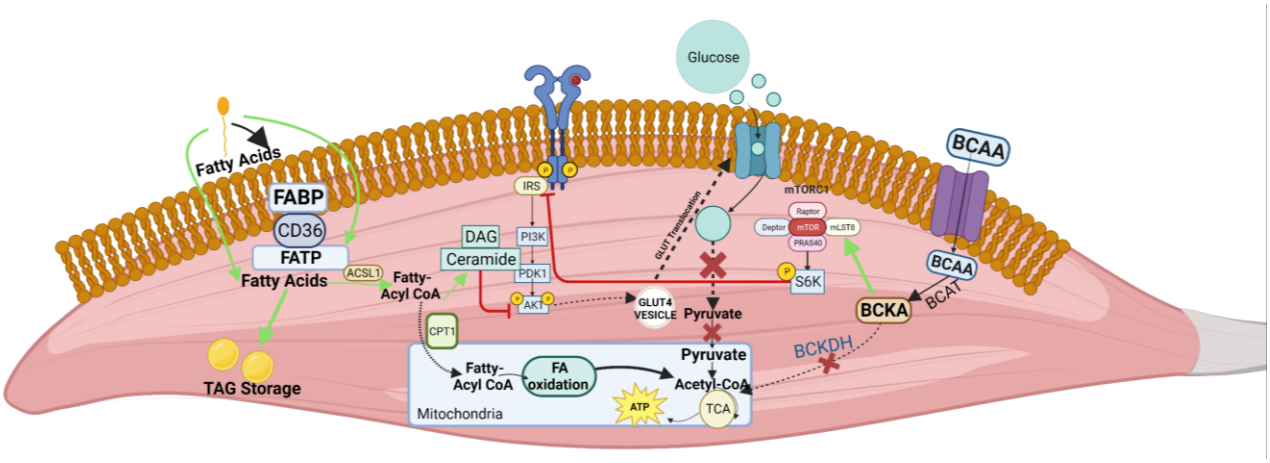

Figure 1.1: Altered skeletal muscle energy metabolism and mitochondrial function during obesity and diabetes.

During skeletal muscle insulin resistance, impaired insulin signaling inhibits glucose oxidation, redirecting glucose intermediates into non-oxidative glucose homeostasis. Decreased reliance on glucose is compensated by enhanced dependence on FAO. Intracellular FA is converted to fatty acyl-CoA that is further processed for mitochondrial β-oxidation pathway to generate ATP through tricarboxylic acid (TCA) cycle. Excess fatty acyl-CoA is either stored as TAG, or converted to DAGs and ceramides, which are lipotoxic intermediates. DAGs and ceramides inhibit Akt function, attenuating glucose uptake and oxidation. Additionally, under conditions of nutrient overload, BCKA oxidation in the TCA cycle is inhibited, and accumulation of BCKAs leads to overactivation of mTORC1, which activates S6K which phosphorylates and inhibits IRS-1, impairing insulin signaling. Solid black arrow: indicate reaction is proceeding forward in a single step; Dashed black arrow: reaction is proceeding in multiple steps; Solid green arrow: indicate reaction is pathologically increased; Solid red line: indicate reaction is inhibited. Solid red X indicates reaction is halted.

1.5 Secretion Associated Ras Related GTPase 1b and amino acid sensing

1.5.1 Structure, localization, and canonical role of Sar1b

Encoded by the SARA2 gene, the Sar1 protein is a member of the ADP-ribosylation factor (ARF) family of guanine-nucleotide-like (G) proteins, a family of proteins that regulate membrane structure and organelle trafficking[101]. Via its GTPase activity, Sar1 acts as a molecular switch to direct vesicle budding from the ER[102]. Sar1 is structurally distinct from other ARF family proteins, with an NH_2 terminus containing a conserved hydrophobic region facilitating membrane recruitment and an alpha1' amphipathic helix responsible for cargo selection during ER export[103].

Sar1 has one paralog in invertebrates and two paralogs in vertebrates and mammals; Sar1a and Sar1b are structurally similar but differ in their physiological roles[104]. Encoded by the SARA2 or SAR1B gene, Sar1b is a 22kDa small GTPase[104]. While both paralogs engage in vesicular trafficking, genetic data and recent studies have pointed toward distinct physiological roles and a specific role in lipoprotein secretion for Sar1b[104]. Sar1-GDP is an essential factor of the coat protein complex II (COPII), which facilitates the transport of newly synthesized TAGs, packaged intro pre-chylomicrons[104,105]. In the COPII complex, Sar1-GDP recruits the heterodimers Sec23/24 and Sec13/31 to the ER membrane, allowing for the formation of pre-chylomicron (CM) transport vesicles and their transport to the Golgi apparatus[106,107]. Investigations into the biochemical differences between the two paralogs have shown that Sar1a can exchange GTP more rapidly than Sar1b due to being adjacent to the GTP binding pocket, making it more useful for faster, smaller cargo trafficking [104]. Sar1b has a higher affinity for binding SEC23A, critical for chylomicron transport and lipoprotein secretion[104]. Therefore, Sar1b plays a distinct role from its paralog in lipoprotein secretion, though both are necessary for efficient CM secretion.

1.5.2 Canonical and non-canonical role of Sar1b in health and disease

Anderson disease, also known as chylomicron retention disease (CRD), is a rare autosomal recessive disorder [108-110] caused by genetic loss of function mutations in the Sar1b gene[111]. Indeed, the loss of function of Sar1b inhibits CM trafficking to the Golgi, resulting in the accumulation of TAGs in enterocytes and a failure to release CMs into circulation[108-110]. Sar1b mutant mice, mutated at a single allele, recapitulated the characteristic features of chylomicron retention disease such as reduced CM secretion, inefficient fat malabsorption[112] and lipogenesis and dysregulated fatty acid oxidation[113] whereas whole body Sar1b deletion resulted in the embryonic lethality of

homozygotes[112]. Sar1b-/- in Caco-2/15 cells increases perilipin 2 (PLIN2) expression, augments mitochondrial fatty acid oxidation and reduces lipogenesis [113].

When studying the tissue distribution of Sar1b, multiple groups uncovered that Sar1b's mRNA expression is significantly higher in the skeletal muscle compared to other tissues[100,114]. Early studies concluded that Sar1b's high skeletal muscle expression was due to its involvement in COPII-dependent[115,116] calcium trafficking. However, in their 2021 study, Chen et al., demonstrated that Sar1b is the only COPII component highly expressed in the mouse skeletal muscle and strikingly Sar1b is a bona fide leucine sensor[100]. Further, its expression pattern differs from the other leucine sensor and mTOR inhibitor, Sestrin2, which is abundant in adipose tissues[100]. During leucine deficiency, Sar1b physically interacts with GATOR2, preventing GATOR2 from activating mTORC1[100]. However, leucine abundance causes Sar1b-leucine binding, dissociating Sar1B from GATOR2 and permitting GATOR2 to activate mTOR, inducing protein synthesis (Figure 1.2)[100]. Notably, increased expression of Sar1b inhibits cell proliferation, attributed to impaired protein synthesis in fibroblast cells. Sar1b was identified to sense leucine and modulate these processes in a COPII-independent manner[100]. Given that Sar1b not only acts as a leucine sensor but also as an inhibitor of mTOR in conditions of low leucine, it remains to be examined whether Sar1b exerts a role in skeletal muscle insulin and mTOR signaling.

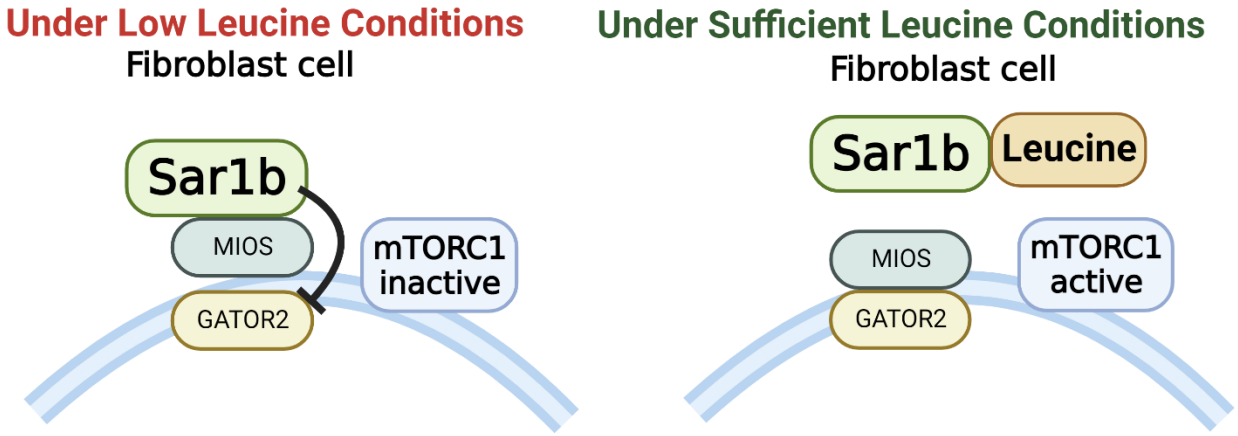

Figure 1.2: Sar1b acts as a leucine sensor to modulate mTOR activation.

Under low leucine conditions, Sar1b binds to and inactivates GATOR2, inhibiting it from binding and activating mTORC1. In the presence of sufficient leucine, Sar1b preferentially binds to leucine, making it unable to bind to GATOR2. GATOR2 is free to bind to MIOS and activate the mTORC1 complex, facilitating its lysosomal recruitment.

1.6 Summary and Rationale

Insulin is a critical regulator of the transition from nutrient uptake to storage to allow for proper energy balance from nutrient sources in animals. Under normal conditions, proper insulin secretion and function allow for carbohydrate uptake and storage, allowing for whole-body glucose homeostasis and proper metabolic function[11]. However, the malfunction of insulin under conditions of nutrient overload, such as in obesity, can cause devastating metabolic effects and result in the development of insulin resistance, T2D and cardiovascular diseases[9,117]. Being the major site of insulin-stimulated glucose uptake in the body, the skeletal muscle is a critical point for insulin signaling and homeostasis. A growing understanding of proper insulin signaling and the mechanisms contributing to insulin resistance under nutrient overload in the skeletal muscle is required to develop therapeutic strategies to combat the growing obesity and T2D epidemics.

We postulate that recently identified leucine-sensor Sar1b could be a novel putative regulator of skeletal muscle insulin signaling and influence functional outcomes of insulin resistance. Given its high expression in the skeletal muscle, it stands to reason that Sar1b has a potential role in governing glucose homeostasis in the skeletal muscle by influencing insulin-stimulated glucose uptake.

In my thesis, I hypothesized that nutrient overload in the skeletal muscle alters Sar1b content and that Sar1b silencing in the muscle perturbs insulin signaling, mitogenic and mTOR signaling, and perturbing skeletal muscle metabolism (Figure 1.3). To elucidate the role of the novel leucine-sensor Sar1b in the skeletal muscle, I aim to:

1. Examine whether exposure of skeletal and cardiac muscle to higher lipids and/or amino acids alters Sar1b protein content.
2. Determine whether altered Sar1b content impacts intracellular BCAA and BCKA levels.
3. Characterize the impact of altered Sar1b availability on myocyte insulin, mitogenic and mTOR signaling.

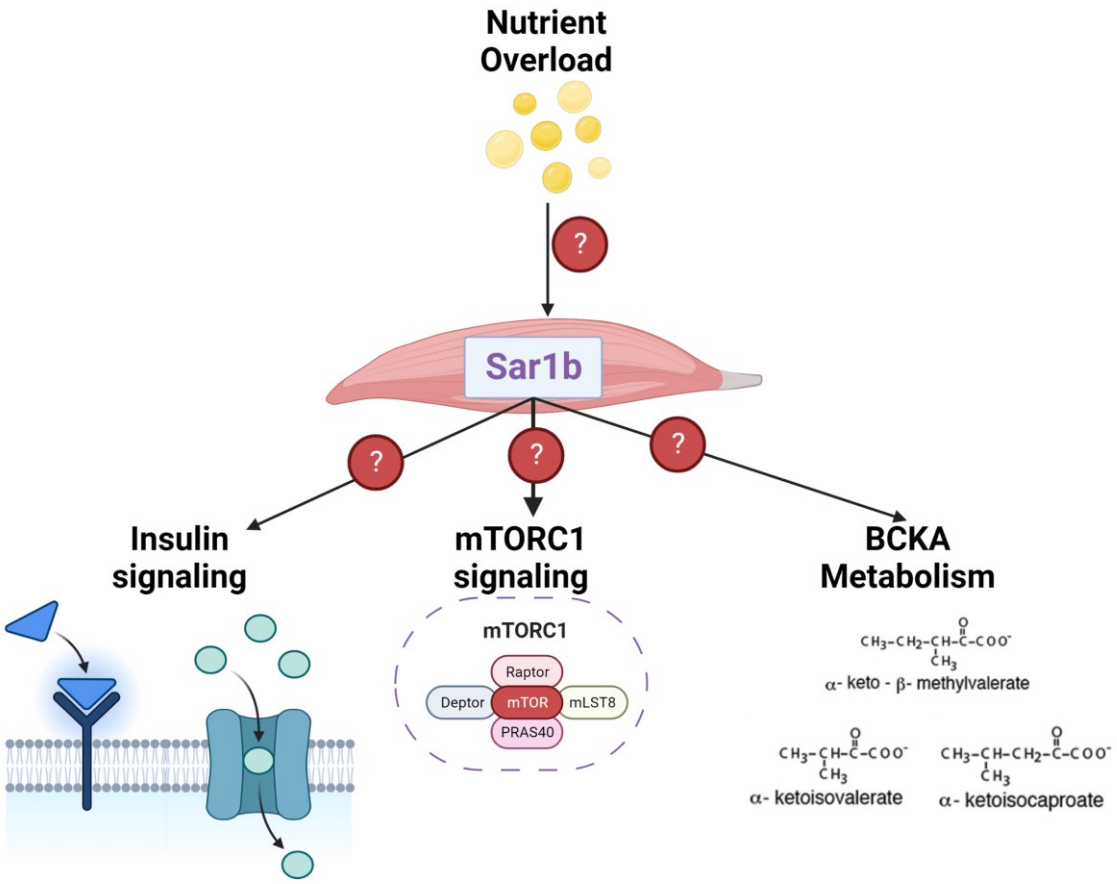

Figure 1.3: Model describing the hypothesis and proposed role of Sar1b in the muscle and potential impacts on insulin signaling, mTORC1 and BCKA metabolism.

Chapter 2: Experimental methods

2.1 Animal studies

All protocols involving rodents were approved by the Dalhousie University, Institutional Animal Care and Use Committee.

2.1.1 High-Fat High-Sucrose diet feeding time course

C57BL/6J mice were procured from the Jackson Laboratory (stock numbers: 000664). Mice were housed on a 12 h light and 12 h dark cycle with access to water and food ad libitum. 8-week-old mice were randomly assigned to either chow (5001; Lab diet, St Louis, MO, USA; with 13.5 kcal% from fat) or high-fat high-sucrose (HFHS) diet (12451; Research Diets, New Brunswick, NJ, USA; with 45kcal% from fat and 17kcal% from sucrose). Body weight gain was recorded weekly. Mice were euthanized following overnight fast after 4, 8, and 13 weeks of diet (N = 5 for each group). Gastrocnemius, EDL, and tibialis muscle were collected, flash-frozen in liquid nitrogen and stored at -80°C until further analysis.

2.1.2 Fasting and refeeding

10-week-old C57BL/6J mice were divided into three groups and either: fed *ad libitum*, fasted for 16, or refed for 4h after fasting (n = 5 for each group). Prior to euthanasia, animals were weighed and had their blood glucose measured. Gastrocnemius muscles were flash-frozen in liquid nitrogen and stored at -80°C until further analysis.

2.2 Cell culture experiments

C2C12 mouse embryonic cardiomyoblast (CRL-1772; ATCC) cells and H9C2 rat embryonic cardiomyoblast (CRL-1446; ATCC) cells were cultured at a cell density of 2.5 $x10^5$ in 35 mm plates/ $5x10^5$ in 60mm plates and maintained in Dulbecco's modified Eagle's high glucose medium (SH30243.01; DMEM-HG; Hyclone Laboratories, UT, USA) supplemented with 10% fetal bovine serum (FBS; 12483020; Gibco) and grown to 80% confluence. C2C12 cardio myoblasts were allowed to differentiate for 48 hr in DMEM-HG supplemented with 0.2% FBS. H9C2 cardiomyoblasts were allowed to differentiate for 48 hr in DMEM-1X medium (11966025; Thermo Fisher Scientific, MA, USA) supplemented with 0.5% FBS and 5 mM glucose (0188; Amresco).

2.2.1 siRNA transfection

Small interfering RNA (siRNA) knockdown of Sar1b was performed using Ambion silencer select siRNA oligonucleotides (4390771; Thermo-Fisher Scientific). For C2C12, mouse siRNAs used were mo-siSAR1B#1: #s83171 targeting exon 6, mo-siSAR1B#2: #s83170 targeting exon 5,

mo-siSar1b#3: #s83172 targeting exons 4 and 5. For H9C2, rat siRNAs used were: ra-si-Sar1b#1: #s142278 targeting exons 2-3, and ra-si-Sar1b#2: #s142280 targeting exons 5-6. siRNA negative control (4390844; Thermo-Fisher Scientific) was included in all C2C12 and H9C2 cell experiments. For siRNA transfection, siRNA was diluted in Opti-MEM (31985062; Life Technologies) and added to Lipofectamine RNAiMAX (13778150; Life Technologies), resulting in a complex with 4 or 6uL of Lipofectamine and a final concentration of 10 or 15nM of siRNA per plate, as indicated in figure legends. The siRNA: lipofectamine solution was prepared in sterile 5mL tubes and incubated for 15-20 min at room temperature to aid complexation. Subsequently, media on plates was replaced with 1.8mL (35mm plates) or 2.75mL (60mm plates) of the cells' respective differentiation media (section 2.12). 200µL (35mm plates) or 250µL (60mm plates) of the siRNA: lipid complex was added dropwise to the appropriate plates, and then cells were incubated 48hr with the siRNA complex before cell harvest or additional treatment.

2.2.2 Insulin signaling

Following 48h of siRNA transfection, differentiated C2C12 myotube cells were incubated for 6h in DMEM1X (11966025; Life Technologies) media supplemented with 5mM glucose (0188; Amresco). Bovine insulin (I0516; Sigma) was diluted to a final concentration of 100nM in DMEM1X media with 5mm glucose, and cells were incubated in 100nM insulin solution or media only control for 15 min at 37°C. After incubation, plates were placed on ice to stop the reaction and subsequently washed in warm 1X phosphate-buffered saline (PBS; Corning; MT21040), prior to harvest for protein analysis (as described in section 2.3.1).

2.2.3 Fatty acid treatments

Bovine serum albumin (BSA): FA solutions were prepared in DMEM 1X medium supplemented with 5mM glucose. 100mM stock solutions of sodium palmitate (P9767; Sigma) were prepared in DMEM1X + 5mM glucose media at a total volume of 7.5mL and heated to 95°C in a boiling water bath to dissolve FA. 2% FA-free BSA (68700; Proliant Biologicals) solution was prepared in DMEM1x + 5mM glucose, wherein BSA was dissolved by centrifugation for 5min at 2500g, and subsequently warmed at 50°C to dissolve further. 100mM stocks of palmitate were diluted to final concentrations of 0.4 or 0.8mM, as indicated in figure legends, in pre-warmed 2% BSA. The resulting FA: BSA (1.5:1) solution was incubated at 50°C for 20 min to complex, prior to sterile filtering for cell culture treatment. Media in wells was replaced with FA: BSA treatment and incubated for 16hr at 37ºC prior to harvest or further treatment.

2.2.4 BCKA treatment

C2C12 cells were incubated for 16h in serum-free DMEM low glucose, leucine-free medium (D9443; Sigma) before treating with 4-methyl 2-oxopentanoic acid sodium salt (KIC; W387101; Sigma), sodium-3-methyl-2-oxobutyrate (KIV; 198994; Sigma), 3-methyl-2-oxovaleric acid sodium salt (KMV; 198978; Sigma), or a combination of all three (BCKAs). BCKAs were prepared in 1:6 HCl/H_2O solution and diluted to a final concentration of 5mM in DMEM low glucose, leucine-free medium. C2C12 cells were treated with 5mM BCKAs or the appropriate vehicle control (VEH; 1:6 HCl/H_2O solution) for 30min prior to cell harvest or subsequent treatments.

2.2.5 SUnSET method

Protein synthesis was measured in vitro by the surface sensing of translation (SUnSET) assay. The SUnSET assay measures protein synthesis by quantifying puromycin incorporation into newly synthesized proteins. C2C12 myotubes were siRNA transfected and incubated for 48hr, control cells were incubated 48hr in differentiation media. This was followed by 6hr serum starvation and incubation in DMEM1X media with 5mM glucose. 50mM puromycin dihydrochloride (P8833; Sigma) was prepared in ddH_2O. The stock solution was further diluted in DMEM1X media with 5mM glucose to 1mM, and a puromycin solution was prepared at a final concentration of 1µM. Media in wells was replaced with 1µM puromycin treatment, or media-only control, in which cells were incubated for 30min at 37°C. Cells were subsequently washed with warm 1X PBS, harvested, and prepared for further protein analysis (as described in section 2.3.1). Puromycin incorporation was detected by western blotting using the monoclonal puromycin antibody (MABE343; Millipore) at a final concentration of 1:5000.

2.2.6 Mitochondrial analysis

Oxygen flux in C2C12 myotubes was measured using the Oxygraph-2k (OROBOROS Instruments). Following 48hr siRNA transfection, cells were rinsed with warm PBS prior to 15-minute incubation with warm accutase (sigma; A6964) to detach cells. Detached cells were collected and centrifuged at 300g for 5min. Subsequently, Accutase was discarded, and cells were resuspended in mitochondrial respiration medium (MiR05) buffer (table 2.1) and diluted to a final concentration of 250,000 cells/mL. Subsequently, cells were permeabilized with 3 µg/mL digitonin to prepare for respirational analysis in 2mL oxygenated-MiR05 buffer at 37°C in oxygraph chambers. Respiration and glucose oxidation was estimated after the sequential addition of malate, pyruvate, and adenosine diphosphate (ADP). Details of the addition and titration of substrates and

inhibitors are listed in table 2.2. The instrument baseline was allowed to stabilize between each addition. Following respirational analysis, cells were collected into 2.0mL tubes from oxygraph chambers and centrifuged at 10 000 g for 5 min at 4°C. The supernatant was aspirated, and the resulting protein pellet was stored at -80°C before analysis of protein concentration by BCA protein assay, as described in section 2.3.1. Mitochondrial respiration was normalized to cell number and protein concentration in µg/mL.

Table 2.2.1: Chemical components, concentrations, and vendor information for components of mitochondrial respiration medium (MiR05) buffer.

Chemical Compound	Concentration	Vendor; Catalog Number
EGTA	0.5 mM	Sigma; E4378
$MgCl_2$-$6H_20$	3 mM	Scharlau; MA0036
Lactobionic acid	60 mM	Sigma; 153516
Taurine	20 mM	Sigma; T0625
KH_2PO_4	10 mM	Merck; 104873
HEPES	20 mM	Sigma; H7523
Sucrose	110 mM	Sigma; 84097
Fatty acid-free-BSA	1 g/l	Sigma; A6003

Table 2.2.2: Substrate uncoupler inhibitor titration protocol to examine pyruvate oxidation in digitonin-permeabilized C2C12 myotubes.

Chemical	Concentration	Mark	Vendor; Catalog Number
Digitonin	3 µM	Dig	Sigma; D5628
Malate	0.5mM	M	Sigma; M1000
Pyruvate	5mM	Pyr	Sigma; P5280
ADP	0.1mM	D 0.1	Sigma; A2754
ADP	0.5mM	D 0.5	Sigma; A2754
ADP	5mM	D 5	Sigma; A2754
FCCP	0.5µM	FCCP	Sigma; C2920
Rotenone	0.5µM	R	Sigma; R8875
Succinate	10µM	S	Sigma; S3674
Antimycin A	5µM	AmA	Sigma; A8674

2.2.7 BCAA and BCKA measurements by UPLC-MS

Following 48hr siRNA transfection, C2C12 cells were incubated with serum-free DMEM low glucose, leucine-free medium (D9443; Sigma), or serum-free DMEM low glucose, leucine-free medium containing 0.4mM palmitate and 2% BSA, for 16h, prior to harvesting and pelleting of cells as described in section 2.3.1.

Intracellular BCKA and BCAA levels were measured by UPLC mass spectrometry as described previously[93]. For intracellular BCKA and BCAA extraction, 500,000 cells, 120 µL of internal standard (ISTD; 4 ug/ml in H_2O containing leucine-d3 (CDN Isotopes; D-1973) and 0.8 ng/µL in H_2O containing sodium-2-Keto-3-methyl-d3-butyrate-3,4,4,4d4 (KIVd7; CDN Isotopes), 120 µl of 3M perchloric acid (CA71007-908; VWR) were combined and lysed using an ultra sonicator. Proteins were precipitated in two sequential steps, with 2 min of sonication at room temperature followed by five min in the ice bath, and then centrifuged at 16,500 g for 15 min at 4ºC. The pellet was subsequently resuspended in 120 uL of 1M perchloric acid and centrifuged at 16,500 g for 2 min at 4ºC. The pellet was frozen at -80C for protein quantification.

Supernatant collected from all precipitation steps were combined and split into two portions for measuring BCKAs (180µL) and BCAAs (150 µL). Samples were subsequently derivatized according to previously established protocols[118,119].

BCKA derivatization and quantification were performed by combining 180 µL of extract and 500 µL of 25 mM OPD in 2M HCl (made from o-Phenylenediamine, 98%; VWR). The mixture was vortexed and then incubated at 80ºC for 20 min, followed by incubation on ice for 10 min and centrifugation at 500 g for 15 min. The supernatant was transferred to a tube containing 0.08 g sodium sulphate (BDH9302; VWR) and 500 µL of ethyl acetate (CABDH83621.400; VWR), which was then centrifuged at 500g at RT for 15 min. This step was repeated twice, and the supernatant collected was vacuum centrifuged at 30ºC for 45 min. Samples were then reconstituted in 60 µL of 200 mM ammonium acetate (made from ammonium Acetate, 98%; CABDH9204 VWR) and transferred to amber glass UPLC vials (Waters). BCKAs were quantified with a Waters Acquity UPLC, Xevo-µTandem Mass Spectrometer and an Acquity UPLC BEH C18 (1.7 µm, 2.1mm X 50 mm; Waters) and ACQBEHC18 VanGuard (130Å, 1.7µm, 2.1mm X 5mm; Waters) using multiple reaction monitoring (MRM) and internal standard calibration according to established protocol[92].

Prior to amino acid derivatization, 150 µL of the extract was neutralized with 120-150 of 2M KOH to a pH of 6-10 (VWR, CABH9262-500G). The sample was centrifuged at 16,500 g, and the supernatant was transferred to a new Eppendorf tube. The neutralized extract was dried via a freeze dryer for 2-4 hours (hole in closed cap). The dried sample was resuspended in 50 µL of 50:50 Methanol: MilliQ water. For amino acid quantification and derivatization, 10 µL of the reconstituted extract was transferred to an autosampler vial and was combined with 70 µL of borate buffer (186009283; Waters) from the Waters AccQ-Tag derivatization kit (target pH: 8–10) and vortexed. 20 µL of AccQ-Tag Derivatization Agent (Waters, 186003836) was added, vortexed, and left standing for 1 min. Samples were derivatized (55 °C, 10 min) and vortexed. Derivatized samples were quantified with a Waters Acquity UPLC, Xevo-µ Tandem Mass Spectrometer and an AccQ-Tag Ultra RP Column 130 Å, 1.7-µm, 2.1-mm, 100-mm column using multiple-reaction monitoring and internal standard calibration[92,93].

2.3 Immunoblotting

2.3.1 Sample processing and protein lysate preparation

Gastrocnemius, tibialis, and EDL muscle strips were powdered and homogenized using a tissue homogenizer (Omni TH, Omni International) in ice-cold lysis buffer (containing 20 mM Tris-HCl pH 7.4 (M151; VWR), 5 mM EDTA (4010; Calbiochem), 10 mM Na_4P_2O7 (P8010; Sigma), 100 mM NaF (S6521; Sigma), 1% Nonidet P-40 (I3021; Sigma), 2 mM Na_3VO_4 (567540; Millipore), protease inhibitor (P8340; 10 mg/ml; Sigma), and phosphatase inhibitor (524628; 10 mg/ml; Calbiochem)). Homogenates were centrifuged at 1200g for 30 min, and supernatants were collected to determine protein concentration. Cells were harvested in ice-cold PBS, transferred to microcentrifuge tubes, and pelleted by centrifugation at 10,000g for 10 min. Ice-cold lysis buffer was added, and cell pellets were subsequently sonicated three times for ten seconds, with 5 seconds each on the ice between each sonication. Lysates were allowed to settle on the ice before being centrifuged for 18 min at 1500 g. The supernatant (total lysate) was aspirated and stored at -80º C until needed. Cell and tissue lysates were diluted 1:10 prior to using the Pierce BCA Protein Assay Kit (23225; Thermo Fisher Scientific) to determine protein concentration, according to the manufacturer's instructions. Protein samples (10-30µg) were diluted in 4X Laemmli Buffer with 1mM dithiothreitol (DTT) and boiled for 5min at 100°C.

2.3.2 Western blotting

Protein samples were denatured and electrophoresed using 10% Mini-Protean Sodium dodecyl sulphate (SDS) polyacrylamide gel electrophoresis or by pre-cast Criterion™ TGX™ 4-20% acrylamide gradient gels (5671095; Bio-Rad). Samples were loaded alongside Precision Plus Protein™ Standards Kaleidoscope™ ladder (1610375; BioRad). Mini-Protean self-cast gels were run at 90V at room temperature in 1X Tris/Glycine/SDS Electrophoresis Buffer (1610772; BioRad); Criterion™ gels were run at 90V for 30 min and 120V for 90 min on ice. Protein was transferred to nitrocellulose membranes (0.2µM; 1620112; Biorad) at 90V for 1h30min at 4°C in 1X Tris/Glycine Transfer Buffer (1610771EDU; Biorad) with 20 % methanol. Following the transfer, membranes were rinsed in ddH_2O and stained with the Pierce Reversible Protein Stain Kit (24580; Thermo Fisher Scientific) to assess loading and transfer efficiency. Membranes were imaged using a ChemiDoc MP Imaging system, and the stain was removed using Pierce Stain Eraser. Subsequently, membranes were blocked with 5% skim milk made in tris-buffered saline (TBS) with 0.05% Tween-20 (0777; VWR) (TBS-T) before overnight incubation at 4°C in primary antibodies (1%

milk-TBS-T with sodium azide) targeting Sar1b (GTX109170; Genetex), pMTOR Ser2448 (2971; Cell Signaling), mTOR (2970; Cell Signaling), pAKT Ser473 (9271; Cell Signaling), AKT1 (05-591; Millipore), pP70S6K Thr389 (9234; Cell Signaling), P70S6K (2708; Cell Signaling), pS6 Ser240/244 (2215; Cell Signaling), S6 (2217; Cell Signaling), Cleaved Caspase-3 (9664; Cell Signaling), Phospho-p44/42 MAPK (Erk1/2) Thr202/Tyr204 (9101; Cell Signaling), ERK (9102; Cell Signaling), pGSK3β ser9 (9336; Cell Signaling), GSK3β (9318; Cell Signaling) Actin (1616; Santa Cruz), Ran GTPase (610341; BD Transduction Laboratories), GAPDH (5174; Cell Signaling), Caspase-3 (9662; Cell Signaling), or Myogenin (12732; Santa Cruz). Membranes were incubated with horseradish peroxidase (HRP)-tagged anti-mouse (1:1000-5000; 7076S, Cell Signaling), anti-rabbit (1:1000-5000; 7074S, Cell Signaling) secondary antibody diluted in 5% milk-TBS-T for 2 hours at room temperature. Proteins were visualized using Western Lightning Plus chemiluminescent substrate (NEL103E001EA; PerkinElmer) or Clarity™ Western Enhanced Chemiluminescence Substrate (1705060S; BioRad). To strip the protein from the blots prior to re-probing, membranes were incubated in 50 mL of 0.5M Tris-HCl/SDS buffer supplemented with 250µ β-mercaptoethanol (6010; OmniPur®) for 1 hour at 50°C.

2.3.3 Densitometry

Densitometric analysis was performed using Image lab software v6.1 (Bio-Rad). Protein content in arbitrary units was calculated by measuring the relative integrated density of the target protein stain normalized to the total protein density of the appropriate MemCode-stained blot. MemCode stain allows for the visualization of proteins and the efficiency of transfer to the nitrocellulose membrane and serves as a normalization tool and confirmation of equal protein loading.

2.4 Quantitative polymerase chain reaction (qPCR)

2.4.1 RNA extraction

RNA was extracted from cell pellets using two methods. For the phenol-chloroform method using RiboZol RNA extraction reagent (VWR), cell pellets were resuspended in 1mL of RiboZol (VWRVN580; VWR) in RNase/DNase free tubes. Samples were sonicated for 30s, before 350µL of chloroform (613312; Sigma Aldrich) was added. Samples were inverted by hand 5-10x, and incubated at room temperature for 3min until two separate layers were indistinguishable. Samples were centrifuged at 12,000g for 20min at 4ºC to separate phases. The upper, colourless aqueous phase was transferred to a fresh RNase/DNase-free tube, while the lower phenol-red organic and

interphases were discarded. This was followed by a second extraction with an additional 100µL of chloroform added to the upper phase. Samples were again inverted and incubated at room temperature before another centrifugation at 12,000g for 20min at 4ºC. Again, the upper phase was transferred to a fresh RNase/DNase-free tube, and the lower phenol-red organic and interphases were discarded. Ice-cold 100% isopropanol (500µL; Sigma-Aldrich) was added to the aqueous phase, and the tubes were inverted by hand before incubation at room temperature for 10 min. Samples were centrifuged at 12,000g for 20 min at 4ºC to pellet the RNA. The supernatant was discarded, and the RNA pellet was then rinsed and resuspended in 1mL ice-cold 75% ethanol prepared in nuclease-free water (10977-015; Life Technologies). Samples were briefly vortexed and then centrifuged at 7500g for 5min at 4ºC. The ethanol wash was discarded, and the RNA pellet was left to air dry for 30 min. The RNA pellet was re-suspended in 20-50 µL of nuclease-free water. Samples were briefly vortex and spun, and RNA was quantified using the BioTek Synergy H4 and Take3 plate by reading absorbance at 260nM.

Conversely, RNA was isolated from other cell culture pellets using The Extracta Plus RNA kit (95214; QuantaBio). Briefly, cell pellets were resuspended in 350µL of buffer EPRL supplemented with β-mercaptoethanol, pipetting vigorously to homogenize pellets. The samples were then transferred to Extracta Plus DNA Removal Columns and centrifuged at 8000g for 30s. 300µL of 70% ethanol was added to the flow through, which was subsequently transferred to Extracta Plus RNA Spin Columns and centrifuged at 8000g for 15s. Flow through was discarded, and 700µL of Buffer EPRW1 was added, and the samples were centrifuged at 8000g for 15s. This was followed by adding 500µL of EPRW2 and additional centrifugation at 8000g for 15s, after which flow through was discarded, 500µL of buffer EPRW2 was added, and the samples were centrifuged at 8000g for 2min. Finally, the spin columns were transferred to fresh collection tubes and centrifuged at 8000g for 1min. Spin columns were then transferred to 1.5 ml collection tubes, and 30µL of RNAse-free water was added to the spin column. Samples were centrifuged at 8000g for 1min to elute RNA. RNA was quantified using the BioTek Synergy H4 and Take3 plate by reading absorbance at 260nM.

2.4.2 Complementary DNA (cDNA) synthesis

cDNA was synthesized for each sample by loading the volume equivalency of 500ng RNA template, 2µL of 5X qScript cDNA supermix (95048; Quantabio) and RNAse-free water up to a total volume of 10µL into RNase/DNase-free strip-tubes. The reaction was briefly vortexed and

centrifuged prior to incubation at 25ºC for 5 min, 42ºC for 30 min, 85ºC for 5 min and then held at 4ºC using a Master cycler Nexus Gradient Thermocycler (Eppendorf). cDNA was stored at -80°C until needed.

2.4.3 Primer-pair validation and development of standard curves

Primer pairs (Invitrogen; Sequences listed in table 2.3) were designed using the NCBI primer designing tool and predicted primer products were cross-referenced with NCBI's Basic Local Alignment Search Tool (BLAST) to ensure target gene sequence specificity. Primer-pair PCR product size was validated, and primers were investigated for dimerization using an automated QIAxcel Advanced microcapillary electrophoresis system. For each primer-pair, a reaction master mix was prepared, containing 25µL AccuStart II GelTrack PCR SuperMix (2X; 95136; Quanta Biosciences™), 2.5µL 10µM forward primer, 2.5µL 10µM reverse primer, and 15µL nuclease-free water, to which 5µL of the appropriate cDNA was added. The reaction mix was briefly vortexed and centrifuged prior to incubation at 94ºC for 1min, 10 cycles of incubation at 94ºC for 30s, 65ºC for 30s and 72ºC for 40s, 25 cycles of incubation at 94ºC for 30s, 55ºC for 30s and 72ºC for 40s, incubation at 72ºC for 4min and then held at 4ºC. Primers were then quantified by QIAxcel (DNA High Resolution) microcapillary electrophoresis in accordance with the manufacturer's guidelines. PCR product sample mixtures were diluted 1 in 5 in sample buffer, loading 10µL into the QIAxcel, alongside a 100bp ladder (239035; Qiagen). After validation that the correct amplicon size was generated for each primer pair, PCR products were column purified by MinElute PCR Purification Kit (28004; Qiagen). The resulting cDNA product was eluted in 20µL of nuclease-free water, and amplicon amount was determined using Synergy H4 Take3, nucleic acid quantification.

The total copy number (molecules) was calculated using the quantified amplicon amount (ng) and dsDNA amplicon length (base pairs), calculated on http://cels.uri.edu/gsc/cndna.html, using the following formula:

$$\boldsymbol{number\ of\ copies} = (\boldsymbol{amount} * \boldsymbol{6.022x1023})(\boldsymbol{length} * \boldsymbol{1x109} * \boldsymbol{650}).$$

After the copy number was determined, 8-point standard curves were subsequently created by serial-diluting the PCR product in RNAse-free water from $1x10^8$ to $1x10^2$ copies/µL, with nuclease-free water (a no-template control (NTC)) serving as the 8^{th} point of the standard curve.

2.4.4 Applied Biosystems qPCR

qPCR reactions were conducted in 96-well plates on a ViiA7 Real-time PCR machine (Thermo Fisher Scientific). Each well contained 2µL standard curve or cDNA template diluted 1:3-

5, 5µL of Perfecta SYBR green Supermix Low ROX supermix (95053; Quantabio), 0.25 µl of each forward and reverse primer and 2.5µL of nuclease-free water in a total of 10 µl per reaction mixture. The qPCR plate was centrifuged at 300 g for 1min prior to incubating the reaction mix at 95ºC for 20s followed by 32 cycles for 1s at 95ºC, 20s at 60ºC, and for 5min at 20ºC. Data were normalized to the geometric mean of two reference genes and quantified by the 2- ΔΔCt method.

Table 2.2.3: Sequences of mouse and rat primers.

Primer	Primer Sequence (5'-3')
Mouse-Sar1b F	TGCCGGGAAAACAACTTTGC
Mouse-Sar1b R	AAGTGGGATGTAGCGTTGGG
Mouse-Sar1a F	CTGGTCTGTGTGGTGCTCTGAGG
Mouse-Sar1a R	ATTGATGCTTACAACGGC CC
Mouse-RER1 F	GCCTTGGGAATTTACCACCT
Mouse-RER1 R	CTTCGAATGAAGGGACGAAA
Mouse-Rpl7 F	ACGGTGGAGCCTTATGTGAC
Mouse-Rpl7 R	ACGGTGGAGCCTTATGTGAC
Rat-Sar1b F	GTGTTCATGTGCAGTGTGCT
Rat-Sar1b R	CTAGTCGATGTACTGCGCCAT
Rat-GAPDH F	GGCCGAGGGCCCACTA
Rat-GAPDH R	TGTTGAAGTCACAGGAGACAACCT
Rat-HPRT1 F	CCCAGCGTCGTGATTAGTGATG
Rat-HPRT1 R	TTCAGTCCTGTCCATAATCAGTC

2.5 Immunofluorescence microscopy experiments

C2C12 cells were plated at $1.5x10^5$ on glass coverslips in 35mm dishes, grown to 80% confluency prior and differentiated for 48 h, as described in section 2.1, and siRNA transfected for 48h as described in section 2.2. After 48h transfection, cells were washed in warm PBS before being fixed in pre-warmed 4% paraformaldehyde in PBS (PFA; PX005503; Millipore) for 15 min. Following fixation, cells were washed 2x in PBS. Cells were then permeabilized in 0.1% Triton-X-100 for 15 min, and subsequently blocked with 3% BSA in PBS for 45 min. Following blocking and permeabilization, cells were washed 3X in PBS and then incubated in AlexaFluor 488 Phalloidin stain (A12379; Thermo Fisher) diluted 1:1000 in 1X PBS (Corning; MT21040) for 30 min protected

from light. Phalloidin staining was followed by 1h incubation with primary antibodies against SAR1B (GTX109170; Genetex, 22292-1-AP; ProteinTech) and 2 h incubation with fluorophore-conjugated secondary antibody Alexa Fluor 594 goat-anti-rabbit (2534079; Thermo Fisher). Cells were washed 2X in PBS again and then counterstained with Hoescht 33342, made to a final concentration of 2µg/mL in PBS. Cells were incubated in Hoechst for 3min, protected from light, after which Hoechst was discarded, and coverslips were rinsed 2X in PBS. Coverslips were mounted onto glass slides using ProLong Gold Antifade Reagent (P36391; ThermoFisher). Coverslips were allowed to harden for 48h prior to imaging slides on Zeiss LSM 900 with Airyscan 2 detector.

2.6 Statistical analysis

Statistical analyses were performed in Graph Pad Prism 9. Data sets with three or more groups were analyzed using one-way or two-way analysis of variance (ANOVA). Significant differences between individual groups were assessed with Tukey's post-hoc test. A pairwise comparison between data sets with two groups was performed using a two-tailed Student's t-test. P-values less than 0.05 were considered statistically significant. Unless otherwise indicated, data are presented with a standard error of the mean (±SEM).

Chapter 3: Results

3.1 8 and 13 weeks of high-fat high-sucrose diet feeding reduces Sar1b protein content in murine gastrocnemius tissue

Sar1b protein content is the highest in skeletal muscle compared to other tissues[100]. To examine if Sar1b is nutritionally regulated in the skeletal muscle, we examined whether nutrient overload could modulate skeletal muscle Sar1b levels in a model of DIO. Male C57BL/6J mice were fed HFHS or chow diet, and gastrocnemius, soleus, tibialis, and EDL were collected at 4, 8, and 13 weeks after feeding, and Sar1b protein content was determined (Figure 3.1. A). Sar1b protein level was unchanged after four weeks of HFHS feeding and was reduced in the gastrocnemius muscle after 8 and 13 weeks of HFHS feeding when compared to chow-fed animals (Figure 3.1. B-C). Further, Sar1b protein quantity was significantly lower after 13 weeks of chow-feeding compared to animals fed chow for 4 weeks. Interestingly, Sar1b protein content was not significantly altered in the tibialis and EDL after 13 weeks of HFHS feeding (Figure 3.2. A-C). The gastrocnemius and tibialis are mixed glycolytic/oxidative tissues, while the EDL is glycolytic. Decreased Sar1b protein level, specifically in the gastrocnemius tissue, indicates a plausible depot-specific regulation of Sar1b under nutrient overload. Published data from our lab show that after 13 weeks of HFHS feeding, serum BCKA levels were upregulated and that 13 weeks of HFHS feeding down-regulated enzymes involved in BCAA catabolism[93]. Strikingly, Sar1b protein quantity was decreased at 13 weeks when serum BCKA levels were upregulated, raising the question of whether changes in Sar1b levels occur in response to increased intramyocellular BCKA content.

We also examined whether the impact of chronic alterations in nutrient content on Sar1b protein quantity in the skeletal muscle is distinct from short-term changes in nutrient intake or starvation (fasting). Our prior data showed that serum BCKA levels significantly increased in fasted mice and normalized following refeeding[93]. Given that HFHS-feeding (nutrient overload), reduced Sar1b protein quantity in the gastrocnemius with concomitant increases in BCKA levels, we hypothesized that fasting (nutrient insufficiency) might alter Sar1b content in the skeletal muscle. C57BL6 mice were divided into three groups; fed ad libitum (fed), fasted 16hr (fasted) or fasted 16hr and refed 4hr (refed) prior to collecting tissues to analyze Sar1b protein quantity (Figure 3.3. A). Notably, Sar1b protein quantity in the gastrocnemius muscle remained unchanged between randomly fed, fasted, and refed mice (Figure 3.3 B-C), suggesting that Sar1b protein quantity is differentially regulated between physiological and pathological changes in nutrient content.

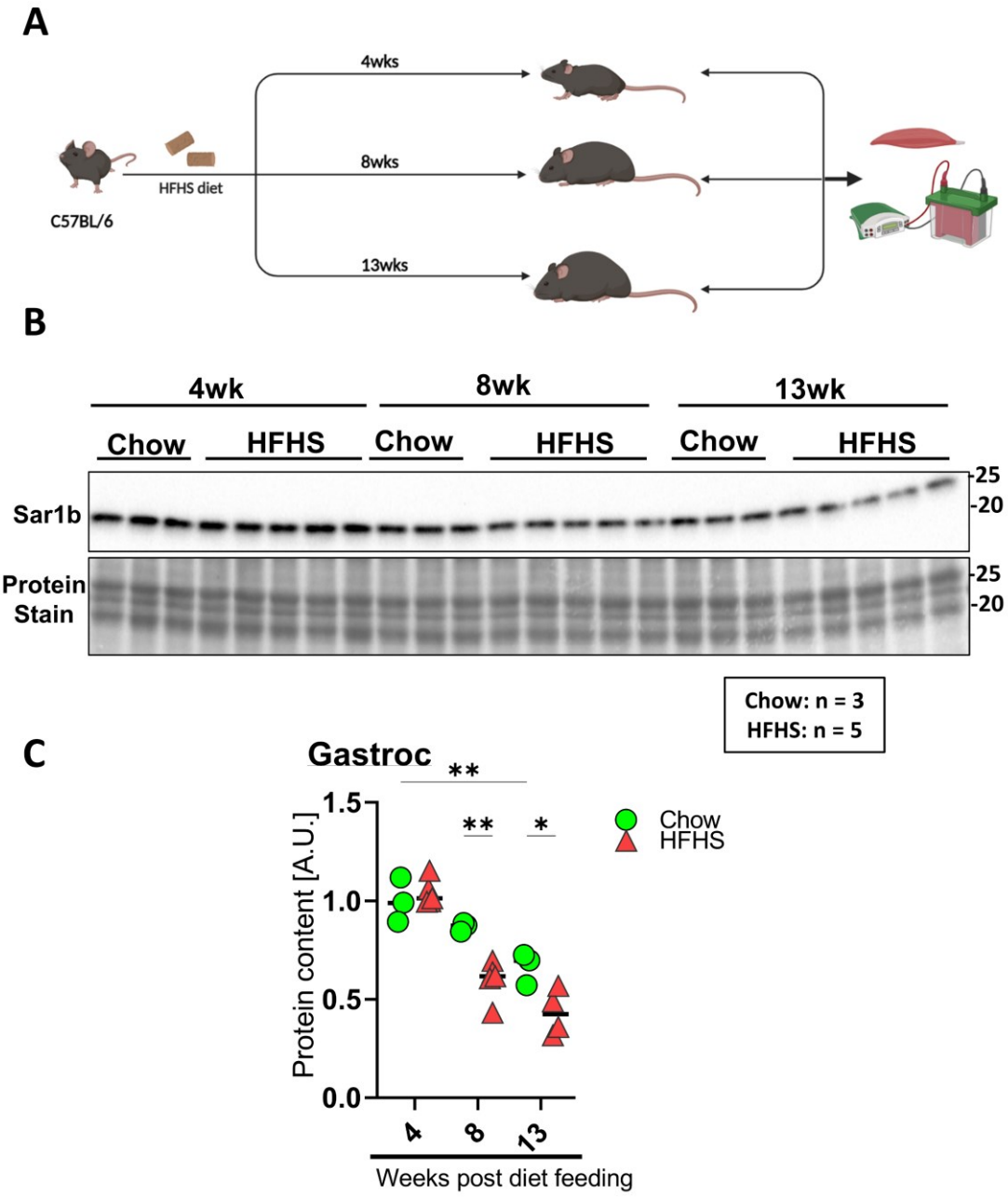

Figure 3.1: Sar1b protein content is decreased in the gastrocnemius muscle of C57BL6J mice at 8- and 13-weeks post HFHS-diet feeding.

(A) study design of HFHS (45% KCAL from fat) diet feeding of C57BL/6Jmice at 4, 8, and 13 weeks. (B-C) Immunoblot and densitometric analysis of Sar1b protein expression in gastrocnemius muscle of mice fed HFHS and chow diet, Graph represents mean ± S.E.M., statistical analysis is performed using two-way ANOVA with Tukey's multiple comparison tests *P<0.05, **P<0.01; AU; Arbitrary Unit. Note: all all the presented lanes are from the same membranes.

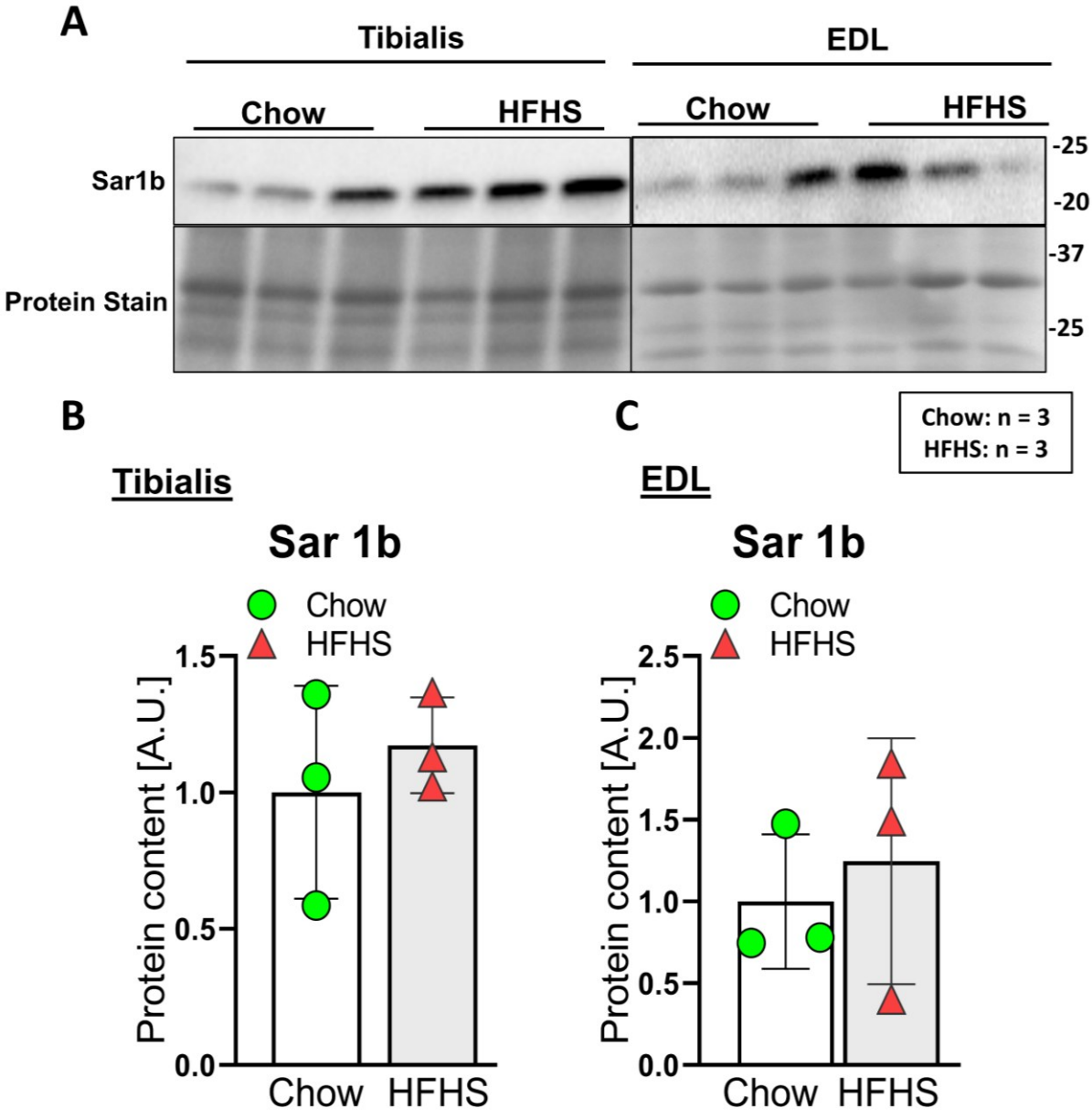

Figure 3.2: Sar1b protein content remains unchanged in tibialis and EDL after 13 weeks of HFHS feeding.

(A-C) Immunoblot and densitometric analysis of Sar1b expression in tibialis and EDL muscle of mice fed HFHS and chow diet. Graph represents mean ± S.E.M., statistical analysis was performed using students T-test, AU, Arbitrary Unit. Note: all the presented lanes are from the same membranes. Non-adjacent lanes from the same membranes are separated by black line between the lanes.

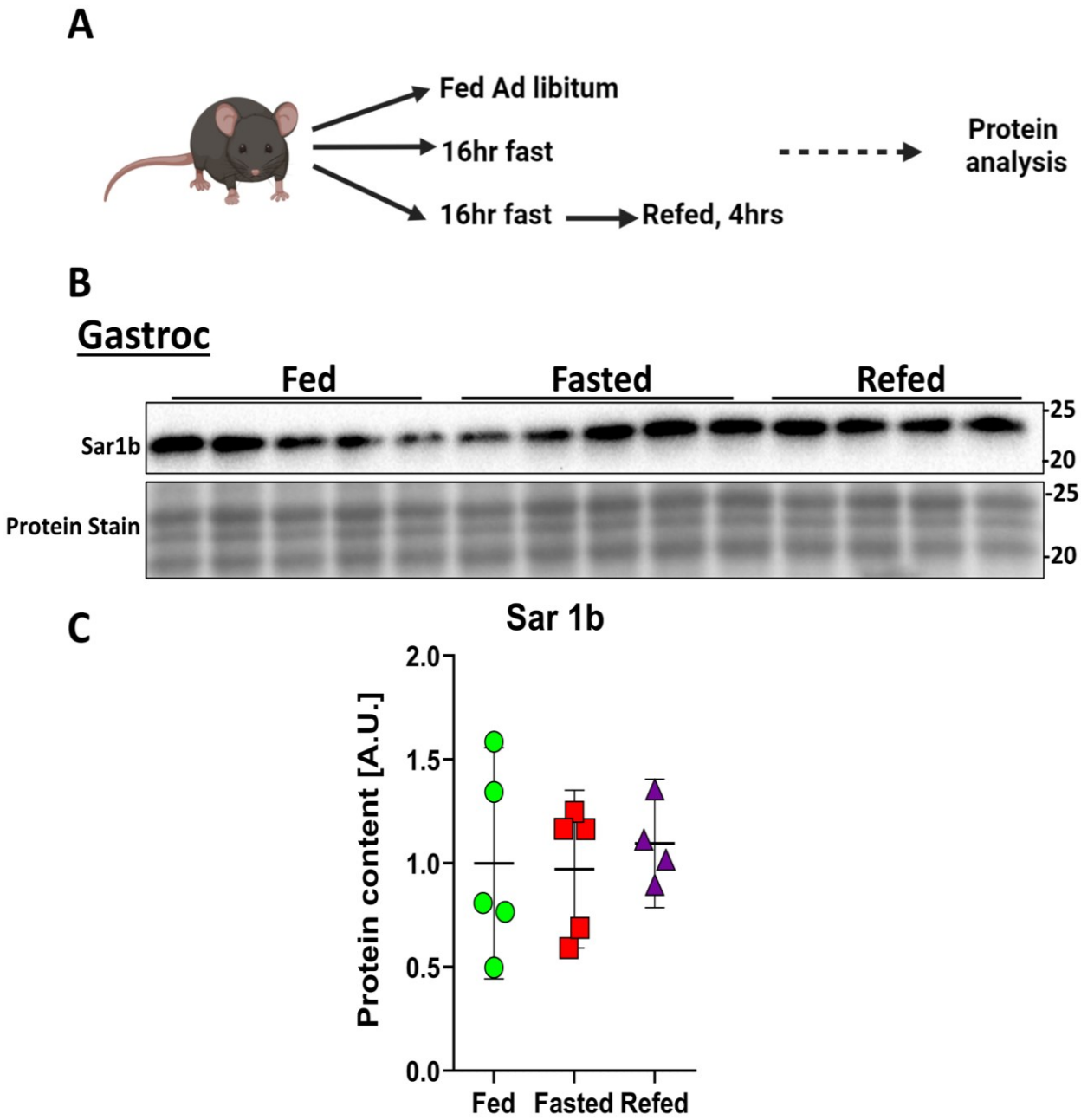

Figure 3.3: Sar1b protein content in the gastrocnemius tissue is unaffected after fasting. (A) Study design outlining feeding, fasting, or fasting and refeeding of C57BL6 mice. (B-C) Immunoblot and densitometric analysis of Sar1b expression in gastrocnemius muscle following feeding, fasting, or fasting and refeeding. Graph represents mean ± S.E.M., statistical analyses were performed using one-way ANOVA with Tukey's multiple comparison tests, N =5 each group, AU; Arbitrary Unit. Note: all the presented lanes are from the same membranes.

3.2 Sar1b protein quantity remains unchanged during the process of myoblast to myotube differentiation

A functional readout of muscle function is its ability to differentiate, a trait which requires metabolic and signaling inputs[120]. We next ascertained if changes in Sar1b corresponded with C2C12 cell differentiation. C2C12 myotubes were grown to 80% confluency prior to the initiation of myotube differentiation by incubating cells in 0.2% FBS. Cells were imaged and collected at eight time points throughout the differentiation process, and myogenin and Sar1b protein quantity was examined (Figure 3.4. A-C). The MyoD family of muscle-specific transcription factors, including MyoD and myogenin[121], regulates skeletal muscle differentiation. Myogenin is essential for myotube formation and is a marker for the progression of differentiation, alongside morphological changes, and the formation of elongated fibre-shaped myotubes from spindle-shaped myoblasts[120,121]. The C2C12 cells morphologically took on the elongated shape of myotubes throughout the 72 hours (Figure 3.4. A), and myogenin content was significantly increased after 24-72 hours of differentiation (Figure 3.4. B). Sar1b protein quantity was unchanged throughout the differentiation process (Figure 3.4. C). Therefore, at the protein level, Sar1b content is not regulated by muscle differentiation, suggesting that in C2C12 cells, any observed metabolic or signaling changes will be independent of the differentiation process.

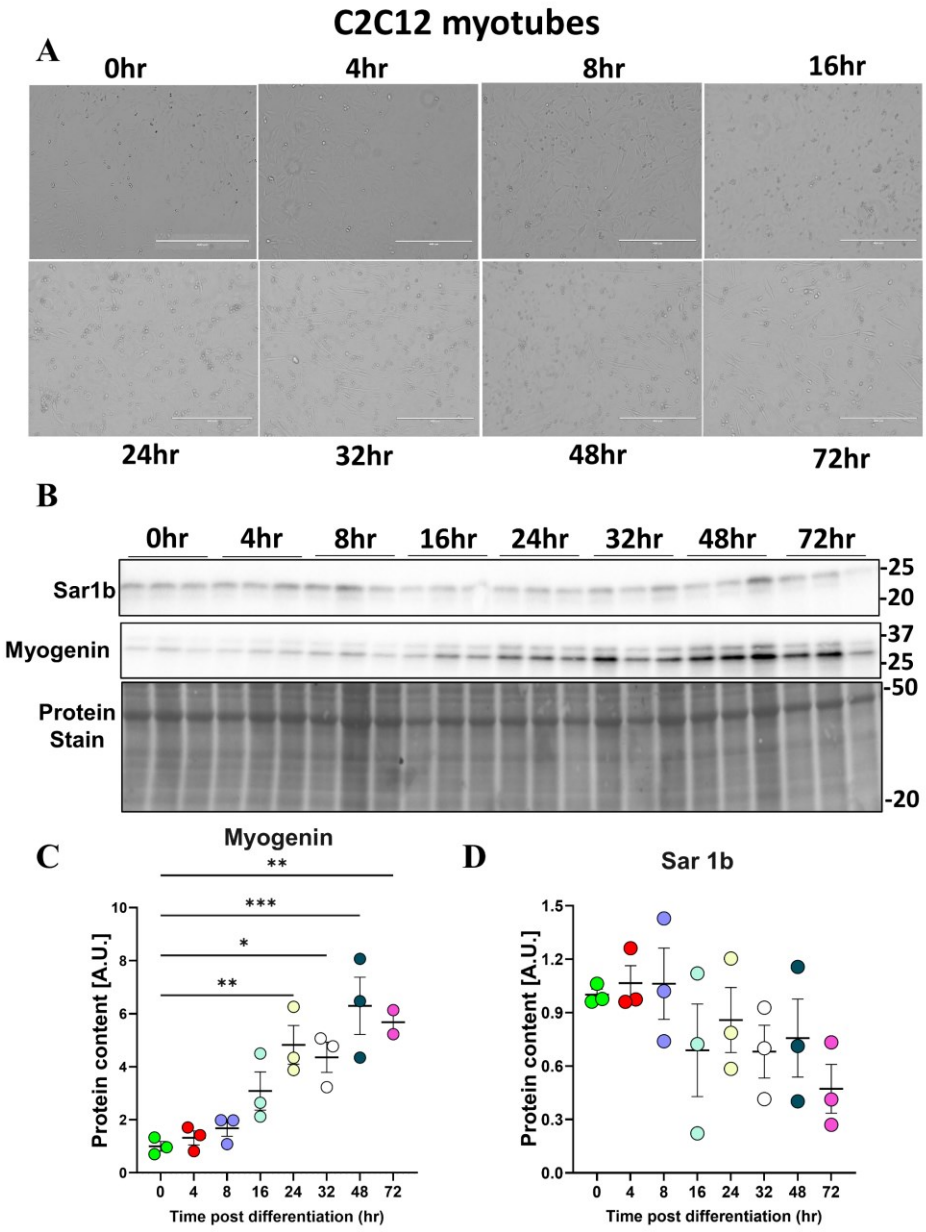

Figure 3.4: Sar1b protein content remains unchanged during C2C12 differentiation.

C2C12 cells were grown to 80% confluency prior to the initiation of myotube differentiation. (A) C2C12 myotubes were visualized at 10X magnification and harvested after 0, 4, 8, 16, 24, 32, 48 and 72hr of differentiation. (B) Immunoblot and (C, D) densitometric analyses were performed to examine protein levels of muscle differentiation marker myogenin (C) and Sar1b (D). Graph represents mean ± S.E.M., **P<0.01, ***P<0.005, one-way ANOVA with Dunnett's multiple comparisons, n = 3, A.U.; arbitrary unit. Note: All the presented lanes are from the same membranes, experiment was repeated twice.

3.3 BCKA and Palmitate treatment alone does not change Sar1b protein quantity in C2C12 myotubes

Since Sar1b protein levels were decreased after 8 weeks of DIO, we sought to investigate whether in vitro exposure to fatty acids or elevated BCKAs altered Sar1b protein quantity in C2C12 cells. To simulate the gradual increase in FAs observed during HFHS feeding, C2C12 cells were treated with low (0.2mM), intermediate (0.4mM) and high (0.8mM) palmitate for 16h, or 2% BSA as a control (Figure 3.5. A-C). High palmitate treatment significantly decreased AKT1 phosphorylation at ser473, consistent with palmitate's effect on downregulating insulin signaling proteins[93] (Figure 3.5. C). However, palmitate treatment did not alter Sar1b protein quantity, suggesting that palmitate alone was not enough to mimic the observed impact of DIO on decreasing Sar1b protein quantity in the gastrocnemius tissue (Figure 3.5. B).

Given that serum BCKA levels were elevated in vivo when Sar1b protein quantity was decreased after HFHS feeding, we postulated that exogenous BCKA treatment might significantly alter Sar1b protein quantity in C2C12 cells. C2C12 myotubes were incubated with 0.05 mM of individual BCKA (KIC, KIV and KMV) for 30min (Figure 3.6. A-C). Sar1b protein quantity remained unchanged after 30 min of treatment with individual BCKA's compared to the VEH group (Figure 3.6. A-B). Consistent with previous findings[93], KIC and KMV but not KIV treatment increased phosphorylation of S6K1 at threonine-389 (Figure 3.6. C). Thus, palmitate and BCKA exposure alone did not alter Sar1b myotube protein content. Therefore, decreases observed in Sar1b protein during DIO could be related to its synthesis or degradation (turnover) or secondary to changes in ER/Golgi function and merits investigation. Moreover, we did not superimpose hyperglycemia in the palmitate or BCKA treatment groups, the impact of which cannot be dismissed in vivo.

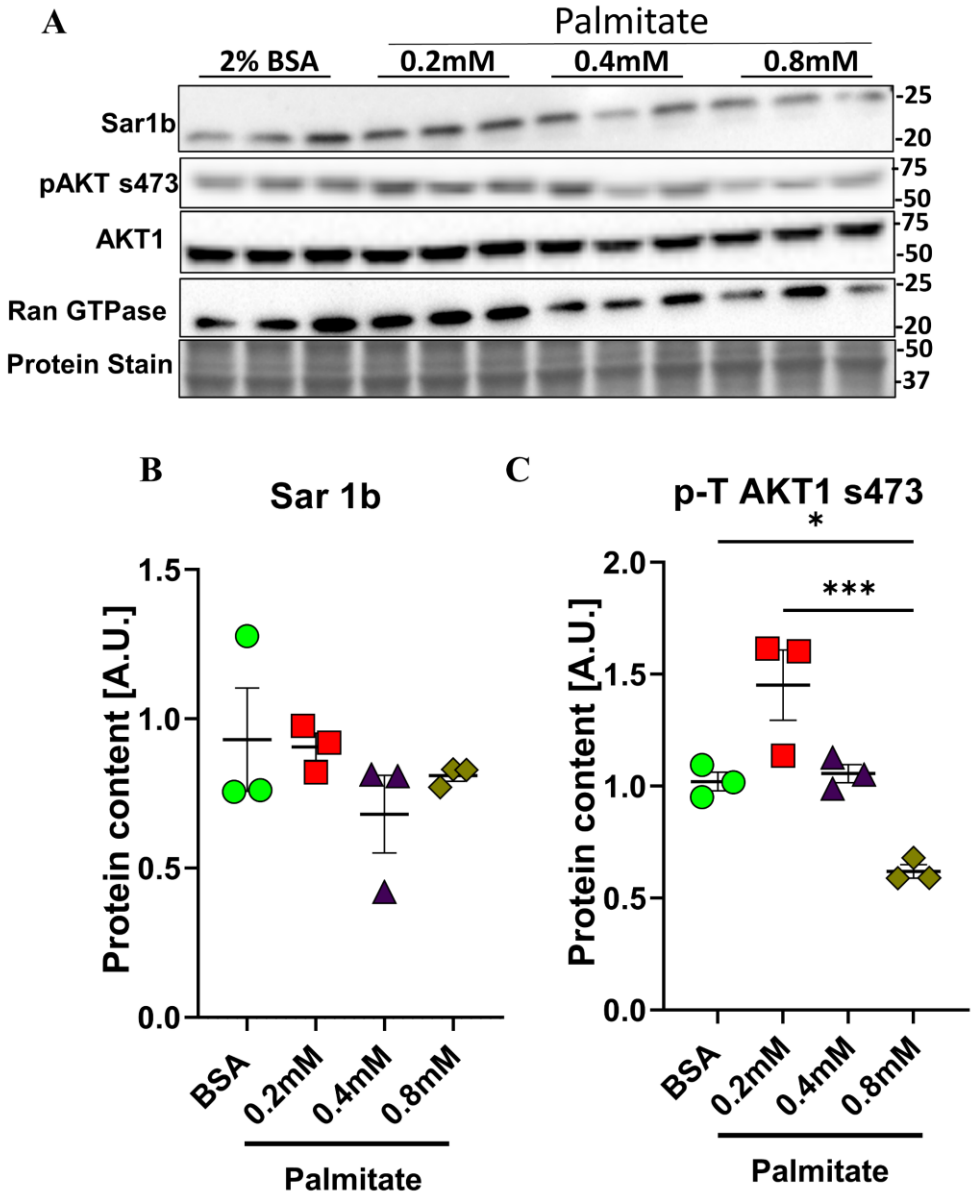

Figure 3.5: Sar1b protein content is unchanged by palmitate treatment in C2C12 cells.

C2C12 cells were incubated with (A-C) palmitate (0.2, 0.4 or 0.8mM) or 2% BSA for 16h. (A) Immunoblot and (B, C) densitometric analysis of proteins (A-C) Sar1b and phosphorylated and total AKT1 at ser473 normalized to protein stain. Ran GTPase served as a loading control. Graphs represent mean ± S.E.M., statistical analysis were performed using one-way ANOVA with Tukey's multiple comparisons test, *P<0.05, and ***P<0.001, n =3, AU; Arbitrary Unit. Note: all the presented lanes are from the same membrane. Experiments were repeated three times.

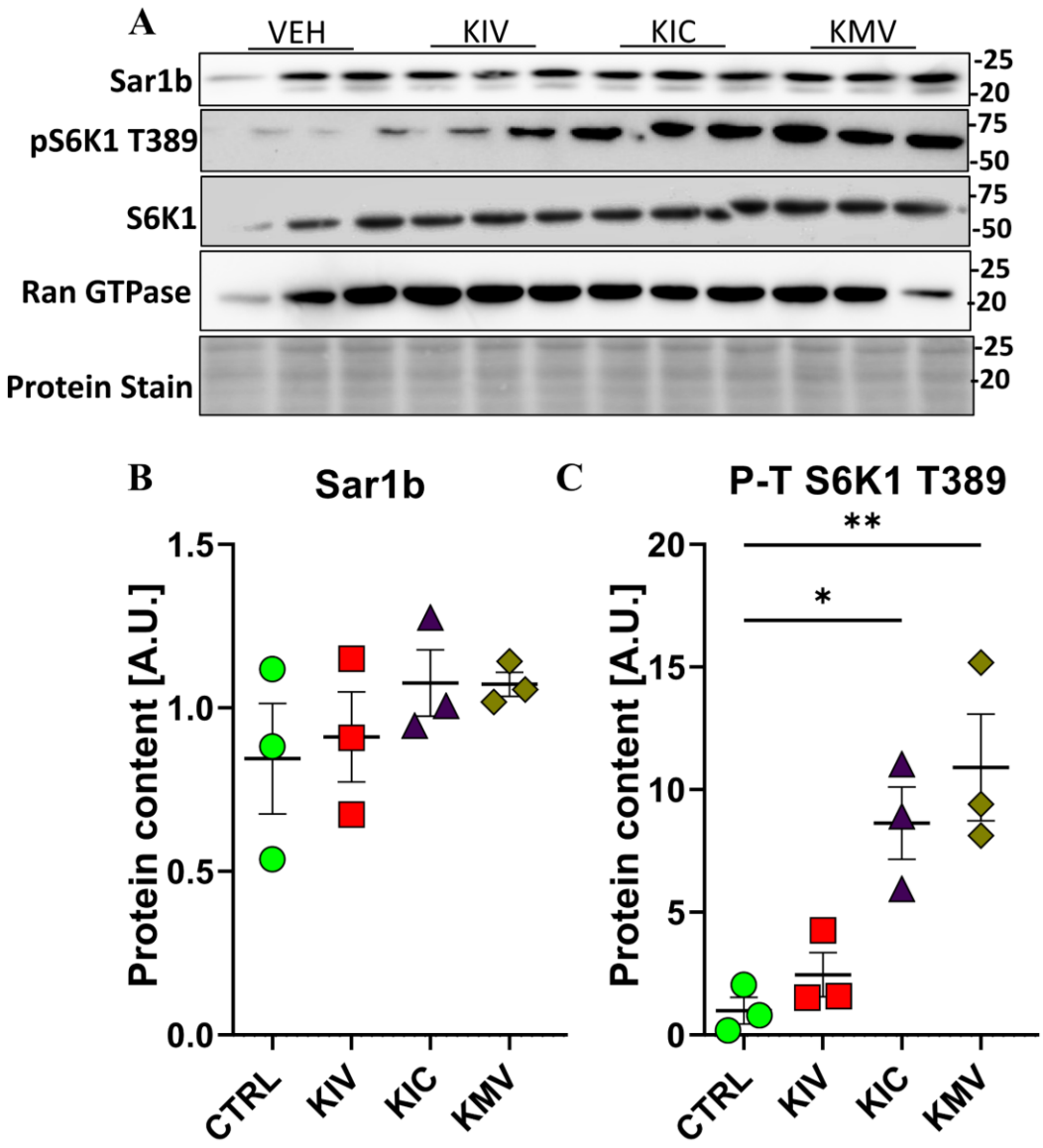

Figure 3.6: Sar1b protein content is unchanged by exogenous BCKA treatment in C2C12 myotubes.

C2C12 cells were incubated with (A-C) 0.05mM individual BCKAs (KIV, KIC and KMV) or vehicle (VEH) for 30min prior to cell harvest. (A) Immunoblot and (B, C) densitometric analysis were performed to examine the protein levels of Sar1b, phosphorylated-S6K1 T389 and total S6K1 normalized to protein stain. Ran GTPase was used as a loading control. Graph represents mean ± S.E.M., statistical analyses were performed using one-way ANOVA with Tukey's multiple comparisons test, *P<0.05, **P<0.01, ***P<0.001, n =3, AU; Arbitrary Unit. Note: all the presented lanes are from the same membranes. Experiments were repeated twice.

3.4 Validation of small interfering RNA targeting exons 4-6 of Sar1b in H9C2 and C2C12 cells

Sar1b protein quantity is decreased in the gastrocnemius muscle during DIO (Figure 3.1) with concomitant impairment of insulin action and hyperactivated mTORC1 signaling[93]. We questioned whether a decrease in Sar1bcontent was protective or detrimental during DIO and drove changes in insulin action and mTOR signaling. To simulate the loss of Sar1b action, we silenced Sar1b in C2C12 and H9C2 cells using siRNA and examined changes in insulin and mTOR signaling.

Differentiated H9C2 cells were transfected 48h with either rat-si-Sar1b#1 targeting exon 2-3 and rat-si-Sar1b#2 targeting exon 5-6 at a concentration of 10nM, with 4uL of lipofectamine RNAimax (Figure 3.7. A-C). Rat-specific siRNA, ra-si-Sar1b#1 targeting Sar1b decreased Sar1b mRNA expression by 70% and by 65% using ra-si-Sar1b#2 compared to scrambled control siRNA (Figure 3.7. A). Correspondingly, Sar1b protein content was decreased by ~ 65% using both rat siRNAs targeting Sar1b (Figure 3.7. B-C).

Differentiated C2C12 cells were transfected with 10nM mouse specific-siSar1b#1 targeting exon 6 and mo-siSar1b#2 targeting exon 5 using 4uL of lipofectamine. Mo-siSar1b#1 and #2 reduced Sar1b protein quantity by 90% and mRNA expression by 85-90% (Figure 3.8. A-C). We also validated a third mouse-specific siRNA, mo-siSar1b#3: targeting exons 4 and 5. Transfection with 15nM siSar1b#3 decreased Sar1b protein quantity by ~50% and mRNA expression by 90% (Figure 3.8 D-F). In my thesis, I successfully validated three distinct siRNA targeting Sar1b in two cell lines.

Sar1b is one of the two mammalian paralogues of the Sar1 gene, including Sar1a[104]. To ensure that siRNA knockdown approaches were specific to Sar1b, we examined Sar1a protein and gene expression in cells 48hr post-Sar1b siRNA transfection (Figure 3.9). In C2C12 cells, the Sar1a gene and protein quantity was unaltered by treatment with 10nM mo-siRNA#1 or #2, highlighting the specificity and effects of Sar1b siRNAs, which are independent of Sar1a.

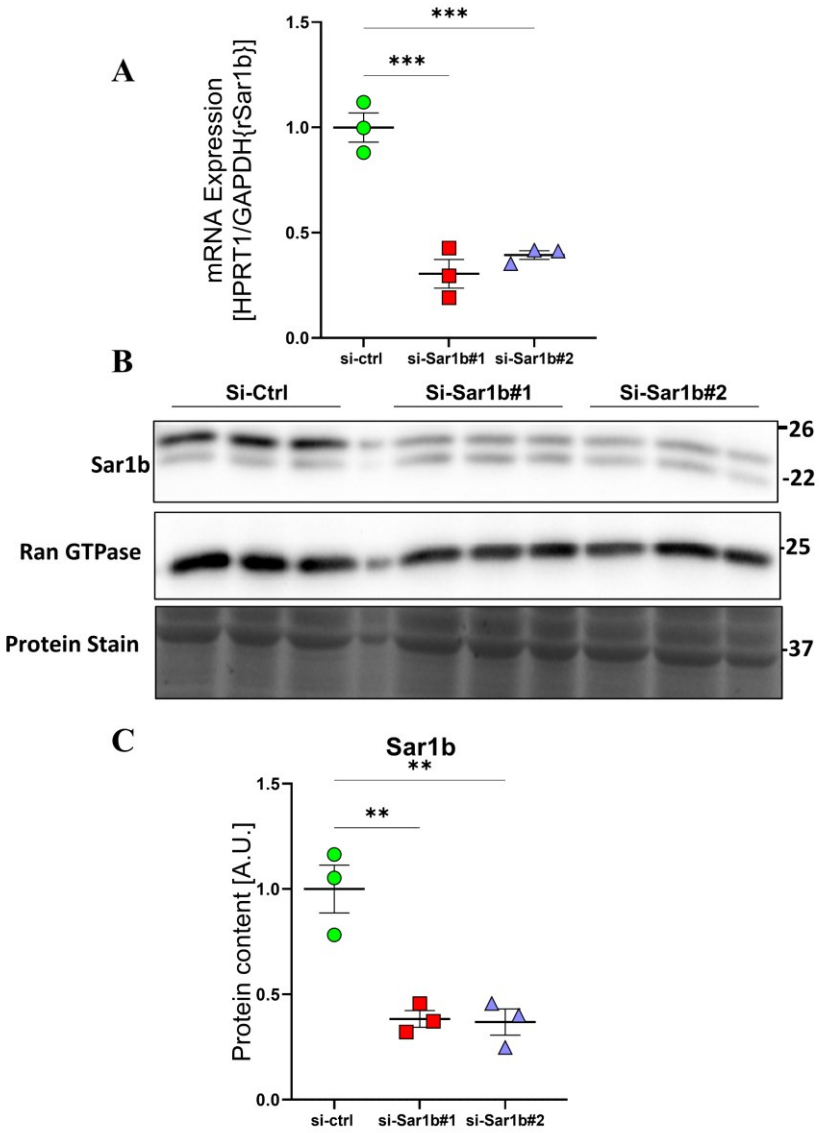

Figure 3.7: Rat-specific small interfering (si)-RNA silencing of Sar1b in H9C2 rat cardiomyoblast

Differentiated H9C2 cells were transfected 48h with either rat-si-Sar1b#1 targeting exon 2-3 and rat-si-Sar1b#2 targeting exon 5-6 at a concentration of 10nM. (A) Sar1b mRNA expression in H9C2 cells. Data quantification by normalizing to GAPDH/HPRT1 reference genes. (B-C) Immunoblot and densitometric analyses of Sar1b protein. Data normalized to protein stain. RAN GTPase served as the loading control. Graph represents mean ± S.E.M.; statistical analyses was performed using one-way ANOVA with Tukey's multiple comparisons, n = 3, A.U.; arbitrary unit. **P<0.01, ***P<0.001. All presented lanes are from the same membranes. Experiments were repeated three times

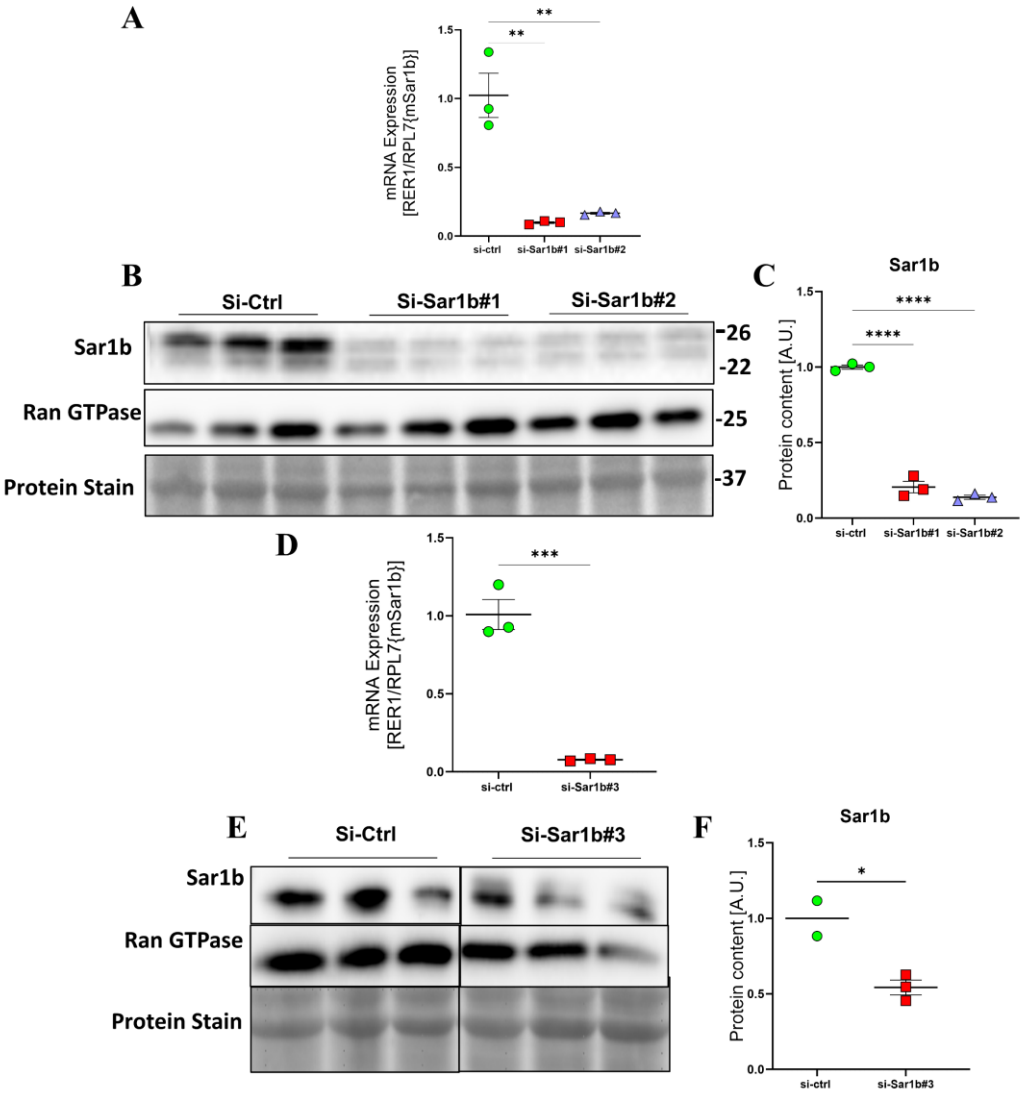
A
**
**
mRNA Expression
[RER1/RPL7(mSar1b)]
1.5
1.0
0.5
0.0
si-ctrl
si-Sar1b#1
si-Sar1b#2
B
Si-Ctrl
Si-Sar1b#1
Si-Sar1b#2
Sar1b
Ran GTPase
Protein Stain
-26
-22
-25
-37
C
Sar1b
****
****
Protein content [A.U.]
1.5
1.0
0.5
0.0
si-ctrl
si-Sar1b#1
si-Sar1b#2
D
***
mRNA Expression
[RER1/RPL7(mSar1b)]
1.5
1.0
0.5
0.0
si-ctrl
si-Sar1b#3
E
Si-Ctrl
Si-Sar1b#3
Sar1b
Ran GTPase
Protein Stain
F
Sar1b
*
Protein content [A.U.]
1.5
1.0
0.5
0.0
si-ctrl
si-Sar1b#3

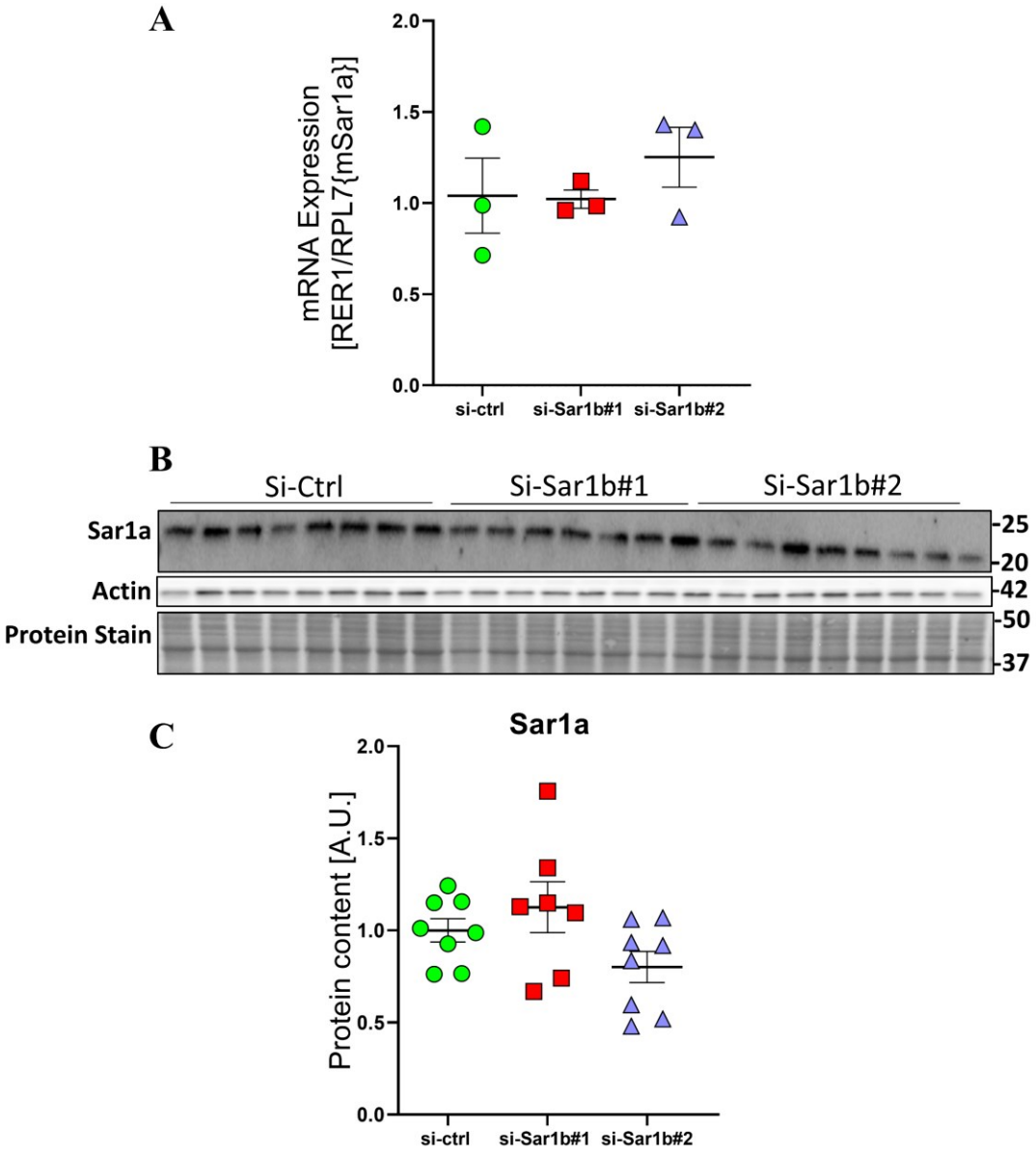

Figure 3.9: Sar1b silencing does not change Sar 1a gene and protein content.

Differentiated C2C12 myotubes were transfected for 48h with mo-siSAR1B#1 targeting exon 6 and mo-siSAR1B#2 targeting exon 5. Cells were transfected 48h prior to harvest. (A) Sar1a mRNA expression in C2C12 cells. Data quantification by normalizing to RER1 and Rpl7 reference genes. (B-C) Immunoblot and densitometric analyses of Sar1a protein. Actin served as the loading control. Graph represents mean ± S.E.M., statistical analyses were performed using one-way ANOVA with Tukey's multiple comparisons test, $p<0.05$. n =3, AU; Arbitrary Unit. Note: all the presented lanes are from the same membranes.

3.5 Unsuccessful screening of commercial antibodies to detect Sar1b in protein in C2C12 cells

We next employed immunofluorescence imaging as a tertiary method to confirm Sar1b knockdown and localization in C2C12 cells. After 48hr siRNA transfection with si-ctrl, si-sar1b#1 and si-sar1b#2, C2C12 cells were fixed with 4% PFA and permeabilized prior to staining with Alexa Fluor 488 Phalloidin stain and incubated with primary antibodies against Sar1b. The Zeiss LSM Airyscan super-resolution microscope was used to visualize Sar1b in cells incubated with fluorophore-conjugated secondary antibody Alexa Fluor 594 goat-anti-rabbit before (Figure 3.10). Unfortunately, none of the employed antibodies changed Alexa Fluor 594 fluorescence signal between the cells treated with si-ctrl or si-Sar1b, indicating that the commercial antibodies could not detect Sar1b (Figure 3.10). Due to time and reagent constraints, we did not pursue further validation of antibodies specific to detecting Sar1b.

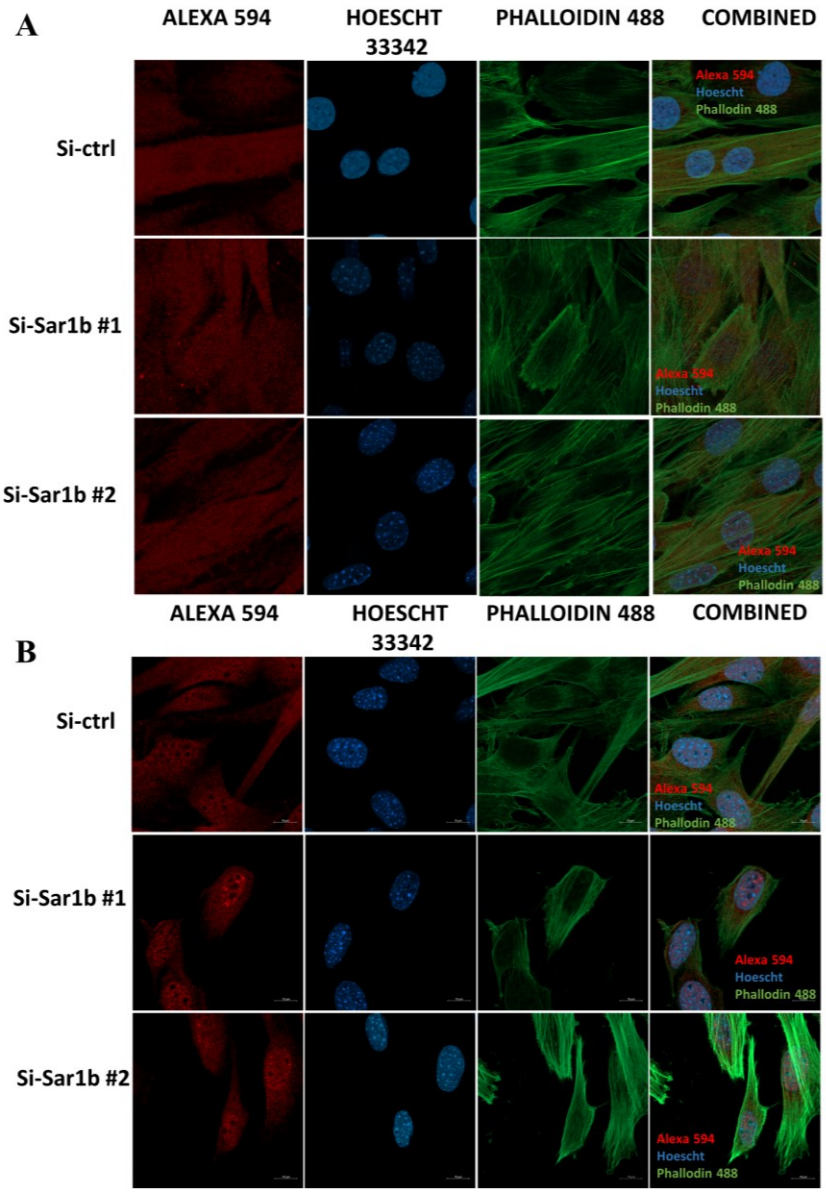

Figure 3.10: Unsuccessful screening of commercial antibodies to detect Sar1b in C2C12 myotubes.

(A-B) Differentiated C2C12 myotubes were transfected for 48h with mo-siSar1b#1 targeting exon 6 and mo-siSar1b#2 targeting exon 5 at a concentration of 10nM with 4uL of lipofectamine. After 48h, cells fixed in 4% formaldehyde in PBS (PFA) for 15 min and then then stained with Alexa Fluor 488 Phalloidin and incubated with primary antibodies against Sar1b (A) GTX109170 and (B) 22292-1-AP and fluorophore-conjugated secondary antibody Alexa Fluor 594 goat-anti-rabbit. Representative fluorescence microscopy images from C2C12 cells with and without siRNA targeting Sar1b are shown.

3.6 Sar1b knockdown increases intracellular BCKA levels in C2C12 myotubes

Having established a model of Sar1b knockdown in myotubes, we sought to establish whether inhibiting leucine-sensor Sar1b would alter the content and flux of intracellular BCAA and BCKA. Given that Sar1b levels were decreased *in vivo* under HFHS-fed conditions when BCKA levels were increased, we hypothesized that altering Sar1b availability may impact intracellular BCKAs, specifically ketoleucine.

To examine whether knockdown of Sar1b altered intracellular BCKA levels, C2C12 cells were transfected with si-Sar1b#1 and #3 and incubated 16hr in leucine-deplete media. Cells were subsequently collected for BCKA extraction and quantification via UPLC MS (Figure 3.11 A). Compared to si-ctrl treated cells, total BCKA levels increased 3-fold after treatment with si-Sar1b#1 and ~3.5-fold after treatment with si-Sar1b#3, which had the higher degree of knockdown amongst the two siRNAs (Figure 3.11. B). Strikingly, KIC, the keto-acid of leucine, was undetectable in si-ctrl treated samples yet had average levels up to 20pmol/million cells in the si-Sar1b treated cells. KIV levels showed a smaller but significant increase when Sar1b was silenced, increasing 1.5-1.6-fold compared to si-ctrl group (Figure 3.11. B). Treatment with si-Sar1b#1 trended to show an increase in KMV levels, albeit did not reach statistical significance, while treatment with si-Sar1b#3 resulted in a 4-fold increase in intracellular KMV compared to si-ctrl (Figure 3.11. B). Furthermore, to examine if changes in BCKA reflected in increased reamination to BCAA, intracellular BCAA levels were determined, and data is expressed as BCKA/BCAA ratio (Figure 3.11. C). Treatment with si-Sar1b#1 and si-Sar1b#3 significantly increased the total BCKA/BCAA ratio and the individual ratio for KIV/leucine without leucine (Figure 3.11. C). Treatment with si-Sar1b#1 did not significantly increase the KMV/isoleucine ratio, though treatment with si-Sar1b#3 did. Interestingly, the KIV/valine ratio displayed an increasing trend, but changes were not statistically significant after treatment with si-Sar1b#1 and si-Sar1b#3 (Figure 3.11. C). Overall, C2C12 cells cultured without leucine showed increases in intracellular BCKA and BCKA/BCAA ratio after Sar1b silencing.

We next examined if intracellular BCKA levels were altered in the absence of Sar1b in leucine-repleted media. C2C12 cells were transfected with si-Sar1b#1 and #3 and incubated 16hr in leucine-repleted DMEM1X media with 5mM glucose (Figure 3.12. A). When Sar1b was silenced, total BCKA levels were significantly increased in the presence of leucine. Treatment with si-Sar1b#1 resulted in an average of 4-fold increase and si-Sar1b#3 with a 5-fold increase compared to treatment with si-ctrl, though overall BCKA levels were lower (Figure 3.12. B) than in the leucine deplete media

studies (Figure 3.11). This is plausibly due to the lower detection limit of KIC and KMV in all treatment groups in leucine-replete studies. Strikingly, changes in KIV in response to Sar1b knockdown appeared to be driving the changes in intracellular BCKA levels, increasing 2-fold and 4-fold compared to treatment with si-ctrl with si-Sar1b#1 and si-Sar1b#3, respectively (Figure 3.12. B). The BCAA/BCKA ratio was significantly increased after treatment with both si-Sar1b#1 and si-Sar1b#3, as was the KIV/valine ratio after treatment with si-Sar1b#3 (Figure 3.12. C). These data suggest that the effect of Sar1b silencing on intracellular BCKA levels depends on the amino acid microenvironment to which the cells are exposed, and alterations in BCKA levels are not necessarily dependent on intracellular changes in their respective BCAAs.

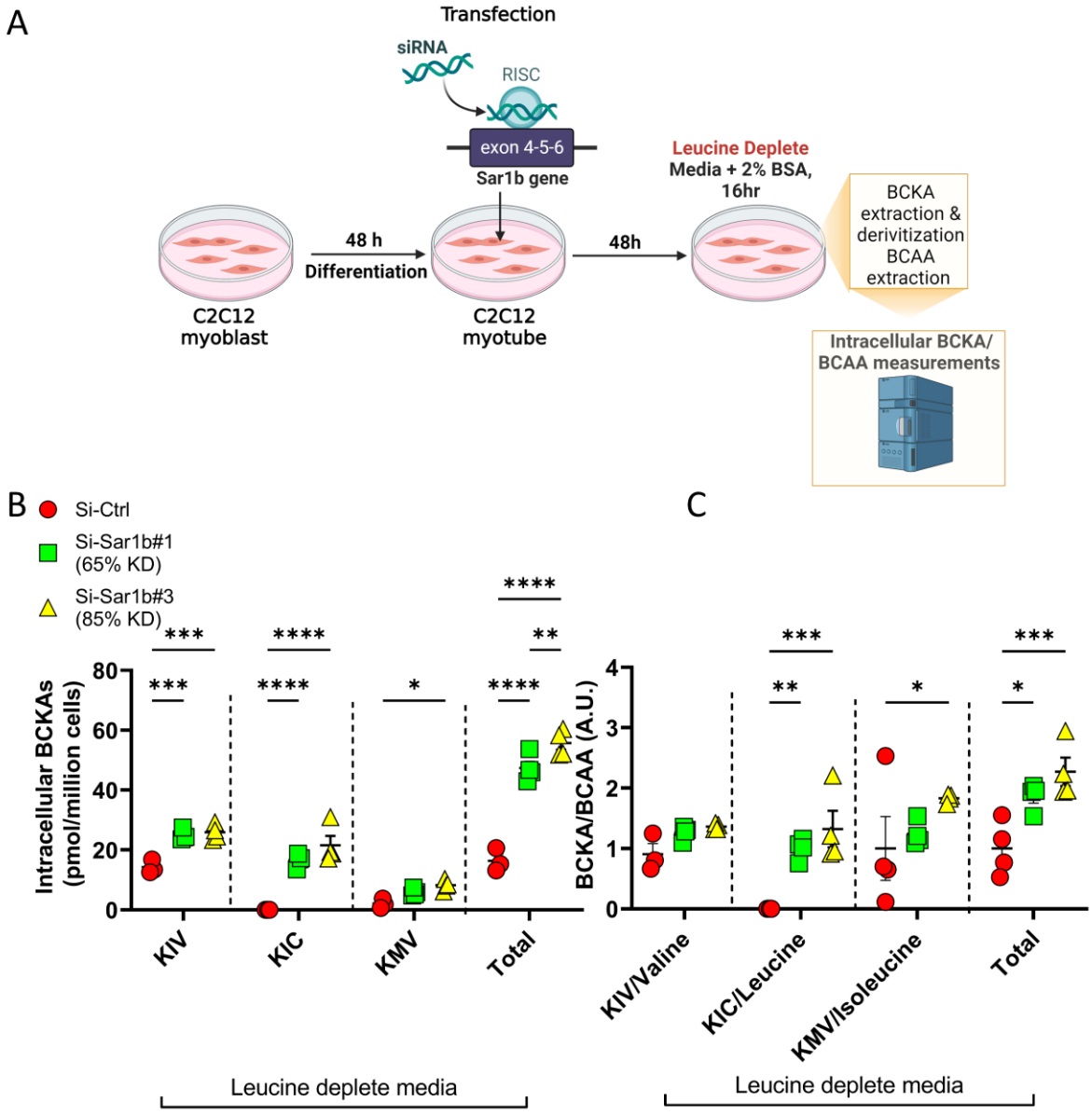

Figure 3.11: Sar1b knockdown significantly increases intracellular BCKA levels and BCKA/BCAA ratio in C2C12 cells cultured in leucine-deficient media.

(A) Outline of study design where sar1b was knocked down in C2C12 cells, prior to incubation in leucine depleted media followed by sample harvest for intracellular BCKA measurements by UPLC mass spectrometric analysis. (B) Intracellular BCKA levels in C2C12 myotubes treated with 15nM si-ctrl, si-Sar1b#1 and si-Sar1b#3. (C) Ratio of intracellular BCKA/BCAA levels in C2C12 myotubes. Graph represents mean ± S.E.M, statistical analyses were performed using two-way ANOVA with Tukey's multiple comparisons test, n =3. *P<0.05, **P<0.01, ***P<0.001, ****P <0.0001, AU; Arbitrary Unit.

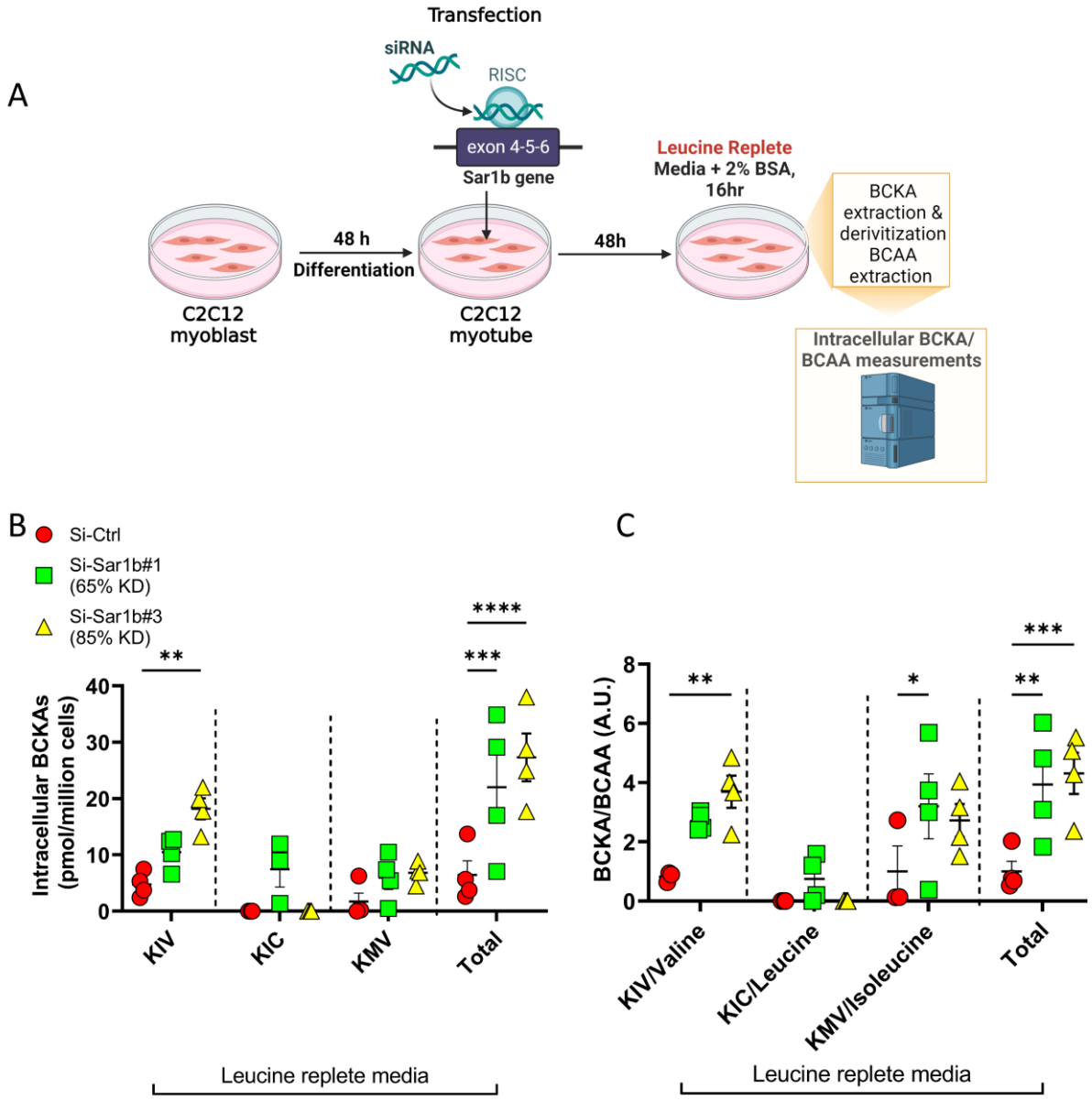

Figure 3.12: Sar1b knockdown significantly increases intracellular KIV but not KMV and KIC levels in C2C12 cells cultured in leucine-replete media.

(A) Outline of study design where Sar1b was knocked down in C2C12 cells prior to incubation in leucine replete media and followed by sample harvest for intracellular BCKA/BCAA measurements by UPLC MS. (B) Intracellular BCKA levels in C2C12 myotubes treated with 15nM si-ctrl, si-Sar1b#1 and si-Sar1b#3. (C) Ratio of intracellular BCKA/BCAA levels in C2C12 myotubes. Graph represents mean ± S.E.M, statistical analyses were performed using two-way ANOVA with Tukey's multiple comparisons test, n =3. *P<0.05, **P<0.01, ***P<0.001, ****P <0.0001, AU; Arbitrary Unit.

3.7 Loss of Sar1b decreases insulin-stimulated protein kinase B (AKT) and glycogen synthase kinase-3 (GSK3) phosphorylation in C2C12 myotubes

Prior studies from our laboratory showed that BCKA overload inhibits skeletal muscle insulin signaling[93]. Since intracellular BCKA levels were elevated following Sar1b inhibition, we queried if Sar1b knockdown would perturb insulin signaling in C2C12 cells. C2C12 cells are insulin responsive and are a widely used model to study insulin signaling and insulin resistance in the muscle[120].

After differentiation and transfection with mo-si-Sar1b#1 and #2 for 48h, C2C12 cells were serum starved for 6h in DMEM1X with 5mM glucose. After starvation, cells were incubated with or without 100nM insulin for 15 min, prior to measurement of Sar1b and protein quantity of total and phosphorylated forms of insulin signaling targets AKT, GSK3 and IRS-1 (Figure 3.13). Sar1b protein quantity decreased by 90% in response to treatment with si-Sar1b#1 and si-Sar1b#2 (Figure 3.13. A-B). Treatment with si-Sar1b#1 reduced insulin-stimulated AKT1 phosphorylation at ser-473 three-fold compared to treatment with si-ctrl, while basal AKT1 phosphorylation was decreased by >50% when Sar1b was silenced by si-Sar1b#1 and #2 (Figure 3.13. C). Interestingly, treatment with si-Sar1b#2 only decreased insulin-stimulated AKT1 phosphorylation by ~30% compared to insulin-stimulated cells treated with si-ctrl, a statistically non-significant change (Figure 3.13. C). Furthermore, since AKT phosphorylates and activates GSK3, we also examined Serine 9 GSK3β phosphorylation in our model. Insulin-stimulated GSK3β phosphorylation was reduced nearly 4-fold in Sar1b silenced cells, while basal GSK3β phosphorylation was decreased by over 50% in the absence of insulin in si-Sar1b treated cells (Figure 3.13. D). Therefore, when muscle Sar1b content is decreased, insulin-stimulated substrate phosphorylation is decreased. Moreover, Sar1b silencing is sufficient to decrease AKT and GSK3 phosphorylation in the absence of insulin, suggesting that Sar1b exerts an insulin-independent effect to inhibit the AKT-GSK3 axis.

We next examined if the effect of Sar1b on distal components of the insulin signaling pathway, notably AKT and GSK3 phosphorylation, were secondary to changes in the markers of the proximal insulin signaling pathway, such as IRS-1. Interestingly, when C2C12 cells were treated with si-Sar1b#1 and #2 and stimulated with 100nM insulin, no significant change was observed in IRS-1 phosphorylation at Y612, a site phosphorylated by insulin. In all three groups (si-ctrl, si-Sar1b#1 and si-Sar1b#2), insulin treatment significantly increased IRS-1 phosphorylation at Y612

greater than 5-fold (Figure 3.14. A, C). This indicates that regulation of the insulin signaling pathway by Sar1b occurs downstream of IRS-1 and is likely reflective of AKT activation status.

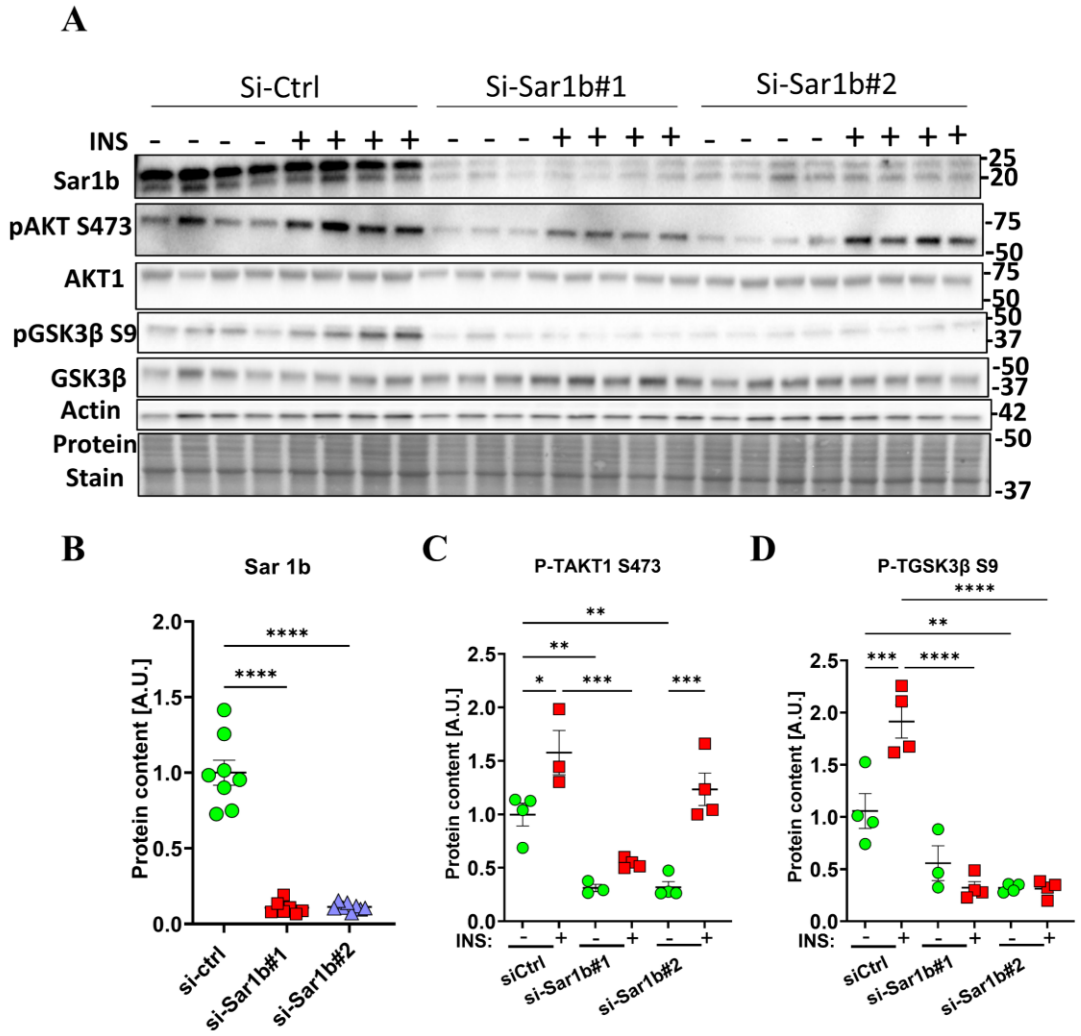

Figure 3.13: Loss of Sar1b protein content decreases protein kinase B (AKT) and glycogen synthase kinase-3 (GSK3) phosphorylation in C2C12 myotubes, both in the presence or absence of insulin.

Differentiated C2C12 myotubes were transfected for 48h with 10nM mo-siSAR1B#1 targeting exon 6 and mo-siSAR1B#2 targeting exon 5. After 48h, cells were serum-starved 6h DMEM1X media with 5mM glucose prior to being stimulated with 100nM insulin (+ INS) or media only (- INS) for 15min, followed by cell harvest. (A-D) Immunoblot and densitometric analyses of Sar1b, total and phosphorylated AKT1 Ser-473, and total and phosphorylated GSK3β Ser-9. Data is normalized to protein stain. Actin served as a protein loading control. Graph represents mean ± S.E.M, statistical analyses were performed using one (B) or two (C-D)-way ANOVA with Tukey's multiple comparisons test, *P<0.05, **P<0.01, ***P<0.001, ****P <0.0001, n=4 AU; Arbitrary Unit. Note: all the presented lanes are from the same membrane.

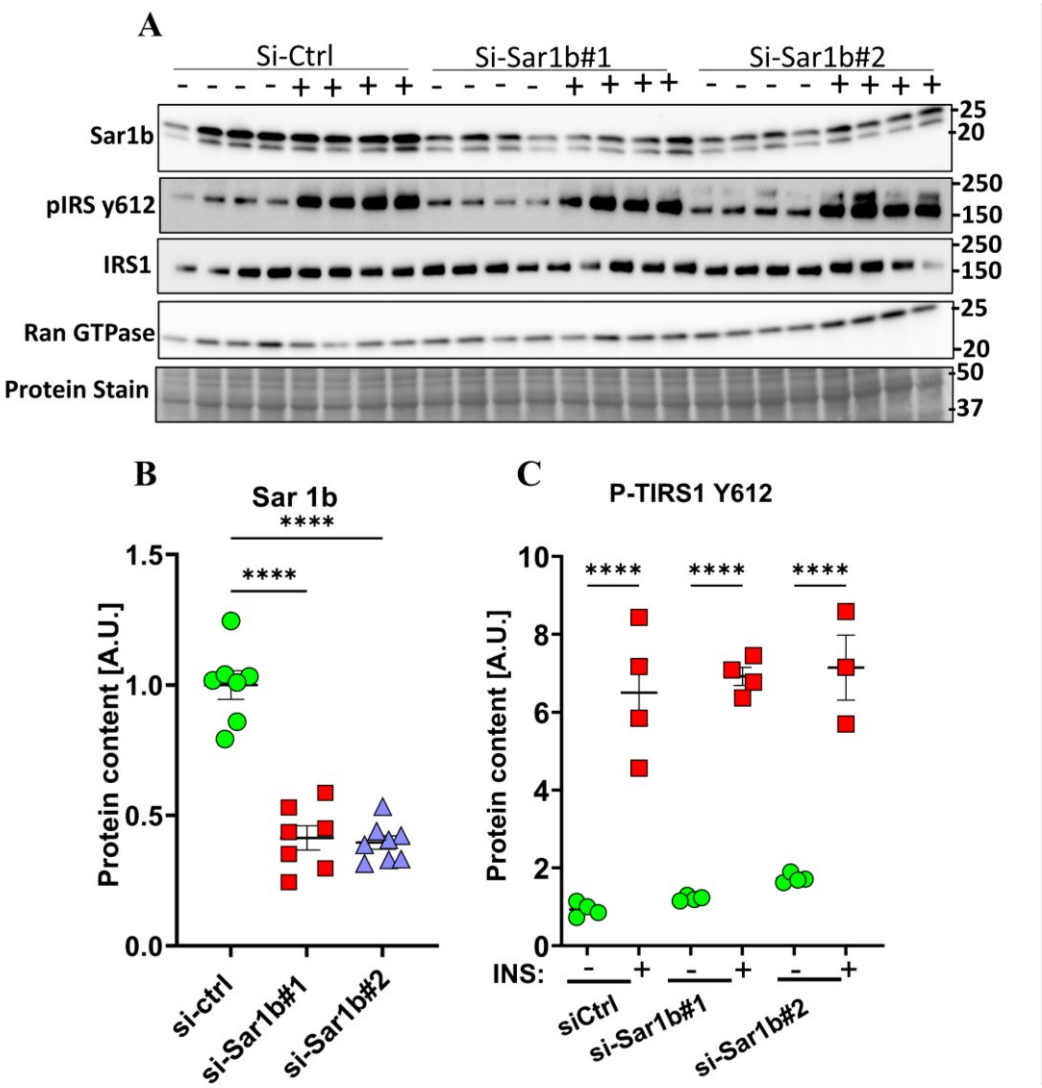

Figure 3.14: Insulin-induced IRS-1 phosphorylation in C2C12 myotubes is unchanged after Sar1b knockdown.

Differentiated C2C12 myotubes were transfected for 48h with 10nM mo-siSAR1B#1 targeting exon 6 and mo-siSAR1B#2 targeting exon 5. After 48h, cells were serum-starved 6h in DMEM1X media with 5mM glucose prior to being stimulated with 100nM insulin (+ INS) or media only (- INS) for 15min, followed by cell harvest. (A-D) Immunoblot and densitometric analyses of Sar1b, and total and phosphorylated IRS-1 Y612. Data is normalized to protein stain. Ran GTPase served as a protein loading control. Graph represents mean ± S.E.M, statistical analyses were performed using one (B) or two (C)-way ANOVA with Tukey's multiple comparisons test, ****P <0.0001, n=4, AU; Arbitrary Unit. Note: all the presented lanes are from the same membranes. Experiment was repeated three times.

3.8 Loss of Sar1b decreases insulin dependent ERK phosphorylation in C2C12 myotubes

In addition to the proximal insulin signaling pathway, we investigated the impact of Sar1b silencing on mitogenic signaling downstream of insulin in C2C12 cells. The readout for insulin-induced activation of mitogenic signaling is increased phosphorylation of ERK1-2 at threonine and tyrosine residues and subsequent dimerization and activation to regulate gene expression, cell proliferation, and growth. Sar1b silencing in C2C12 cells (Figure 3.15. A-B) stimulated with 100nM insulin showed significantly decreased ERK phosphorylation at T202/204 compared to cells treated with si-ctrl (Figure 3.15. A, C). However, no significant changes in ERK phosphorylation were observed in the absence of insulin in Sar1b silenced cells (Figure 3.15. C). Therefore, Sar1b modifies insulin-dependent ERK phosphorylation with a plausible role in governing the mitogenic signaling pathway.

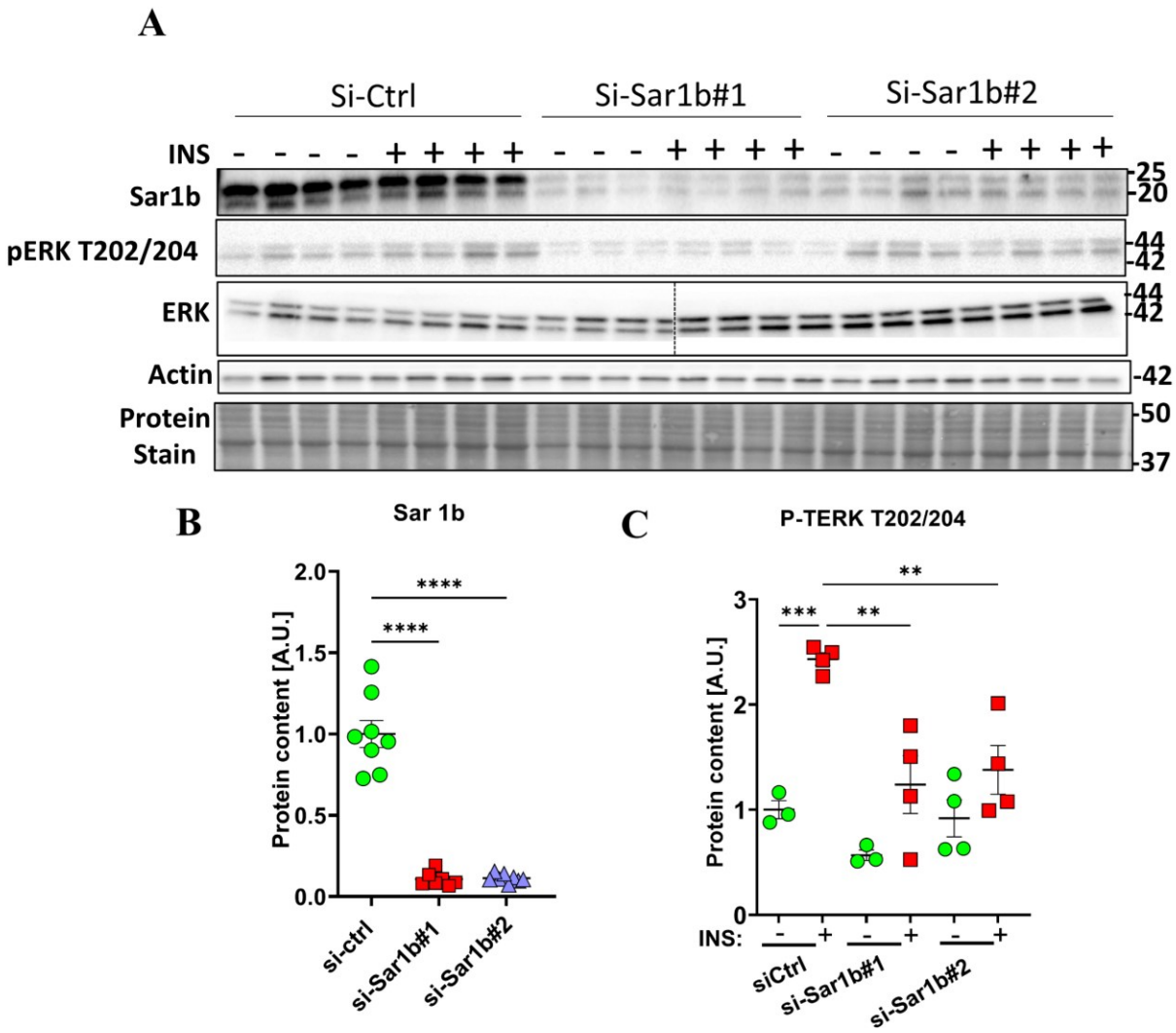

Figure 3.15: Sar1b silencing decreases insulin-dependent extracellular receptor kinase (ERK) phosphorylation in C2C12 myotubes.

Differentiated C2C12 myotubes were transfected for 48h with 10nM mo-siSAR1B#1 targeting exon 6 and mo-siSAR1B#2 targeting exon 5. After 48h, cells were serum-starved 6h in DMEM1X media with 5mM glucose prior to being stimulated with 100nM insulin (+ INS) or media only (- INS) for 15min, followed by cell harvest. (A-D) Immunoblot and densitometric analyses of Sar1b, and total and phosphorylated ERK Thr202/204. Data is normalized to protein stain. Actin served as a protein loading control. Graph represents mean ± S.E.M, statistical analyses were performed using one (B) or two (C)-way ANOVA with Tukey's multiple comparisons test, **P<0.01, ***P<0.001, ****P <0.0001, n=4, AU; Arbitrary Unit. Note: all the presented lanes are from the same membranes. Dotted line indicates a break in the membrane. Experiment was repeated three times with N = 2 technical replicates.

3.9 Sar1b silencing in C2C12 myotubes decreased mTOR, S6K, and S6 phosphorylation in basal and insulin-stimulated states

During leucine deficiency, Sar1b binds to the GATOR2 complex, inhibiting the activation of mTORC1, a driver of protein synthesis[100]. However, in the presence of leucine, Sar1b preferentially binds to leucine and relieves inhibition on GATOR2, thereby activating mTOR. Therefore, we postulated that loss of Sar1b may increase mTORC1 phosphorylation and activation of downstream mTOR substrates. However, silencing of Sar1b decreased total mTOR protein quantity, resulting in slightly decreased phosphorylated mTOR ser2448 protein in the basal and insulin-stimulated state, though these were not statistically significant changes (Figure 3.14. C). The impact of Sar1b on mTOR phosphorylation is secondary to changes in total protein. This opposed our hypothesis that loss of Sar1b should increase activating phosphorylation of mTOR. However, loss of Sar1b significantly decreased S6K1 phosphorylation at Thr389 by 3-4-fold in both the basal and insulin-stimulated states compared to the control (Figure 3.16. D). A similar trend was observed in the phosphorylation of S6K1 substrate rS6 at ser240/244, with 2-3-fold decreases in S6 phosphorylation following Sar1b silencing (Figure 3.16. E). These data suggest that Sar1b protein quantity regulates the total protein content of mTOR, S6K1, and S6, plausibly by regulating its transcription and/or turnover, which remains to be investigated.

Phosphorylation and activation of S6K1 and downstream substrates such as ribosomal S6 and 4EBP1 are critical for the onset of protein translation and protein synthesis. Given the significant impact of Sar1b knockdown on the quantity of total and phosphorylated S6K1 and S6, we examined if these changes reflected in the functional impact of Sar1b knockdown on protein synthesis in C2C12 cells. To ascertain this, we used the SUnSET assay to measure protein synthesis in C2C12 cells transfected with si-ctrl, si-Sar1b#1 or si-Sar1b#2. The SUnSET method measures the incorporation of puromycin into the nascent peptide chain, which reflects the rate of in vitro protein translation[122]. After 48h siRNA transfection, C2C12 cells were incubated with 1µM puromycin for 30min prior to harvest and immunoblotting with monoclonal puromycin antibody to detect puromycin levels in C2C12 samples (Figure 3.17A-B). A 50% decrease in Sar1b protein did not change puromycin incorporation and protein synthesis, suggesting that a higher silencing of Sar1b protein is likely needed to observe effects on protein synthesis.

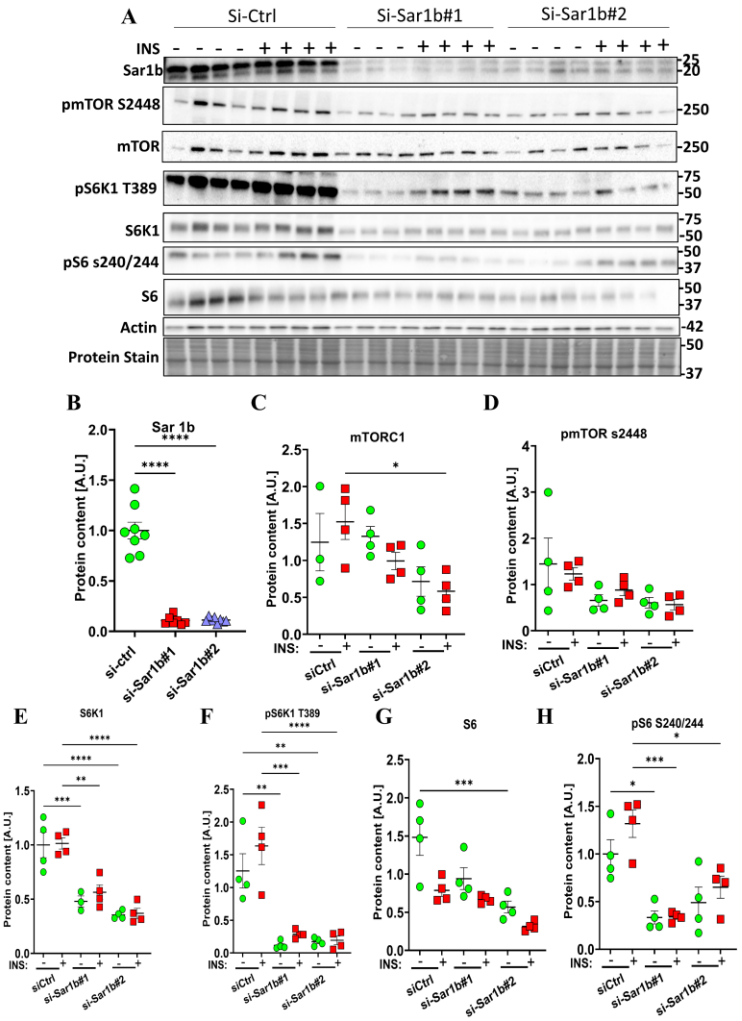

Figure 3.16: Silencing Sar1b decreases total protein content of mTOR, P70S6 kinase and s6 and reduces activating phosphorylation of P70S6K and S6 but not mTOR in C2C12 myotubes. Differentiated C2C12 myotubes were transfected for 48h with 10nM mo-siSAR1B#1 targeting exon 6 and mo-siSAR1B#2 targeting exon 5. After 48h, cells were serum-starved 6h in DMEM1X media with 5mM glucose prior to being stimulated with 100nM insulin (+ INS) or media only (- INS) for 15min. (A-H) Immunoblot and densitometric analyses of Sar1b, and total and phosphorylated mTOR Ser-2448, S6K1 Thr389, and S6 ser240/244. Data normalized to protein stain. Actin served as the protein loading control. Graph represents mean ± S.E.M, statistical analyses were performed using one (B) or two (C-H)-way ANOVA with Tukey's multiple comparisons test, *P<0.05, **P<0.01, ***P<0.001, ****P <0.0001, n=4; AU; Arbitrary Unit. Note: all the presented lanes are from the same membranes. Experiment was repeated three times, with the best run repeated with N = 2 technical replicates.

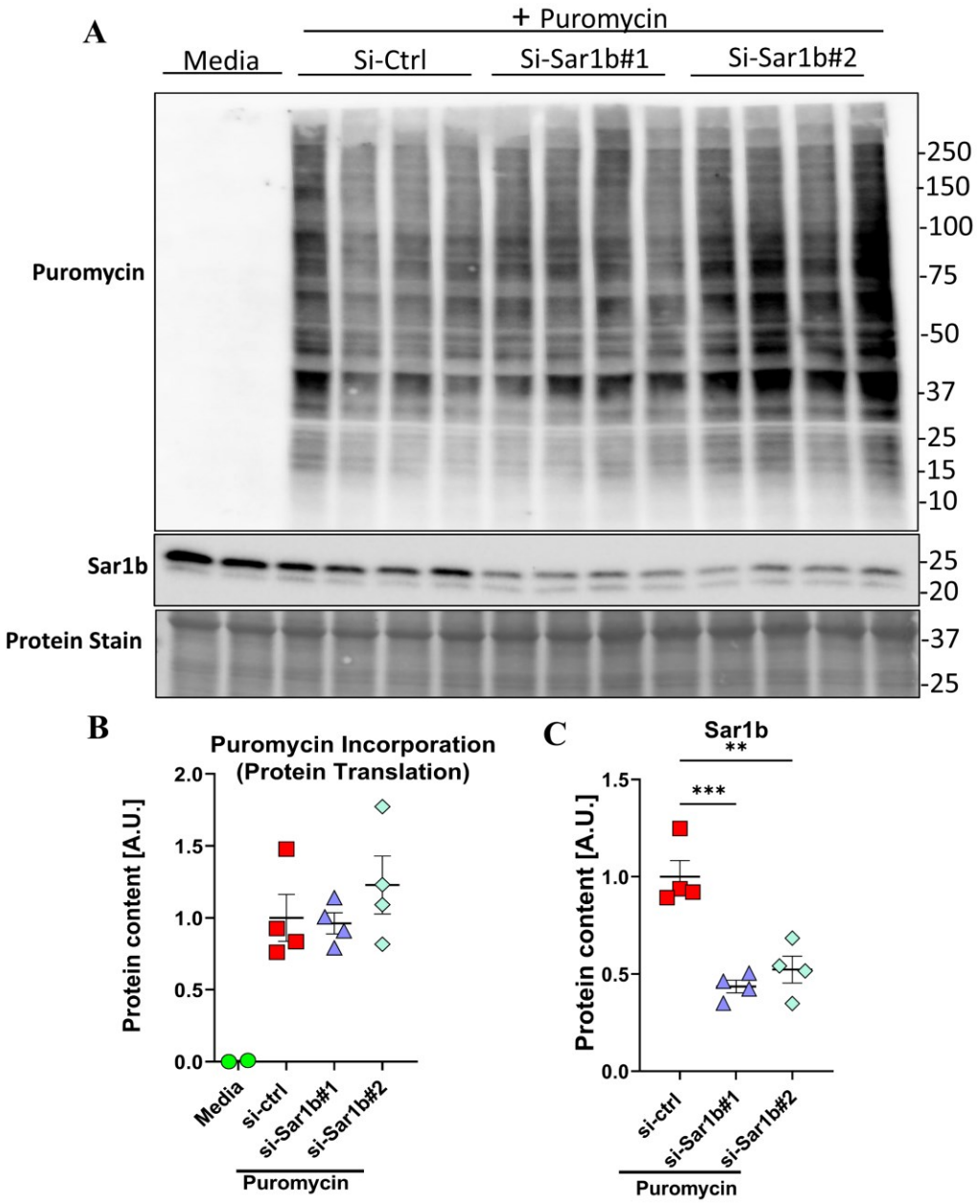

Figure 3.17: Protein translation is unchanged following Sar1b silencing in C2C12 myotubes

Differentiated C2C12 myotubes were transfected for 48h with 10nM mo-siSAR1B#1 targeting exon 6 and mo-siSAR1B#2 targeting exon. After 48h, cells were serum-starved 6h in DMEM1X media with 5mM glucose prior to incubation with 1 µm puromycin for 30 min (A-C). Immunoblot and densitometric analysis of puromycin incorporation. Graph represents mean ± S.E.M, statistical analyses were performed using one-way ANOVA with Tukey's multiple comparisons test, **P<0.01, ***P<0.001, n=4, AU; Arbitrary Unit. Note: all the presented lanes are from the same membranes. Experiment was repeated three times.

3.10 Sar1b knockdown reduces pyruvate-linked respiration in C2C12 cells

Given Sar1b's impact on downregulating insulin and mTOR signaling nodes for regulating substrate oxidation and growth, we next sought to understand whether Sar1b insufficiency would impact mitochondrial respiration in C2C12 cells. C2C12 myotubes treated with si-ctrl, si-Sar1b#1, and si-Sar1b#3 for 48h were examined for pyruvate (pyr)-linked respiration using the Oroboros-O2k oxygraph unit. Treatment with si-Sar1b#1 and si-Sar1b#3 resulted in 65 and 80% knockdown in Sar1b mRNA expression, respectively (Figure 3.18. A). The pyruvate-linked respiration protocol allows for evaluating changes in oxygen flux after the sequential addition of different electron transport substrates and inhibitors in the electron transport system (ETS) as outlined in figure 3.18. B. Knockdown of Sar1b resulted in significantly decreased pyruvate-linked respiration in the presence of non-saturating, physiological concentrations of ADP (0.1mM; D 0.1; Figure 3.18. D-E). si-Sar1b#1 and si-Sar1b#3 treatment decreased oxygen flux in C2C12 myotubes by 30% and 40%, respectively, compared to si-ctrl (Figure 3.18. D-E). While si-ctrl myotubes still responded to increasing ADP concentrations by increasing their oxygen flux in response to malate and pyruvate, this response was impaired in cells lacking Sar1b. Notably, uncoupled respiration, in response to FCCP, decreased significantly only with si-Sar1b#1 but not si-Sar1b#3 (Figure 3.18. F). Complex II respiration induced by succinate addition was comparable between all groups (Figure 3.18. G).

Our data show that inhibition of Sar1b inhibits mitochondrial respiration in C2C12 cells, which could be a cause or a consequence of diminished insulin and mTORC1 signaling, which merits investigation (Figure 3.19).

Figure 3.18: Sar1b knockdown decreases Pyr-linked oxygen consumption in C2C12 cells Differentiated C2C12 myotubes were transfected with Sar1b targeting siRNA prior to analysis of pyruvate-linked respirational analysis with Oroboros O2K oxygraph. (A) quantification of Sar1b mRNA expression corrected to RER1 and Rpl7 reference genes in siRNA treated C2C12 cells (B) Schematic depicting changes in oxygen flux during an ETS protocol measuring pyr-linked respiration. (C) Sample trace of oxygen flux in C2C12 cells treated with si-ctrl. (D) Oxygen consumption rate of siRNA treated C2C12 cells following substrate and inhibitor addition. (E) Pyr-linked oxygen-consumption rate in presence of 100μM ADP. (F) Uncoupled oxygen consumption rate in the presence of uncoupling agent FCCP. (G) Complex II oxygen consumption rate in the presence of CII substrate succinate. Presented values were corrected to corrected to ug protein and the oxygen consumption rate following AMA addition**.** Graphs represents mean ± S.E.M, statistical analyses were performed using one (A, F-G) or two (D-E)-way ANOVA with Tukey's multiple comparisons test, *P<0.05, **P<0.01, ***P<0.001, ****P <0.0001. Presented data comes from N = 3 trials, with n = 4 replicates included in each trial.

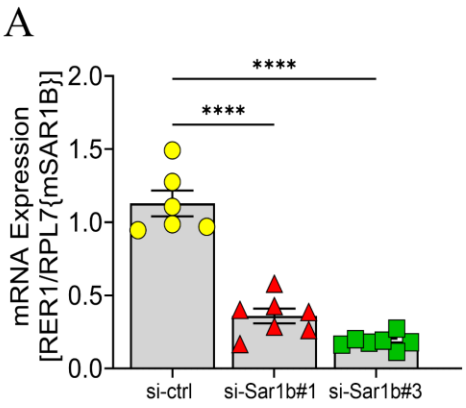

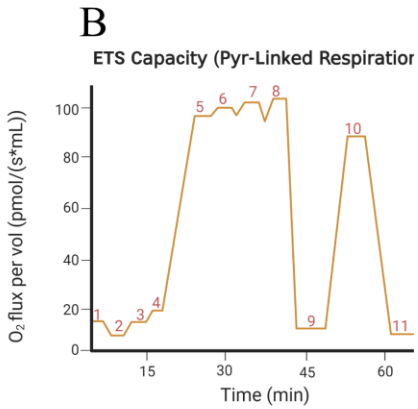

Label	Chemical added	Concentration
1	Basal state	----
2	Digitonin	3 µM
3	Malate	0.5mM
4	Pyruvate	5mM
5	ADP	0.1mM
6	ADP	0.5mM
7	ADP	5mM
8	FCCP	0.5µM
9	Rotenone	0.5µM
10	Succinate	10µM
11	Antimycin A	5µM

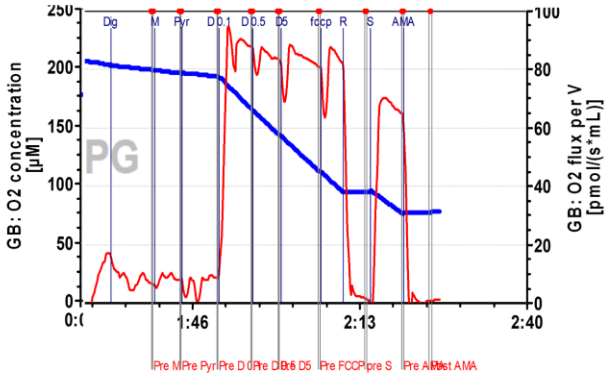

Chemical	Concentration	Mark
Digitonin	3 µM	Dig
Malate	0.5mM	M
Pyruvate	5mM	Pyr
ADP	0.1mM	D 0.1
ADP	0.5mM	D 0.5
ADP	5mM	D 5
FCCP	0.5µM	FCCP
Rotenone	0.5µM	R
Succinate	10µM	S
Antimycin A	5µM	AmA

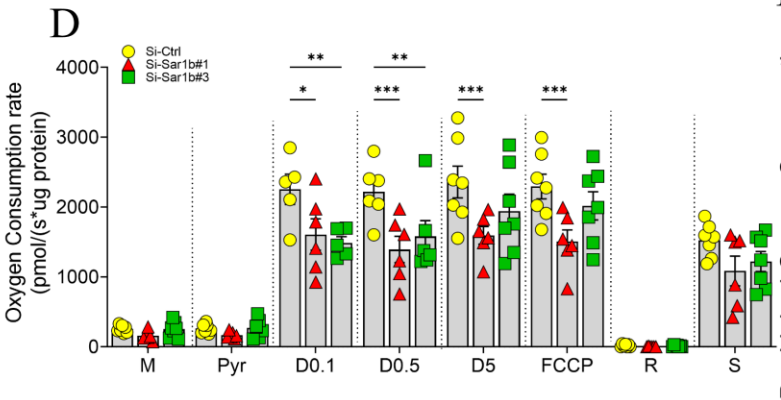

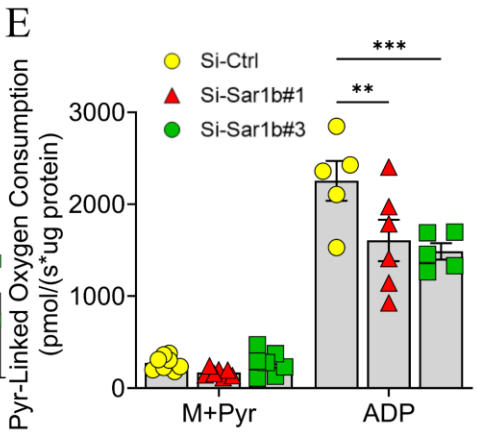

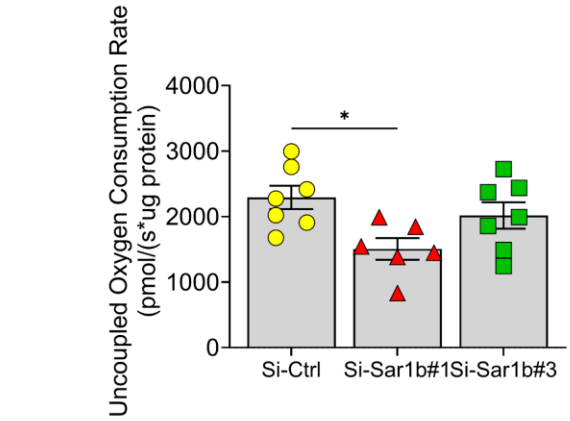

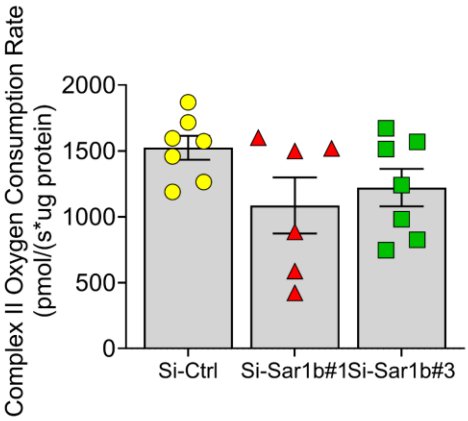

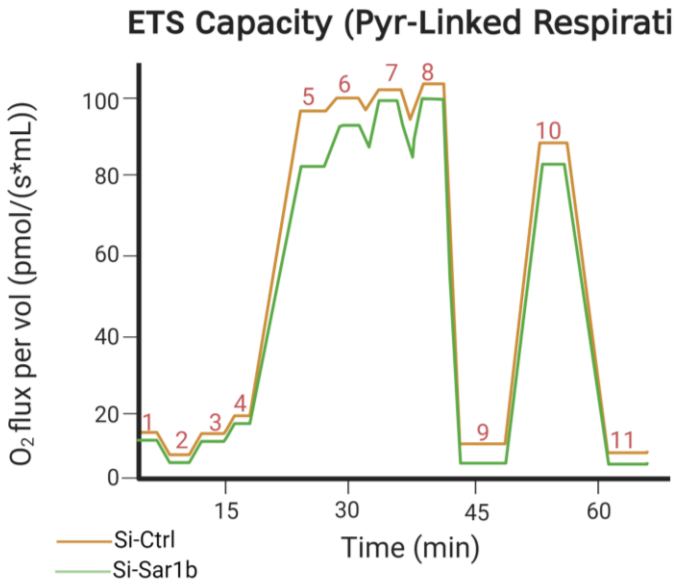

Label	Chemical added	Concentration
1	Basal state	----
2	Digitonin	3 µM
3	Malate	0.5mM
4	Pyruvate	5mM
5	ADP	0.1mM
6	ADP	0.5mM
7	ADP	5mM
8	FCCP	0.5µM
9	Rotenone	0.5µM
10	Succinate	10µM
11	Antimycin A	5µM

Figure 3.19: Working model describing the impact of Sar1b knockdown on ETS capacity

Schematic depicting changes in oxygen flux during an ETS protocol measuring pyr-linked respiration in C2C12 cells treated with control siRNA (orange) and siRNA targeting Sar1b (green) in response to the addition of electron transport chain substrates and inhibitors

Chapter 4: Discussion

4.1 Study overview & summary of findings:

Chronically elevated glucose, fatty acids, amino acids, hormones, and cytokines drive insulin resistance, metabolic remodeling, and maladaptive tissue function during obesity[6,7]. Persistent tissue insulin resistance increases predisposition to T2D[6,7]. The impact of insulin resistance in the skeletal muscle has profound implications on whole-body glucose homeostasis, as skeletal muscle is the body's largest insulin-sensitive tissue. Skeletal muscle insulin resistance is significantly impacted at the level of glucose transport[58], perturbing glucose utilization, which leads to compensatory changes in lipids and amino acid metabolism[6,7]. Therapies to improve skeletal muscle insulin signaling should restore metabolic homeostasis during obesity and T2D[2,9]. However, a limited understanding of mechanisms driving insulin resistance and metabolic inflexibility in the skeletal muscle poses challenges to developing newer therapies.

The current dogma suggests that obesity and T2D induce insulin resistance primarily by increasing intracellular FA content and accumulation of lipotoxic species that impair insulin signaling[9]. This is accompanied by diminished glucose utilization and accumulation of non-oxidative metabolites of glucose, leading to glucotoxicity, which is sufficient to promote insulin resistance. Lipotoxicity and glucotoxicity are together referred to as "glucolipotoxicity", and this combination in the skeletal muscle impairs glucose homeostasis, metabolic flexibility, and mitochondrial function[51-54]. Rodent models suggest that the deregulation of insulin-dependent glucose uptake is attributed to dysfunction in the proximal and distal axes of insulin signaling, independent of the allosteric modification of GLUT4[11]. Therefore, it is critical to understand the signaling markers downstream of AKT that indirectly modulate and contribute to skeletal muscle insulin resistance.

In addition to glucolipotoxicity driving insulin resistance, the mTORC1 pathway is a negative regulator of insulin signaling and an important initiator of insulin resistance[47,84]. Nutrient overload in the skeletal muscle activates mitogenic signaling and the mTORC1 pathway. Indeed, rodent models have demonstrated that inhibition of the mTORC1 pathway and S6K1 deletion improves insulin resistance in mice[12]. The mTORC1 pathway is also activated by the accumulation of BCAA and BCKA following the dysregulation of BCAA catabolism. Dysregulation in BCAA metabolism and subsequent overactivation of the mTOR pathway is sufficient to disrupt skeletal

muscle insulin signaling[93]. However, mechanistically, how these alterations in skeletal muscle BCAA/BCKA ratio are sensed and relayed to change mTOR and insulin signaling remains unclear.

Sar1b was recently identified as a leucine-sensing protein which inhibits mTOR activation when leucine levels are low[100]. Given its high content in the skeletal muscle and its inhibition of mTOR, a negative regulator of insulin signaling, Sar1b may have a role in governing insulin-dependent glucose homeostasis in the skeletal muscle, which was previously unexplored. My thesis work uncovered a potential role for leucine-sensor Sar1b in skeletal muscle mTOR and insulin signaling and a novel connection between Sar1b, nutrient overload, and intracellular BCKA levels. Data from my thesis (Table 4.1) suggests that 1) during diet-induced obesity, when serum BCKA levels are elevated, protein quantity of Sar1b is decreased in the gastrocnemius tissue, indicating a decline in Sar1b protein quantity under nutrient overload; 2) *in vitro,* when Sar1b is knocked down there is an elevation in intracellular BCKA levels in C2C12 cells, an effect that is independent of the presence of leucine; 3) knockdown of Sar1b inhibits the phosphorylation of distal insulin signaling markers AKT1 and GSK3β, while also inhibiting pyruvate-linked glucose oxidation in C2C12 myotubes; 4) Sar1b knockdown in C2C12 myotubes inhibits ERK phosphorylation downstream of insulin, highlighting altered mitogenic signaling; 5) Contrary to Sar1b's identification as an mTOR inhibitor, strikingly, loss of Sar1b reduces S6K1 and S6 phosphorylation in C2C12 myotubes, without significantly altering protein synthesis. Findings from my thesis present an increased understanding of the role of Sar1b in regulating myocellular processes critical for substrate metabolism, mitochondrial function, and insulin signaling.

4.2 Physiological impact of altered Sar1b availability in vivo

Biallelic mutations in the Sar1b gene cause chylomicron retention disease (ANDD/CRD), characterized by failed intestinal lipid transport resulting from impaired COPII-coated vesicular transport of CMs from the ER to the Golgi of the enterocyte, thereby inhibiting CM maturation and transport[108-110]. Despite the highest expression of Sar1b in the skeletal muscle[100], the impact of Sar1b changes on muscle metabolism and physiology was minimally explored. Data from my thesis showed that Sar1b protein quantity was decreased in the gastrocnemius tissue of animals fed an HFHS diet. To which cell type within the muscle this decrease is specific/autonomous to remains to be investigated, since gastrocnemius is a heterocellular tissue containing myocytes, immune cells, lipid cells, fibroblasts, and smooth muscle cells. Our data point to a non-canonical role for Sar1b in

the skeletal muscle, distinct from its role in the COPII complex, given that only Sar1b, not other COPII components, are highly expressed in mouse skeletal muscle[100].

In contrast to our data, a 2015 study demonstrated that transgenic mice overexpressing Sar1b ($Sar1b^{+/+}$) at the whole body level are more susceptible to weight gain, fat deposition, dyslipidemia, and increased intestinal fat absorption when fed a high-fat diet[123]. Within this study, Sar1b overexpression contributed specifically to lipid accumulation in the liver, intestine, and plasma[123]. Further, $Sar1b^{+/+}$ mice also had decreased insulin insensitivity, based on HOMA-IR index, and significantly decreased glucose tolerance after high-fat diet feeding[123]. Therefore, Sar1b abundance *in vivo* was shown to cause more significant complications and aberrations in response to high-fat feeding. Authors surmised that overexpressing Sar1b drives intestinal fat absorption, causing excess lipoprotein secretion into the circulation used by the liver, adipose tissue and muscle in excess, antagonizing insulin sensitivity[123]. The effect on the skeletal muscle is plausibly secondary to insulin resistance in the liver and/or adipose tissue due to greater TAG accumulation in insulin-responsive tissues. These findings suggest that Sar1b changes at the whole-body level could indirectly impact skeletal muscle substrate metabolism and function. Alternatively, Sar1b changes within the muscle in a cell-autonomous manner could directly alter insulin action, nutrient metabolism, and mitochondrial function, mechanisms that warrant additional studies. Furthermore, it is unknown whether changes in Sar1b in the whole body versus skeletal muscle alone could affect the metabolism of different nutrients.

4.3 Absence of Sar1b increases intramyocellular BCKA content and impairs insulin signaling

Secretion Associated Ras-related GTPase-1b (Sar1b) was recently identified as a leucine-sensing protein. During leucine deficiency, Sar1b physically interacts with GATOR2, preventing it from binding to MIOS and activating mTORC1. However, leucine abundance causes Sar1b-leucine binding, dissociating Sar1b from GATOR2 and permitting GATOR2 to activate mTOR, thereby inducing protein synthesis[100]. Since the BCAAs leucine, isoleucine, and valine and their BCKA metabolites modify insulin signaling in the skeletal muscle[93], it is pertinent to understand if Sar1b interacts with BCKAs or the other BCAAs in addition to leucine.

Data from my thesis show that silencing Sar1b in C2C12 cells led to an accumulation of individual and total BCKAs in leucine-deplete conditions, like what was observed in C2C12 cells exposed to high palmitate[93]. Interestingly, our data demonstrate that increases in intracellular BCKA levels in response to Sar1b knockdown were less pronounced in leucine-replete media. It remains to

be examined how the presence of leucine and the availability of Sar1b influence intramyocellular BCKA accumulation. Notably, in rodent models with obesity and IR, BCAA catabolizing enzymes BCATm, PPM1K and BCKDHA are decreased by lipid accumulation in adipose tissue and skeletal muscle [13, 21, 22]. Moreover, Sar1b-/- in Caco-15 cells impaired lipid absorption resulting in lipid overload [113]. Therefore, we surmise that Sar1b knockdown might alter intracellular lipid metabolism to inhibit BCAA catabolizing enzymes and render changes in BCKA content.

Increased intracellular BCKA content also contributes to impaired skeletal muscle insulin signaling in C2C12 cells and activates the mTORC1 complex, a negative regulator of insulin signaling[93]. Similarly, decreased Sar1b levels in the skeletal muscle of mice fed an HFHS diet are also associated with elevated plasma BCKA levels, suggesting that altering Sar1b availability coincides with impaired insulin signaling and increased accumulation of BCKA and lipid intermediates. Therefore, Sar1b's role as a BCKA regulator in the skeletal muscle might alter muscle insulin and mTOR signaling. Indeed, the loss of Sar1b function inhibited the phosphorylation of AKT1 at Ser473 and its downstream target GSK3β at Ser9. Additionally, increased intracellular BCKAs in C2C12 myotubes resulted in decreased insulin stimulated AKT1 phosphorylation at ser473[93]. Notably, increased intracellular BCKA content during Sar1b insufficiency correlated with decreased AKT1 and GSK3β phosphorylation even in the absence of insulin, suggesting that Sar1b per se regulates AKT activation through an uncharacterized mechanism. Sar1b might plausibly regulate upstream activators of AKT or function as an inhibitor of AKT deactivators such as PTEN or PHLPP1 and PHLPP2. Surprisingly, loss of Sar1b had no impact on activating phosphorylation of IRS-1 at Thr612, in contrast to the inhibitory effect of excess BCKA[93], suggesting that loss of Sar1b inhibits the phosphorylation and activation of distal insulin signaling markers but leaves the proximal insulin signaling proteins unaffected. BCKA overload not only inhibits insulin signaling but also activates mTORC1 and increases protein translation. Since AKT1 is phosphorylated at ser473 by the mTORC2 complex[124] it raises the question if Sar1b could function as an activator or regulator of the mTORC2 complex, preventing phosphorylation and activation of AKT1.

4.4 Sar1b as a regulator of skeletal muscle mTOR signaling

As a mitogenic hormone, insulin prevents amino acid mobilization, enabling the storage of amino acids into proteins[46]. Insulin mediates protein synthesis through the regulation of mTOR activation[48]. We hypothesized that since Sar1b was shown to inhibit mTORC1 in the absence of

leucine the absence of Sar1b might increase the phosphorylation of mTORC1 at S2448. However, the knockdown of Sar1b did not significantly alter mTORC1 phosphorylation, and strikingly Sar1b knockdown exerted pronounced inhibition of S6K1 and S6 phosphorylation, downstream mTOR substrates, in the presence and absence of insulin. Therefore, Sar1b likely regulates AKT and mTOR phosphorylation by two distinct, unrelated mechanisms. Classically, S6K1 is reported to be regulated by other kinases, including the insulin-dependent RAS/MAPK and PI3K pathway[32, 33]. Furthermore, PDK1, an AKT1 regulator, has also been found to phosphorylate threonine residues of S6K1[34]. Since AKT1 and S6K1 phosphorylation were decreased following Sar1b loss of function, Sar1b could potentially alter the activities of MAPK, PI3K or PDK to decrease S6K phosphorylation. S6K1 is also dephosphorylated by phosphatases like PP2A, which could be activated following the inhibition of Sar1b[35]. Notably, prior studies from our lab showed that increased intracellular BCKA augments PP2A activity to inhibit insulin signaling[93], raising the question if Sar1b could alter S6K phosphorylation by modifying PP2A action.

BCKAs activate mTOR, P70S6K, and ribosomal S6 to facilitate muscle protein synthesis. Indeed, our data indicate that exogenous BCKA treatment significantly increased S6K1 phosphorylation at T389 and activated protein synthesis[13] in C2C12 cells. We theorized that inhibiting S6K1 and rS6 phosphorylation following Sar1b silencing would decrease protein synthesis in C2C12 myotubes. However, puromycin incorporation was unaffected by Sar1b knockdown. Most likely, Sar1b post-translationally regulates S6K1 and S6 without affecting protein synthesis or during silencing studies, the inability to achieve 100% knockdown might reflect in unaltered protein synthesis. Puromycin incorporation is only a crude measure of protein synthesis, and a more mechanistic study examining Sar1b's impact on protein synthesis and translation in myotubes is warranted.

Insulin is also a critical regulator and activator of the MAPK pathway, which controls gene expression, mitogenesis (cell growth), and cell differentiation[30, 31]. Our data indicate that the MAPK pathway could plausibly contribute to changes in skeletal muscle insulin signaling following the loss of Sar1b function. Indeed, the knockdown of Sar1b inhibited the phosphorylation of ERK in the presence of insulin. However, Sar1b knockdown did not significantly impact basal ERK phosphorylation, indicating that this is an insulin-dependent relationship observed between altered Sar1b availability and ERK phosphorylation. Therefore, Sar1b blunted mitogenic signaling

downstream of insulin, which likely negatively impacts cell growth and survival and could involve upstream regulators of ERK pathways such as MAP2K and MAP3K family of proteins.

4.5 The role of Sar1b in skeletal muscle mitochondrial function

During insulin resistance and T2D, fewer functional mitochondria impairs mitochondrial function [54]. Reduced insulin-stimulated muscle glucose uptake and/ or metabolism leads to a 40-50% reduction in mitochondrial oxidative phosphorylation (OXPHOS) activity[60]. Insulin-induced glucose uptake by the skeletal muscle leads to the formation of pyruvate via glycolysis. Pyruvate, in the presence of sufficient molecular O_2, undergoes a process of mitochondrial OXPHOS to produce ATP, CO_2 and H_2O[26]. Furthermore, in the skeletal muscle of diabetic patients, sustained insulin infusion failed to promote the expression of mRNA transcripts encoding key mitochondrial proteins[125,126], suggesting that insulin signaling is required for normal mitochondrial function in metabolism. Indeed, BCKA overload inhibits insulin signaling[93] and concomitantly increases mitochondrial ROS production[93], questioning the role of Sar1b in mitochondrial function and its linkages to changes in insulin signaling. We observed that when Sar1b content was decreased in C2C12 myotubes, pyruvate-linked respiration in the presence of physiological ADP concentrations was significantly impaired.

Furthermore, FCCP-linked respiration and CII respiration marginally decreased following Sar1b insufficiency. These data support the notion that Sar1b knockdown inhibited AKT and GSK3 phosphorylation, decreasing glucose uptake and oxidation in myotubes and contributing to the observed decreases in O_2 flux. Our model demonstrates that in addition to acting as a regulator of AKT and downstream GSK3 phosphorylation, Sar1b knockdown inhibits pyruvate-linked respiration.

Prior report showed that loss of Sar1b function resulted in increased FA β-oxidation[18] via upregulation of PPARα, which activates fatty acid oxidation by depleting malonyl-CoA and relieving its inhibition on FAO[18]. Excessive FAO compromises glucose utilization and oxidation.[29] According to the Randle cycle, increased FA uptake and utilization during insulin inaction result from impaired glucose uptake and oxidation[28]. Therefore, a potential mechanistic explanation for the observed decreases in pyruvate-linked glucose oxidation in Sar1b knockdown cells may be attributed to a compensatory increase in FA oxidation. Indeed, deletion of Sar1b in Caco-2/15 cells increases PLIN2 expression and mitochondrial fatty acid oxidation, diminishing lipogenesis and lipid absorption in intestinal cells[113]. Future studies incorporating exposure to increased FA in our

model prior to measuring glucose oxidation or estimating palmitate-linked FAO in our Sar1b knockdown model will address if Sar1b induced changes in glucose metabolism are secondary to changes in lipid uptake and utilization.

Table 4.1: Summary of key observations in C2C12 myotubes with Sar1b knockdown

	Response to Sar1b knockdown	
Phosphorylation/functional readout	(-) Ins	(+) Ins
Intracellular BCKA levels	↑	NM
AKT phosphorylation (Ser473)	↓	↓(si-Sar1b#1) -/-(si-Sar1b#2)
GSK3 phosphorylation (Ser9)	↓	↓
IRS-1 phosphorylation (Tyr612)	-/-	-/-
Pyruvate-linked respiration	↓	NM
ERK phosphorylation (Thr202/204)	-/-	↓
Total mTOR levels	-/-	↓
mTOR phosphorylation (Ser2448)	-/-	-/-
Total S6K levels	↓	↓
S6K phosphorylation (Thr389)	↓	↓
Total S6 levels	↓	-/-
S6 phosphorylation (T202/204)	↓	↓
Protein synthesis	-/-	NM

-/-, no change; NM, not measured; BCKA, branched chain keto acid; GSK3, glycogen synthase kinase; IRS, insulin receptor substrate; ERK, extracellular receptor kinase; mTOR, mechanistic target of rapamycin; S6K, S6 kinase.

4.6 Limitations & future directions:

Several limitations regarding this thesis curtail the scope of the conclusions we can draw from the results. First, aside from an analysis of *in vivo* Sar1b protein quantity, research in this thesis was limited to an in vitro model of Sar1b knockdown in C2C12 myotubes. This allowed for the development of a baseline model and mechanistic insight into Sar1b's role in the skeletal muscle, however, to establish physiological importance, an animal model of Sar1b knockdown or knockout would need to be employed. Additionally, our findings are limited to the use of only one cell line; the inclusion of a knockdown model in an additional in vitro cell line, such as the rat L6 cell line or in a primary cell line, would significantly strengthen the data and findings of this study. Diabetic mouse models, or skeletal muscle-specific Sar1b deletion subjected to diet-induced obesity, would allow us to demonstrate whether altered availability of Sar1b contributes to impaired glucose and insulin tolerance, body weight gain, and adiposity *in vivo*, bringing forth a greater understanding of how Sar1b impacts insulin signaling *in vivo*.

Sar1b is only one of two mammalian paralogues of the Sar1 gene, along with its counterpart Sar1a. Recent studies have pointed toward distinct physiological roles for these two paralogues[104]. I demonstrated that siRNA-mediated knockdown in C2C12 cells was specific to decreasing Sar1b content without altering Sar1a protein and mRNA levels. However, it is unknown if Sar1a has a compensatory role during Sar1b knockdown and might exert functional effects in the skeletal muscle. Compensatory mechanisms from Sar1a could be masking some of the impacts of Sar1b knockdown in the skeletal muscle. This could have been corrected by employing a co-knockdown of both Sar1b and Sar1a, coupled with individual knockdown, which would aid in understanding the paralogue-specific roles. Future directions should continue to explore the specific roles of the two paralogues, which could contribute to a more robust understanding of the specific functional impact of the loss of Sar1b in the skeletal muscle.

For Sar1b to exert its role in COPII vesicle formation, its GTPase activity is required. However, when Chen et al. identified Sar1b to function as a leucine sensor, locking the protein into its GDP or GTP-loaded state and inhibiting its GTPase activity did not alter its role in leucine-sensing and mTOR activation[100]. A limitation of this study is that we never investigated whether Sar1b's identified role in skeletal muscle insulin and mTOR signaling and mitochondrial function was dependent on its activity as a GTPase. To what extent Sar1b's GTPase activity is altered when Sar1b is silenced in the C2C12 model remains to be investigated to underscore the importance of

the COPII complex of Sar1b and its putative non-canonical functions. Furthermore, employing mutations that inhibit the GTPase activity of Sar1b[127] by locking it into its GTP-loaded state, such as Sar1-H79G [128], would enable us to decipher whether the observed effects of Sar1b knockdown in our model could occur in the absence of GTPase activity.

Work in this study was limited to unchallenged, basal state muscle cell function impacted by the loss of Sar1b. Given Sar1b's known impact on lipid metabolism in hepatocytes (CRD)[112], it remains to be seen whether Sar1b has a direct role in lipid metabolism in the skeletal muscle.

An important methodological limitation of this study is the use of solely siRNA-mediated knockdown to reduce Sar1b content. Though experiments were repeated with two or three siRNA constructs to rule out off-target effects of individual siRNA and gain the highest degree of knockdown, there is no telling whether the remaining Sar1b was continuing to exert influence or likewise if the degree of knockdown was enough to exert functional effects. Using a knockout model, such as CRISPR-Cas-9 mediated knockout, in our cell lines would help to confirm whether the phenotype we observed in our knockdown experiments was specific to the loss of Sar1b function and not attributed to off-target effects of siRNA.

Finally, another limitation of this study is the lack of in vitro Sar1b overexpression model to complement findings from the knockdown model. Our understanding of Sar1b's potential role in the skeletal muscle in this study was based upon a loss of function/knockdown model of Sar1b and its effect on skeletal muscle insulin and mTOR signaling. However, to better understand Sar1b's function, it would be critical to investigate the impact of overexpressing Sar1b in the skeletal muscle. In our studies, Sar1b protein quantity was decreased in diet-induced obesity, and Sar1b knockdown impaired insulin signaling and mitochondrial function in the muscle. Thus, a critical future direction based on this project would be to examine if the decline of Sar1b under nutrient overload were to be corrected, would this rescue metabolic anomalies encountered in diet-induced obesity.

4.7 Conclusions

In conclusion, the current study has uncovered and characterized a role for Sar1b in skeletal muscle insulin signaling, mitochondrial function and mTOR signaling while demonstrating that Sar1b protein content is decreased in the skeletal muscle of obesogenic mouse models. Knockdown of Sar1b inhibited skeletal muscle insulin signaling, mitochondrial function, and mitogenic and mTOR signaling. Additionally, this study has established a potential role for Sar1b as a branched-

chain amino acid and keto acid regulator in the skeletal muscle. A greater understanding of the functional impact of the loss of Sar1b is required to understand better the impact of altering its availability on skeletal muscle metabolism and function.

References

1 Gonzalez-Muniesa, P. *et al.* Obesity. *Nat Rev Dis Primers* **3**, 17034, doi:10.1038/nrdp.2017.34 (2017).

2 Lin, X. & Li, H. Obesity: Epidemiology, Pathophysiology, and Therapeutics. *Front Endocrinol (Lausanne)* **12**, 706978, doi:10.3389/fendo.2021.706978 (2021).

3 WHO. *World Health Organization (WHO): Obesity and Overweight*, 2022).

4 Boutari, C. & Mantzoros, C. S. A 2022 update on the epidemiology of obesity and a call to action: as its twin COVID-19 pandemic appears to be receding, the obesity and dysmetabolism pandemic continues to rage on. *Metabolism* **133**, 155217, doi:10.1016/j.metabol.2022.155217 (2022).

5 Bluher, M. Obesity: global epidemiology and pathogenesis. *Nat Rev Endocrinol* **15**, 288-298, doi:10.1038/s41574-019-0176-8 (2019).

6 Lu, X. *et al.* Multidisciplinary Progress in Obesity Research. *Genes (Basel)* **13**, doi:10.3390/genes13101772 (2022).

7 Kahn, S. E. The relative contributions of insulin resistance and beta-cell dysfunction to the pathophysiology of Type 2 diabetes. *Diabetologia* **46**, 3-19, doi:10.1007/s00125-002-1009-0 (2003).

8 Tallis, J., James, R. S. & Seebacher, F. The effects of obesity on skeletal muscle contractile function. *J Exp Biol* **221**, doi:10.1242/jeb.163840 (2018).

9 Lee, S. H., Park, S. Y. & Choi, C. S. Insulin Resistance: From Mechanisms to Therapeutic Strategies. *Diabetes Metab J* **46**, 15-37, doi:10.4093/dmj.2021.0280 (2022).

10 Fuster, J. J., Ouchi, N., Gokce, N. & Walsh, K. Obesity-Induced Changes in Adipose Tissue Microenvironment and Their Impact on Cardiovascular Disease. *Circ Res* **118**, 1786-1807, doi:10.1161/CIRCRESAHA.115.306885 (2016).

11 Carnagarin, R., Dharmarajan, A. M. & Dass, C. R. Molecular aspects of glucose homeostasis in skeletal muscle--A focus on the molecular mechanisms of insulin resistance. *Mol Cell Endocrinol* **417**, 52-62, doi:10.1016/j.mce.2015.09.004 (2015).

12 Wasserman, D. H. Insulin, Muscle Glucose Uptake, and Hexokinase: Revisiting the Road Not Taken. *Physiology (Bethesda)* **37**, 115-127, doi:10.1152/physiol.00034.2021 (2022).

13 Joost, H. G. & Thorens, B. The extended GLUT-family of sugar/polyol transport facilitators: nomenclature, sequence characteristics, and potential function of its novel members (review). *Mol Membr Biol* **18**, 247-256, doi:10.1080/09687680110090456 (2001).

14 Bryant, N. J., Govers, R. & James, D. E. Regulated transport of the glucose transporter GLUT4. *Nat Rev Mol Cell Biol* **3**, 267-277, doi:10.1038/nrm782 (2002).

15 White, M. F. & Kahn, C. R. The insulin signaling system. *J Biol Chem* **269**, 1-4 (1994).

16 Klaman, L. D. *et al.* Increased energy expenditure, decreased adiposity, and tissue-specific insulin sensitivity in protein-tyrosine phosphatase 1B-deficient mice. *Mol Cell Biol* **20**, 5479-5489, doi:10.1128/MCB.20.15.5479-5489.2000 (2000).

17 Elchebly, M. *et al.* Increased insulin sensitivity and obesity resistance in mice lacking the protein tyrosine phosphatase-1B gene. *Science* **283**, 1544-1548, doi:10.1126/science.283.5407.1544 (1999).

18 White, M. F., Shoelson, S. E., Keutmann, H. & Kahn, C. R. A cascade of tyrosine autophosphorylation in the beta-subunit activates the phosphotransferase of the insulin receptor. *J Biol Chem* **263**, 2969-2980 (1988).

19 Long, Y. C., Cheng, Z., Copps, K. D. & White, M. F. Insulin receptor substrates Irs1 and Irs2 coordinate skeletal muscle growth and metabolism via the Akt and AMPK pathways. *Mol Cell Biol* **31**, 430-441, doi:10.1128/MCB.00983-10 (2011).

20 Huang, C., Thirone, A. C., Huang, X. & Klip, A. Differential contribution of insulin receptor substrates 1 versus 2 to insulin signaling and glucose uptake in l6 myotubes. *J Biol Chem* **280**, 19426-19435, doi:10.1074/jbc.M412317200 (2005).

21 Lietzke, S. E. *et al.* Structural basis of 3-phosphoinositide recognition by pleckstrin homology domains. *Mol Cell* **6**, 385-394, doi:10.1016/s1097-2765(00)00038-1 (2000).

22 Jaiswal, N. *et al.* The role of skeletal muscle Akt in the regulation of muscle mass and glucose homeostasis. *Mol Metab* **28**, 1-13, doi:10.1016/j.molmet.2019.08.001 (2019).

23 Wan, M. *et al.* Loss of Akt1 in mice increases energy expenditure and protects against diet-induced obesity. *Mol Cell Biol* **32**, 96-106, doi:10.1128/MCB.05806-11 (2012).

24 Cho, H. *et al.* Insulin resistance and a diabetes mellitus-like syndrome in mice lacking the protein kinase Akt2 (PKB beta). *Science* **292**, 1728-1731, doi:10.1126/science.292.5522.1728 (2001).

25 Katso, R. *et al.* Cellular function of phosphoinositide 3-kinases: implications for development, homeostasis, and cancer. *Annu Rev Cell Dev Biol* **17**, 615-675, doi:10.1146/annurev.cellbio.17.1.615 (2001).

26 Alessi, D. R. *et al.* Mechanism of activation of protein kinase B by insulin and IGF-1. *EMBO J* **15**, 6541-6551 (1996).

27 Brognard, J., Sierecki, E., Gao, T. & Newton, A. C. PHLPP and a second isoform, PHLPP2, differentially attenuate the amplitude of Akt signaling by regulating distinct Akt isoforms. *Mol Cell* **25**, 917-931, doi:10.1016/j.molcel.2007.02.017 (2007).

28 Gao, T., Furnari, F. & Newton, A. C. PHLPP: a phosphatase that directly dephosphorylates Akt, promotes apoptosis, and suppresses tumor growth. *Mol Cell* **18**, 13-24, doi:10.1016/j.molcel.2005.03.008 (2005).

29 Cross, D. A., Alessi, D. R., Cohen, P., Andjelkovich, M. & Hemmings, B. A. Inhibition of glycogen synthase kinase-3 by insulin mediated by protein kinase B. *Nature* **378**, 785-789, doi:10.1038/378785a0 (1995).

30 Thong, F. S., Dugani, C. B. & Klip, A. Turning signals on and off: GLUT4 traffic in the insulin-signaling highway. *Physiology (Bethesda)* **20**, 271-284, doi:10.1152/physiol.00017.2005 (2005).

31 Avruch, J. MAP kinase pathways: the first twenty years. *Biochim Biophys Acta* **1773**, 1150-1160, doi:10.1016/j.bbamcr.2006.11.006 (2007).

32 Skolnik, E. Y. *et al.* The SH2/SH3 domain-containing protein GRB2 interacts with tyrosine-phosphorylated IRS1 and Shc: implications for insulin control of ras signalling. *EMBO J* **12**, 1929-1936, doi:10.1002/j.1460-2075.1993.tb05842.x (1993).

33 Kim, S. J. & Kim, K. H. Insulin rapidly stimulates ERK2 in the membrane of osteoblast-like UMR-106 cell. *Biochem Mol Biol Int* **43**, 1023-1031, doi:10.1080/15216549700204841 (1997).

34 Ramalingam, M., Kwon, Y. D. & Kim, S. J. Insulin as a Potent Stimulator of Akt, ERK and Inhibin-betaE Signaling in Osteoblast-Like UMR-106 Cells. *Biomol Ther (Seoul)* **24**, 589-594, doi:10.4062/biomolther.2016.030 (2016).

35 Boucher, J., Kleinridders, A. & Kahn, C. R. Insulin receptor signaling in normal and insulin-resistant states. *Cold Spring Harb Perspect Biol* **6**, doi:10.1101/cshperspect.a009191 (2014).

36 Cahova, M., Vavrinkova, H. & Kazdova, L. Glucose-fatty acid interaction in skeletal muscle and adipose tissue in insulin resistance. *Physiol Res* **56**, 1-15, doi:10.33549/physiolres.930882 (2007).

37 Colberg, S. R., Simoneau, J. A., Thaete, F. L. & Kelley, D. E. Skeletal muscle utilization of free fatty acids in women with visceral obesity. *J Clin Invest* **95**, 1846-1853, doi:10.1172/JCI117864 (1995).

38 Watanabe, T., Smith, M. M., Robinson, F. W. & Kono, T. Insulin action on glucose transport in cardiac muscle. *The Journal of biological chemistry* **259**, 13117-13122 (1984).

39 Randle, P. J. The biochemical basis of the relation between glucose and fatty acid metabolism. *Acta chirurgica Scandinavica. Supplementum* **498**, 111-114 (1980).

40 Randle, P. J., Garland, P. B., Hales, C. N. & Newsholme, E. A. The glucose fatty-acid cycle. Its role in insulin sensitivity and the metabolic disturbances of diabetes mellitus. *Lancet* **1**, 785-789, doi:10.1016/s0140-6736(63)91500-9 (1963).

41 An, D. & Rodrigues, B. Role of changes in cardiac metabolism in development of diabetic cardiomyopathy. *American journal of physiology. Heart and circulatory physiology* **291**, H1489-1506, doi:10.1152/ajpheart.00278.2006 (2006).

42 Muoio, D. M. & Newgard, C. B. Fatty acid oxidation and insulin action: when less is more. *Diabetes* **57**, 1455-1456, doi:10.2337/db08-0281 (2008).

43 Karwi, Q. G. *et al.* Insulin directly stimulates mitochondrial glucose oxidation in the heart. *Cardiovasc Diabetol* **19**, 207, doi:10.1186/s12933-020-01177-3 (2020).

44 Sloun, B. V. *et al.* The Impact of Amino Acids on Postprandial Glucose and Insulin Kinetics in Humans: A Quantitative Overview. *Nutrients* **12**, doi:10.3390/nu12103211 (2020).

45 Bonadonna, R. C., Saccomani, M. P., Cobelli, C. & DeFronzo, R. A. Effect of insulin on system A amino acid transport in human skeletal muscle. *J Clin Invest* **91**, 514-521, doi:10.1172/JCI116230 (1993).

46 Manchester, K. L. Effect of insulin on protein synthesis. *Diabetes* **21**, 447-452, doi:10.2337/diab.21.2.s447 (1972).

47 Yoon, M. S. The Role of Mammalian Target of Rapamycin (mTOR) in Insulin Signaling. *Nutrients* **9**, doi:10.3390/nu9111176 (2017).

48 Saxton, R. A. & Sabatini, D. M. mTOR Signaling in Growth, Metabolism, and Disease. *Cell* **168**, 960-976, doi:10.1016/j.cell.2017.02.004 (2017).

49 Lee, W. S. & Kim, J. Peroxisome Proliferator-Activated Receptors and the Heart: Lessons from the Past and Future Directions. *PPAR research* **2015**, 271983, doi:10.1155/2015/271983 (2015).

50 Brindley, D. N., Kok, B. P., Kienesberger, P. C., Lehner, R. & Dyck, J. R. Shedding light on the enigma of myocardial lipotoxicity: the involvement of known and putative regulators of fatty acid storage and mobilization. *American journal of physiology. Endocrinology and metabolism* **298**, E897-908, doi:10.1152/ajpendo.00509.2009 (2010).

51 Shannon, C. *et al.* Effect of Chronic Hyperglycemia on Glucose Metabolism in Subjects With Normal Glucose Tolerance. *Diabetes* **67**, 2507-2517, doi:10.2337/db18-0439 (2018).

52 Genders, A. J., Holloway, G. P. & Bishop, D. J. Are Alterations in Skeletal Muscle Mitochondria a Cause or Consequence of Insulin Resistance? *Int J Mol Sci* **21**, doi:10.3390/ijms21186948 (2020).

53 Kim, J. Y., Hickner, R. C., Cortright, R. L., Dohm, G. L. & Houmard, J. A. Lipid oxidation is reduced in obese human skeletal muscle. *Am J Physiol Endocrinol Metab* **279**, E1039-1044, doi:10.1152/ajpendo.2000.279.5.E1039 (2000).

54 Chomentowski, P., Coen, P. M., Radikova, Z., Goodpaster, B. H. & Toledo, F. G. Skeletal muscle mitochondria in insulin resistance: differences in intermyofibrillar versus subsarcolemmal subpopulations and relationship to metabolic flexibility. *J Clin Endocrinol Metab* **96**, 494-503, doi:10.1210/jc.2010-0822 (2011).

55 Matsuda, M. & DeFronzo, R. A. Insulin sensitivity indices obtained from oral glucose tolerance testing: comparison with the euglycemic insulin clamp. *Diabetes Care* **22**, 1462-1470, doi:10.2337/diacare.22.9.1462 (1999).

56 Boushel, R. *et al.* Patients with type 2 diabetes have normal mitochondrial function in skeletal muscle. *Diabetologia* **50**, 790-796, doi:10.1007/s00125-007-0594-3 (2007).

57 James, D. E., Stockli, J. & Birnbaum, M. J. The aetiology and molecular landscape of insulin resistance. *Nat Rev Mol Cell Biol* **22**, 751-771, doi:10.1038/s41580-021-00390-6 (2021).

58 Saltiel, A. R. Insulin signaling in health and disease. *J Clin Invest* **131**, doi:10.1172/JCI142241 (2021).

59 Haeusler, R. A., McGraw, T. E. & Accili, D. Biochemical and cellular properties of insulin receptor signalling. *Nat Rev Mol Cell Biol* **19**, 31-44, doi:10.1038/nrm.2017.89 (2018).

60 Fazakerley, D. J., Krycer, J. R., Kearney, A. L., Hocking, S. L. & James, D. E. Muscle and adipose tissue insulin resistance: malady without mechanism? *J Lipid Res* **60**, 1720-1732, doi:10.1194/jlr.R087510 (2019).

61 Gual, P., Le Marchand-Brustel, Y. & Tanti, J. F. Positive and negative regulation of insulin signaling through IRS-1 phosphorylation. *Biochimie* **87**, 99-109, doi:10.1016/j.biochi.2004.10.019 (2005).

62 Aguirre, V. *et al.* Phosphorylation of Ser307 in insulin receptor substrate-1 blocks interactions with the insulin receptor and inhibits insulin action. *J Biol Chem* **277**, 1531-1537, doi:10.1074/jbc.M101521200 (2002).

63 Esposito, D. L., Li, Y., Cama, A. & Quon, M. J. Tyr(612) and Tyr(632) in human insulin receptor substrate-1 are important for full activation of insulin-stimulated phosphatidylinositol 3-kinase activity and translocation of GLUT4 in adipose cells. *Endocrinology* **142**, 2833-2840, doi:10.1210/endo.142.7.8283 (2001).

64 Li, Y. *et al.* Protein kinase C Theta inhibits insulin signaling by phosphorylating IRS1 at Ser(1101). *J Biol Chem* **279**, 45304-45307, doi:10.1074/jbc.C400186200 (2004).

65 Kim, J. K. *et al.* PKC-theta knockout mice are protected from fat-induced insulin resistance. *J Clin Invest* **114**, 823-827, doi:10.1172/JCI22230 (2004).

66 Pal, M., Febbraio, M. A. & Lancaster, G. I. The roles of c-Jun NH2-terminal kinases (JNKs) in obesity and insulin resistance. *J Physiol* **594**, 267-279, doi:10.1113/JP271457 (2016).

67 Solinas, G. & Becattini, B. JNK at the crossroad of obesity, insulin resistance, and cell stress response. *Mol Metab* **6**, 174-184, doi:10.1016/j.molmet.2016.12.001 (2017).

68 Yung, J. H. M. & Giacca, A. Role of c-Jun N-terminal Kinase (JNK) in Obesity and Type 2 Diabetes. *Cells* **9**, doi:10.3390/cells9030706 (2020).

69 Feng, J. *et al.* The Role of JNk Signaling Pathway in Obesity-Driven Insulin Resistance. *Diabetes Metab Syndr Obes* **13**, 1399-1406, doi:10.2147/DMSO.S236127 (2020).

70 Liu, X. & Yao, Z. Chronic over-nutrition and dysregulation of GSK3 in diseases. *Nutr Metab (Lond)* **13**, 49, doi:10.1186/s12986-016-0108-8 (2016).

71 Leng, S. *et al.* Glycogen synthase kinase 3 beta mediates high glucose-induced ubiquitination and proteasome degradation of insulin receptor substrate 1. *J Endocrinol* **206**, 171-181, doi:10.1677/JOE-09-0456 (2010).

72 Kawahito, S., Kitahata, H. & Oshita, S. Problems associated with glucose toxicity: role of hyperglycemia-induced oxidative stress. *World J Gastroenterol* **15**, 4137-4142, doi:10.3748/wjg.15.4137 (2009).

73 Du, X. *et al.* Inhibition of GAPDH activity by poly(ADP-ribose) polymerase activates three major pathways of hyperglycemic damage in endothelial cells. *The Journal of clinical investigation* **112**, 1049-1057, doi:10.1172/JCI18127 (2003).

74 Poornima, I. G., Parikh, P. & Shannon, R. P. Diabetic cardiomyopathy: the search for a unifying hypothesis. *Circulation research* **98**, 596-605, doi:10.1161/01.RES.0000207406.94146.c2 (2006).

75 Cai, L. & Kang, Y. J. Oxidative stress and diabetic cardiomyopathy: a brief review. *Cardiovascular toxicology* **1**, 181-193 (2001).

76 Wakasaki, H. *et al.* Targeted overexpression of protein kinase C beta2 isoform in myocardium causes cardiomyopathy. *Proceedings of the National Academy of Sciences of the United States of America* **94**, 9320-9325 (1997).

77 Shannon, C. E. *et al.* Effects of Sustained Hyperglycemia on Skeletal Muscle Lipids in Healthy Subjects. *J Clin Endocrinol Metab* **107**, e3177-e3185, doi:10.1210/clinem/dgac306 (2022).

78 Akoumi, A., Haffar, T., Mousterji, M., Kiss, R. S. & Bousette, N. Palmitate mediated diacylglycerol accumulation causes endoplasmic reticulum stress, Plin2 degradation, and cell death in H9C2 cardiomyoblasts. *Exp Cell Res* **354**, 85-94, doi:10.1016/j.yexcr.2017.03.032 (2017).

79 Ertunc, M. E. & Hotamisligil, G. S. Lipid signaling and lipotoxicity in metaflammation: indications for metabolic disease pathogenesis and treatment. *J Lipid Res* **57**, 2099-2114, doi:10.1194/jlr.R066514 (2016).

80 Watt, M. J. Storing up trouble: does accumulation of intramyocellular triglyceride protect skeletal muscle from insulin resistance? *Clin Exp Pharmacol Physiol* **36**, 5-11, doi:10.1111/j.1440-1681.2008.05075.x (2009).

81 Lair, B., Laurens, C., Van Den Bosch, B. & Moro, C. Novel Insights and Mechanisms of Lipotoxicity-Driven Insulin Resistance. *Int J Mol Sci* **21**, doi:10.3390/ijms21176358 (2020).

82 Sokolowska, E. & Blachnio-Zabielska, A. The Role of Ceramides in Insulin Resistance. *Front Endocrinol (Lausanne)* **10**, 577, doi:10.3389/fendo.2019.00577 (2019).

83 Ong, P. S. *et al.* Judicious Toggling of mTOR Activity to Combat Insulin Resistance and Cancer: Current Evidence and Perspectives. *Front Pharmacol* **7**, 395, doi:10.3389/fphar.2016.00395 (2016).

84 Shum, M., Bellmann, K., St-Pierre, P. & Marette, A. Pharmacological inhibition of S6K1 increases glucose metabolism and Akt signalling in vitro and in diet-induced obese mice. *Diabetologia* **59**, 592-603, doi:10.1007/s00125-015-3839-6 (2016).

85 Harrington, L. S. *et al.* The TSC1-2 tumor suppressor controls insulin-PI3K signaling via regulation of IRS proteins. *J Cell Biol* **166**, 213-223, doi:10.1083/jcb.200403069 (2004).

86 Layman, D. K. The role of leucine in weight loss diets and glucose homeostasis. *J Nutr* **133**, 261S-267S, doi:10.1093/jn/133.1.261S (2003).

87 Biswas, D., Duffley, L. & Pulinilkunnil, T. Role of branched-chain amino acid-catabolizing enzymes in intertissue signaling, metabolic remodeling, and energy homeostasis. *FASEB J* **33**, 8711-8731, doi:10.1096/fj.201802842RR (2019).

88 Uddin, G. M. *et al.* Impaired branched chain amino acid oxidation contributes to cardiac insulin resistance in heart failure. *Cardiovasc Diabetol* **18**, 86, doi:10.1186/s12933-019-0892-3 (2019).

89 Li, T. *et al.* Defective Branched-Chain Amino Acid Catabolism Disrupts Glucose Metabolism and Sensitizes the Heart to Ischemia-Reperfusion Injury. *Cell Metab* **25**, 374-385, doi:10.1016/j.cmet.2016.11.005 (2017).

90 Biswas, D. & Pulinilkunnil, T. Disrupted branched-chain amino acid catabolism impair cardiac insulin signaling and is associated with adverse cardiometabolic outcomes. *J Mol Cell Cardiol* **153**, 93-94, doi:10.1016/j.yjmcc.2020.12.011 (2021).

91 Zhou, M. *et al.* Targeting BCAA Catabolism to Treat Obesity-Associated Insulin Resistance. *Diabetes* **68**, 1730-1746, doi:10.2337/db18-0927 (2019).

92 Biswas, D. *et al.* Adverse Outcomes in Obese Cardiac Surgery Patients Correlates With Altered Branched-Chain Amino Acid Catabolism in Adipose Tissue and Heart. *Front Endocrinol (Lausanne)* **11**, 534, doi:10.3389/fendo.2020.00534 (2020).

93 Biswas, D. *et al.* Branched-chain ketoacid overload inhibits insulin action in the muscle. *J Biol Chem* **295**, 15597-15621, doi:10.1074/jbc.RA120.013121 (2020).

94 Felig, P., Owen, O. E., Wahren, J. & Cahill, G. F., Jr. Amino acid metabolism during prolonged starvation. *J Clin Invest* **48**, 584-594, doi:10.1172/JCI106017 (1969).

95 Wolfson, R. L. & Sabatini, D. M. The Dawn of the Age of Amino Acid Sensors for the mTORC1 Pathway. *Cell Metab* **26**, 301-309, doi:10.1016/j.cmet.2017.07.001 (2017).

96 Ye, J. *et al.* GCN2 sustains mTORC1 suppression upon amino acid deprivation by inducing Sestrin2. *Genes Dev* **29**, 2331-2336, doi:10.1101/gad.269324.115 (2015).

97 Nakamura, M., Satoh, N., Horita, S. & Nangaku, M. Insulin-induced mTOR signaling and gluconeogenesis in renal proximal tubules: A mini-review of current evidence and therapeutic potential. *Front Pharmacol* **13**, 1015204, doi:10.3389/fphar.2022.1015204 (2022).

98 Wolfson, R. L. *et al.* Sestrin2 is a leucine sensor for the mTORC1 pathway. *Science* **351**, 43-48, doi:10.1126/science.aab2674 (2016).

99 Kowalsky, A. H. *et al.* The GATOR2-mTORC2 axis mediates Sestrin2-induced AKT Ser/Thr kinase activation. *J Biol Chem* **295**, 1769-1780, doi:10.1074/jbc.RA119.010857 (2020).

100 Chen, J. *et al.* SAR1B senses leucine levels to regulate mTORC1 signalling. *Nature* **596**, 281-284, doi:10.1038/s41586-021-03768-w (2021).

101 Donaldson, J. G. & Jackson, C. L. ARF family G proteins and their regulators: roles in membrane transport, development and disease. *Nat Rev Mol Cell Biol* **12**, 362-375, doi:10.1038/nrm3117 (2011).

102 Springer, S., Spang, A. & Schekman, R. A primer on vesicle budding. *Cell* **97**, 145-148, doi:10.1016/s0092-8674(00)80722-9 (1999).

103 Huang, M. *et al.* Crystal structure of Sar1-GDP at 1.7 A resolution and the role of the NH2 terminus in ER export. *J Cell Biol* **155**, 937-948, doi:10.1083/jcb.200106039 (2001).

104 Melville, D. B., Studer, S. & Schekman, R. Small sequence variations between two mammalian paralogs of the small GTPase SAR1 underlie functional differences in coat protein complex II assembly. *J Biol Chem* **295**, 8401-8412, doi:10.1074/jbc.RA120.012964 (2020).

105 Ackema, K. B. *et al.* Sar1, a Novel Regulator of ER-Mitochondrial Contact Sites. *PLoS One* **11**, e0154280, doi:10.1371/journal.pone.0154280 (2016).

106 Saito, K., Maeda, M. & Katada, T. Regulation of the Sar1 GTPase Cycle Is Necessary for Large Cargo Secretion from the Endoplasmic Reticulum. *Frontiers in Cell and Developmental Biology* **5**, doi:10.3389/fcell.2017.00075 (2017).

107 Levy, E. *et al.* Expression of Sar1b enhances chylomicron assembly and key components of the coat protein complex II system driving vesicle budding. *Arterioscler Thromb Vasc Biol* **31**, 2692-2699, doi:10.1161/ATVBAHA.111.233908 (2011).

108 Sane, A. T. *et al.* Understanding Chylomicron Retention Disease Through Sar1b Gtpase Gene Disruption: Insight From Cell Culture. *Arterioscler Thromb Vasc Biol* **37**, 2243-2251, doi:10.1161/ATVBAHA.117.310121 (2017).

109 Levic, D. S. *et al.* Animal model of Sar1b deficiency presents lipid absorption deficits similar to Anderson disease. *J Mol Med (Berl)* **93**, 165-176, doi:10.1007/s00109-014-1247-x (2015).

110 Levy, E. Insights from human congenital disorders of intestinal lipid metabolism. *J Lipid Res* **56**, 945-962, doi:10.1194/jlr.R052415 (2015).

111 Doya, L. J. *et al.* Chylomicron retention disease caused by a new pathogenic variant in sar1b protein: a rare case report from Syria. *BMC Pediatr* **21**, 449, doi:10.1186/s12887-021-02897-5 (2021).

112 Auclair, N. *et al.* Sar1b mutant mice recapitulate gastrointestinal abnormalities associated with chylomicron retention disease. *J Lipid Res* **62**, 100085, doi:10.1016/j.jlr.2021.100085 (2021).

113 Sane, A. *et al.* SAR1B GTPase is necessary to protect intestinal cells from disorders of lipid homeostasis, oxidative stress, and inflammation. *J Lipid Res* **60**, 1755-1764, doi:10.1194/jlr.RA119000119 (2019).

114 Marcil, V. *et al.* Tissue distribution and regulation of the small Sar1b GTPase in mice. *Cell Physiol Biochem* **33**, 1815-1826, doi:10.1159/000362960 (2014).

115 Zhuang, X., Chowdhury, S., Northup, J. K. & Ray, K. Sar1-dependent trafficking of the human calcium receptor to the cell surface. *Biochem Biophys Res Commun* **396**, 874-880, doi:10.1016/j.bbrc.2010.05.014 (2010).

116 Nori, A., Bortoloso, E., Frasson, F., Valle, G. & Volpe, P. Vesicle budding from endoplasmic reticulum is involved in calsequestrin routing to sarcoplasmic reticulum of skeletal muscles. *Biochem J* **379**, 505-512, doi:10.1042/BJ20031875 (2004).

117 Yaribeygi, H., Farrokhi, F. R., Butler, A. E. & Sahebkar, A. Insulin resistance: Review of the underlying molecular mechanisms. *J Cell Physiol* **234**, 8152-8161, doi:10.1002/jcp.27603 (2019).

118 Armenta, J. M. *et al.* Sensitive and rapid method for amino acid quantitation in malaria biological samples using AccQ.Tag ultra performance liquid chromatography-electrospray ionization-MS/MS with multiple reaction monitoring. *Anal Chem* **82**, 548-558, doi:10.1021/ac901790q (2010).

119 Salazar, C., Armenta, J. M., Cortes, D. F. & Shulaev, V. Combination of an AccQ.Tag-ultra performance liquid chromatographic method with tandem mass spectrometry for the analysis of amino acids. *Methods Mol Biol* **828**, 13-28, doi:10.1007/978-1-61779-445-2_2 (2012).

120 Wong, C. Y., Al-Salami, H. & Dass, C. R. C2C12 cell model: its role in understanding of insulin resistance at the molecular level and pharmaceutical development at the preclinical stage. *J Pharm Pharmacol* **72**, 1667-1693, doi:10.1111/jphp.13359 (2020).

121 Weintraub, H. The MyoD family and myogenesis: redundancy, networks, and thresholds. *Cell* **75**, 1241-1244, doi:10.1016/0092-8674(93)90610-3 (1993).

122 Schmidt, E. K., Clavarino, G., Ceppi, M. & Pierre, P. SUnSET, a nonradioactive method to monitor protein synthesis. *Nat Methods* **6**, 275-277, doi:10.1038/nmeth.1314 (2009).

123 Levy, E. *et al.* Sar1b transgenic male mice are more susceptible to high-fat diet-induced obesity, insulin insensitivity and intestinal chylomicron overproduction. *J Nutr Biochem* **25**, 540-548, doi:10.1016/j.jnutbio.2014.01.004 (2014).

124 Sarbassov, D. D., Guertin, D. A., Ali, S. M. & Sabatini, D. M. Phosphorylation and regulation of Akt/PKB by the rictor-mTOR complex. *Science* **307**, 1098-1101, doi:10.1126/science.1106148 (2005).

125 Barazzoni, R. *et al.* Insulin fails to enhance mTOR phosphorylation, mitochondrial protein synthesis, and ATP production in human skeletal muscle without amino acid replacement. *Am J Physiol Endocrinol Metab* **303**, E1117-1125, doi:10.1152/ajpendo.00067.2012 (2012).

126 Asmann, Y. W. *et al.* Skeletal muscle mitochondrial functions, mitochondrial DNA copy numbers, and gene transcript profiles in type 2 diabetic and nondiabetic subjects at equal levels of low or high insulin and euglycemia. *Diabetes* **55**, 3309-3319, doi:10.2337/db05-1230 (2006).

127 Mondal, S., Hsiao, K. & Goueli, S. A. A Homogenous Bioluminescent System for Measuring GTPase, GTPase Activating Protein, and Guanine Nucleotide Exchange Factor Activities. *Assay Drug Dev Technol* **13**, 444-455, doi:10.1089/adt.2015.643 (2015).

128 Weigel, A. V. *et al.* ER-to-Golgi protein delivery through an interwoven, tubular network extending from ER. *Cell* **184**, 2412-2429 e2416, doi:10.1016/j.cell.2021.03.035 (2021).